UNIVERSITY OF SOUTHAMPTON

IN SEARCH OF ACCURATE QUANTUM MECHANICAL SOLUTIONS

TO SMALL SYSTEMS OF CHEMICAL INTEREST

SIMON JOHN HOLDSHIP

A dissertation submitted in partial fulfilment of the

requirements for the Degree of Doctor of Philosophy at the

University of Southampton.

Department of Chemistry   December 1989.

Contents

UNIVERSITY OF SOUTHAMPTON

ABSTRACT

FACULTY OF SCIENCE

CHEMISTRY

Doctor of Philosophy

IN SEARCH OF ACCURATE QUANTUM MECHANICAL SOLUTIONS
TO SMALL SYSTEMS OF CHEMICAL INTEREST

by Simon John Holdship

An adiabatic separation is applied to a system of two coupled
oscillators with the coupling term of the form x^2y^2. The resulting
approximate quantum mechanical energies are corrected for non-
adiabatic interactions by perturbation theory. The convergence
properties of the perturbation series (based on the Rayleigh-
Schrödinger scheme) are demonstrated for different harmonic
frequencies and magnitude of perturbation. The order in which the
adiabatic separation is made is shown to have little effect on the
accuracy of the energy levels. The results of calculations on the
generalized Henon-Heiles hamiltonian are also presented.
   Multigrid methods are used to tackle the perturbed oscillator
problem in one and two dimensions. The multigrid V- and FMV- cycles
are used in conjunction with Brillouin-Wigner perturbation theory and
the method of inverse iteration. The Numerov correction in two
dimensions is derived and incorporated in the multigrid schemes. The
method of nested iteration is used in a direct approach to the
problem of a pair of coupled oscillators. The difficulties
encountered when applying multigrid methods to systems governed by a
non-positive definite operator are discussed. In particular, the use
of a carefully chosen coarsest grid is shown to play a key rôle in
the convergence of the calculations.
   The hyperspherical coordinate system is used to investigate the
vibration-rotation energy levels of a model X_3 system constrained to
move in a fixed plane. The influence of the rotation on the
structure of the molecule is investigated. Approximate energy levels
are obtained using an adiabatic separation, which readily provides
structual data in an easily visualisable form. The same
hyperspherical system is used to calculate bound state energies of
the Helium atom confined to motion in a plane. The symmetry aspects
of the three body system for zero and non-zero angular momentum are
discussed.

Acknowledgements

I would like to thank my supervisor Dr. Jeremy G. Frey for all his help throughout the duration of this work.

I am deeply indebted to my parents and brother for their continual encouragement and support.

The coloured graphical plots in this work were produced using code written by Mr. M. Pinches (it was worth a drink or two for him).

Finally, I would like to thank various people for putting up with me over the years. They shall remain anonymous to all but themselves and those in the know. They are, Loco, Frog, The Sheds, Jezbo, Ambo, 'Old Boy', all of the other Bo's and Nobby's and all those who 'swung their pants'.

1. General Introduction

1.1 Introduction

The aim of this work was to calculate bound state energies efficiently and accurately for small quantum mechanical systems. The achievement of such an ambition is non-trivial even for calculations where a particle is confined to motion in just two dimensions. The apparently simple form of the Schrödinger wave equation belies the complexity involved when solutions are required for systems of chemical interest. The problem is put into perspective by considering the amount of work carried out on even the simplest of molecules, H_2^+ and related isotopic species. These systems exhibit relativistic effects which have to be included in the calculations in order to achieve a good agreement with accurate well-resolved experimental results (for examples, see [1]). Relativistic quantum mechanical effects have not been considered in this work. Instead, attention is given to improving on standard approximation techniques and to the development of new ways to tackle old problems. To this end, many of the calculations were performed on the system of a pair of coupled oscillators. Chapters 3 and 4 use this system as a model problem for the methods employed in the bound state calculations. Chapter 2 is designed to set the scene for these calculations by outlining some of the numerical tools that were used. The final chapter is devoted to the planar three body problem; specifically a model X_3 molecule and the He atom with the electrons confined to motion in a plane.

The ability to solve a one-dimensional Schrödinger equation is often a crucial part in quantum mechanical calculations. Approximate methods may be used to reduce multi-dimensional coupled wave equations to a set of uncoupled single-dimensional equations. Therefore, it is essential to be able to derive eigenvalues and eigenfunctions for such systems, quickly and efficiently. Throughout this work, this is achieved using the Numerov-Cooley finite difference algorithm [2]. The Numerov integration technique [3] is described in Chapter 2, where examples of its use in one-dimensional problems are given. The Numerov correction in two dimensions is derived in this chapter and a brief example of its use is also

presented. Later on in this study, the Numerov correction is applied more extensively (in two dimensions) to calculations of systems involving coupled harmonic oscillators. Another numerical tool outlined in Chapter 2 is the method of inverse iteration. Inverse iteration is introduced as a means of predicting and improving on eigenvalue/eigenvector calculations from given initial approximations. The iteration process itself uses matrix algebra to describe the appropriate wave equation. Matrix methods in various forms were often used in this work to both define the problem of interest and to find solutions to these problems. They first appear in the method of secular equations where a perturbation is applied to a system of known solutions. The new system hamiltonian is diagonalised in a set of basis functions formed by the eigenfunctions of the zeroth order hamiltonian. An example of this is also given in Chapter 2.

The difficulties associated with directly solving multi-dimensional and multi-particle problems to a high degree of accuracy usually lead to the use of methods of approximating the system of interest. Harmonic oscillators are often used as a first approximation in molecular systems to describe the vibrations of the two atoms in a chemical bonds. More recently, the system has been studied in the hope of shedding light on the onset of classical chaos in quantum systems [4]. A set of N-dimensional uncoupled oscillators is one of the few exactly soluble problems in quantum mechanics. The solution of such a multi-dimensional system is achieved using the method of separation of variables [5], a concept that is often employed in proceeding calculations. The harmonic oscillator itself is too simple a model to be directly applicable to atomic/molecular vibrations (the Morse oscillator gives a better approximation and is used later in this study). However, the situation may be improved by applying perturbations to the original model in the hope of providing a better and more useful description of vibrational motions. Two forms of perturbation theory were used in this work, that of Rayleigh-Schrödinger and Brillouin-Wigner. The first of these is encountered in Chapter 3 and the latter is introduced in Chapter 2 and appears later in Chapter 4.

An often used technique of approximately separating the variables of the problem in hand is described by Born and Oppenheimer [6] in their work on molecular wavefunctions. In this method, the complete wavefunction is obtained by first solving for electronic motion alone (with the nuclei fixed on the electronic time scale) and then solving for the nuclei alone. In the second part of this calculation, the electronic energy as a function of internuclear distance occurs as a potential function. The terms neglected in this approximation, the so-called adiabatic and non-adiabatic corrections, may then be included by means of perturbation theory. This is the approach used in Chapter 3 in the work on a pair of coupled oscillators; the Born-Oppenheimer approximation is applied to produce approximate solutions which are then improved by the incorporation of the correction terms using Rayleigh-Schrödinger perturbation theory. The results of these calculations are used to show the application, effectiveness and drawbacks encountered in the use of such a scheme.

Separating the variables in a problem of interest and attempting to improve on the resulting approximate results can be a complicated and laborious process. The large computational effort that is often required can lead in many cases to scant reward. This is illustrated in Chapter 3. It would be much more convenient if the Schrödinger wave equation under consideration could be solved directly, without having to uncouple the system of equations. Attempts to affect such calculations are given in Chapter 4 on the use of multigrid methods. Multigrid techniques were originally developed to solve boundary value problems on a variety of spatial domains, for instance the Poisson equation in a square domain [7]. The method involves the discretisation of the problem by choosing a set of grid points in the range of the problem and incorporates a series of grids with an ever decreasing number of points. The grid level immediately below the top, finest level has half the number of points than that of the top level. The next lowest grid then has half the number of points than the previous one and the sequence continues until the bottom, coarsest grid level is reached. The equation may then be solved iteratively on the finest grid using standard relaxation techniques, with an initial guess for the

solution. The error components present after relaxation are
diminished by successive relaxations on coarser grids until an exact
solution is sought on the coarsest grid. The process is then
continued by the injection of correction terms on to successively
finer grids and ends with relaxation at the finest level. (This is
actually a description of the 'V' multigrid cycle.) The whole
process may be repeated until satisfactory convergence of the
solution is attained. Details of this method are outlined in Chapter
4. The multigrid method has proved very efficient for such problems
as the Poisson equation in various domains [8]. In order to
guarantee convergence of the iteration scheme, it is required for the
matrix of the linear algebraic system (which results from the finite
difference discretisation) to be positive definite. The roots of
this matrix must be positive which is not necessarily the case for
the operator (H - E). The solution of the Schrödinger equation can
support both positive and negative eigenvalues. The consequences of
this are that standard multigrid techniques are not directly
applicable. Chapter 4 does make use of the standard multigrid
methods in conjunction with the Brillouin-Wigner perturbation scheme
in a new approach to solving the coupled oscillator problem. The
system of equations in this case is no longer in the form of an
eigenvalue problem and can be tackled with a degree of success by the
multigrid scheme. The solution of this problem incorporates the two
dimensional Numerov correction in a manner analogous to the one-
dimensional problems described in Chapter 2. The same coupled-
oscillator problem is also examined using multigrid techniques in
conjunction with the method of inverse iteration. The direct
application of the multigrid method to the same system is attempted
using the scheme described by Hackbusch [8]. This method involves
projecting out correction terms orthogonal to the approximate
solution at a given level and solving exactly on the chosen coarsest
grid using guassian elimination. The effectiveness and limitations
of these methods are all discussed in this section.

The final chapter in this report is devoted to the study of the
planar three body problem using the system of hyperspherical
coordinates. The hyperspherical system has been used extensively in

the full spatial case to describe systems that exhibit large amplitude anharmonic motion [9]. Such motions occur in systems containing light atoms (for example, H_3^+) and/or weakly bound atoms or molecules (for example, noble gas trimers). Van der Waals molecules are typical of such systems and are characterised by low dissociation energies (~1-10 kJ mol^{-1}) and large bond lengths (~4Å) corresponding to weak chemical bonds. The symmetry aspects and flexibility of the hyperspherical coordinate system are ideal in the study of such floppy molecules.

Owing to the complexity of the hyperspherical harmonic functions, previous calculations with this system [10] have been mainly confined to cases with zero total angular momentum. The planar case allows the simple inclusion of angular momentum into the problem of interest. Thus it becomes possible to study the influence of rotation on the structure of the molecular or atomic system in question. In particular, the behaviour of the model X_3 system near dissociation was examined using the system of planar hyperspherical harmonics. The potential term in this case consisted of three coupled Morse oscillators, as defined by Child [11]. The helium atom confined to a plane which was also studied in this work has a potential given by the coulomb interactions between the positively charged nucleus (taken to have infinite mass) and the two electrons. The symmetry aspects of the planar coordinate system were of particular interest and were crucial to the assignment of the calculated energy levels. The approximate energy levels were obtained by a Born-Oppenheimer-type separation of the radial coordinate (the hyperradius, ρ) from the angular coordinates. The adiabatic and non-adiabatic corrections were not included in the calculations; the Born-Oppenheimer approximation proved good enough to describe the qualitative behaviour of the two systems under consideration.

It should be noted that all results tables referred to in the text are to be found at the end of each chapter, before any appendices and references. Other descriptive tables accompany the appropriate section of text.

1.2 References

1. A. Carrington, I. R. McNab and C. A. Montgomerie, J. Phys. B. (At. Mol. and Opt. Phys.), 22, 3551, (1989), and references contained therein.

2. J. K. Cashion, J. Chem. Phys. 39, 1872, (1963).

3. B. Numerov, Publ. Observatoire Central Astroph. Russ., 2, 188, (1933).

4. G. S. Ezra, Chem. Phys. Lett., 101, 259, (1983).

5. L. Pauling and E. B. Wilson, "Introduction to Quantum Mechanics", International Student Edition, McGraw-Hill, (1935).

6. M. Born and J. R. Oppenheimer, Ann. d. Phys., 84, 457, (1927).

7. W. L. Briggs, "A Multigrid Tutorial", Society for Industrial and Applied Mathematics (SIAM), (1987).

8. W. Hackbusch, "Multi-Grid Methods and Applications", Springer-Verlag, (1985).

9. J. L. Ballot and M. Fabre de la Ripelle, Ann. Phys. (NY), 127, 62, (1980) and references contained therein;
H. Klar and M. Klar, J. Phys. B, 13, 1057, (1980);
J. A. Kaye and A. Kupperman, Chem. Phys. Lett., 78, 546, (1981).

10. V. Aquilanti, S. Cavalli And G. Grossi, J. Chem. Phys., 85, 1362, (1986).

11. A. V. Chambers, M. S. Child and R. Pfeiffer, J. Chem. Soc. Faraday Trans. 2, 84, (198

2. Numerical Tools

2.1 Introduction

This chapter is devoted to the presentation of some of the numerical tools which have been used throughout this work. The solution of the one-dimensional Schrödinger equation, essential in much of the work that follows, was achieved using the Numerov-Cooley method as described by Cashion [1]. This algorithm uses a finite-difference approximation for the second order derivative with respect to the radial coordinate. The finite-difference approach immediately introduces an error factor into any attempt to solve differential equations. The simplest approximation gives an accuracy of $O(h^2)$ for the derivatives. The introduction of higher order approximations will improve this (by powers of h^2 for successively higher orders) at the expense of complicating the calculation and increasing computational time. The Numerov integration method has the effect of a higher order approximation without any of these side-effects.

Matrix algebra and matrix manipulation techniques are frequently used to set up and solve quantum mechanical problems, and examples of this nature are presented in this chapter. The matrix method of inverse iteration is outlined as an alternative method of solving one-dimensional problems. The results of this indirect approach to finding eigenvalues and eigenvectors are compared to the direct and more efficient Numerov-Cooley method. Inverse iteration is not restricted to single-dimensional problems but is limited by the computational size of multi-dimensional problems.

The secular equation approach to incorporating perturbations from a fully soluble unperturbed basis is also investigated for a pair of coupled harmonic oscillators. The solution of this problem simply involves the diagonalisation of the full hamiltonian in the harmonic basis. Finally, the Brillouin-Wigner perturbation scheme is introduced as another useful numerical technique.

2.2 Numerov Integration

A. The Radial Schrödinger Equation

The method of Numerov integration [2] has been employed by Cooley [3] to solve the radial Schrödinger equation for the vibrational motion of diatomic molecules. The equation has the form

$$2.2.1 \qquad \frac{d^2\Psi}{dr^2} + V(r)\Psi(r) = 0$$

$$\text{with,} \quad V(r) = 2[E - U(r)]$$

where $\Psi(r)$ is the radial wavefunction, E is the energy and $U(r)$ is the potential energy. The energy, E and the potential, $U(r)$ have been pre-multiplied by the scaling factor $\mu/\hbar^2$, where μ represents the mass of the oscillator. The reduced energy units employed throughout this work are denoted by the symbol u. Numerical treatment of the one-dimensional Schrödinger equation is best achieved when the potential term, $U(r)$ is specified on an equally spaced grid of r values, such that

$$2.2.2 \qquad r_1 \ldots r_i \ldots r_N$$

$$r_{i+1} = r_i + h$$

$$V_1 \ldots V_i \ldots V_N$$

The second order differential term is then expressed as a finite-difference approximation. Equation (2.2.1) may now be written

$$2.2.3 \qquad \Psi_{i-1} - 2\Psi_i + \Psi_{i+1} + h^2 V_i \Psi_i = 0$$

The error in the solution of this finite difference equation for a converged eigenfunction is expected to be of the order of h^2. Numerov integration gives an accuracy of $O(h^4)$ by means of a simple modification to equation (2.2.3). The equation to be solved is now

of the form

2.2.4 $\quad Y_{i-1} - 2Y_i + Y_{i+1} + h^2 V_i \Psi_i = 0$

where

2.2.5 $\quad Y_i = [1 - (h^2/12)V_i]\Psi_i$

A correction term of this form is also valid for the two-dimensional Schrödinger equation and is used later in the text. The derivation of this Numerov correction, which is given in the appendix to this chapter, may be written

2.2.6 $\quad Y_{ij} = [1 - (h^2/12)V_{ij}]\Psi_{ij}$

A two-dimensional example problem is outlined later on in this chapter; the system of a pair of coupled harmonic oscillators is studied using Brillouin-Wigner perturbation theory.

The one-dimensional Numerov-Cooley algorithm consists of an iterative process. The integration of equation (2.2.4) is carried out both inwardly from $i = N$ and outwardly from $i = 0$, with the boundary conditions $\Psi_0 = \Psi_{N+1} = 0$. Where the two integration processes meet, at r_m the two curves are joined and normalised to the condition $\Psi_m = 1$. The correction to the initial energy guess, E is then calculated from the slopes of the two curves at the crossing point r_m. This process is continued until the value of E has converged to a predefined tolerance. The final eigenfunction, Ψ_i is then normalised to the condition

2.2.7 $\quad \int \Psi^2 \, dr = 1$

In order to test this predicted accuracy, calculations were performed on the vibrational energies of $H^{35}Cl$ with zero total angular momentum. The potential was approximated by a Morse potential

2.2.8 $V(r) = D_e[1 - \exp(a(r_e-r))]^2$

where the values for the depth of the potential energy minimum, D_e the equilibrium bond distance, r_e and the constant a were obtained from the values of the equilibrium vibrational frequency ω_e, the reduced mass μ and the anharmonicity constant x_e given by Huber and Herzberg [4];

2.2.9 ω_e =   2990.946 cm^{-1}

             μ =   0.97959272 a.m.u.

             x_e =   0.0174

and D_e and a are given by

2.2.10 $D_e = \dfrac{\omega_e}{4x_e}$ and $a = \left\{\dfrac{\mu}{2D_e}\right\}^{\frac{1}{2}}.\omega_e$

     For the units defined in equation (2.2.9), the multiplying factor for the scaled potential and energy is given by

2.2.11 $2\mu/\hbar^2 = \mu/16.85763042$

     $H^{35}Cl$ has 28 vibrational energy levels below dissociation. In order to observe all of these levels in the calculation, appropriate bounds need to be applied to the radial potential. In all numerical eigenvalue calculations, the problem of finding suitable coordinate ranges is recurrent. By keeping the step-size, h constant, it was found that a radial range of 0.6 to 6.0 Å was enough to converge the $v = 27$ level. Calculations were performed over this range with the total number of points on the radial grid ranging from 200 to 1500. A total of 1500 points proved enough to converge all vibrational levels to at least 7 significant figures.

     Figures I and II show plots of the convergence of chosen eigenvalues against h^4. It can be seen from these plots that the rate of convergence for the lower levels is indeed of the order of h^4, and is still the case even for eigenvalues with many nodes. The convergence rate slows down as dissociation is approached, but even for the highest energy level, the rate is approximately proportional

to h^4.

Figure I

Convergence plots of vibrational energy versus computational step-size, h^4 for levels v = 3 (upper) and v = 11 for $H^{35}Cl$.
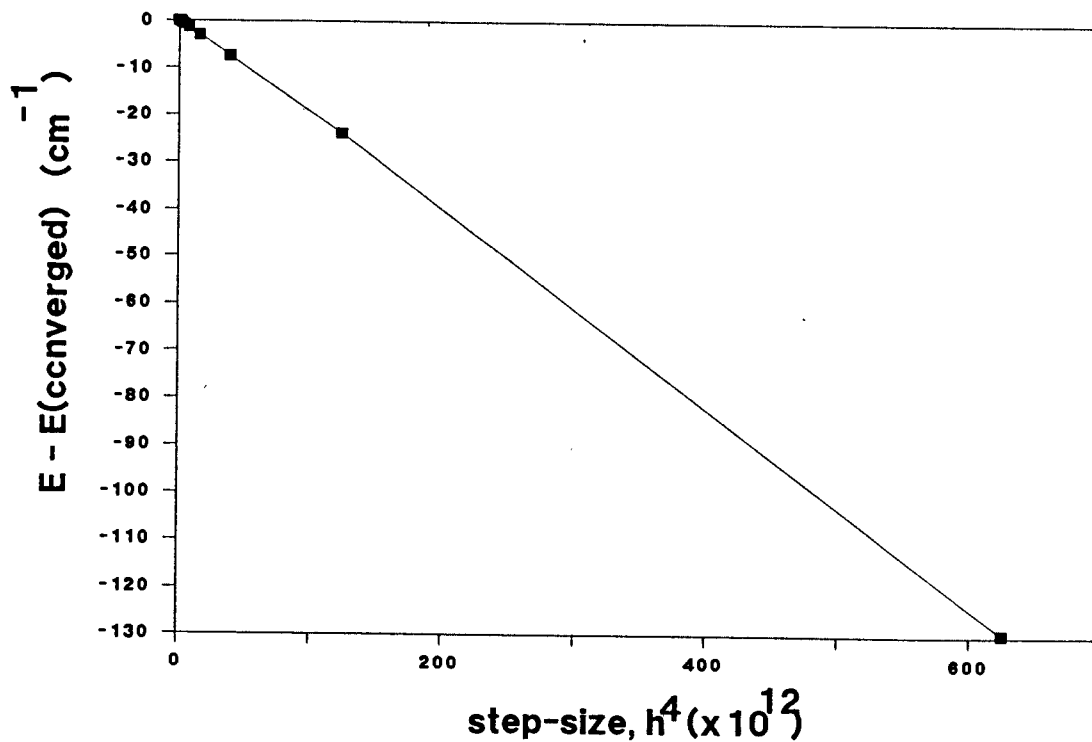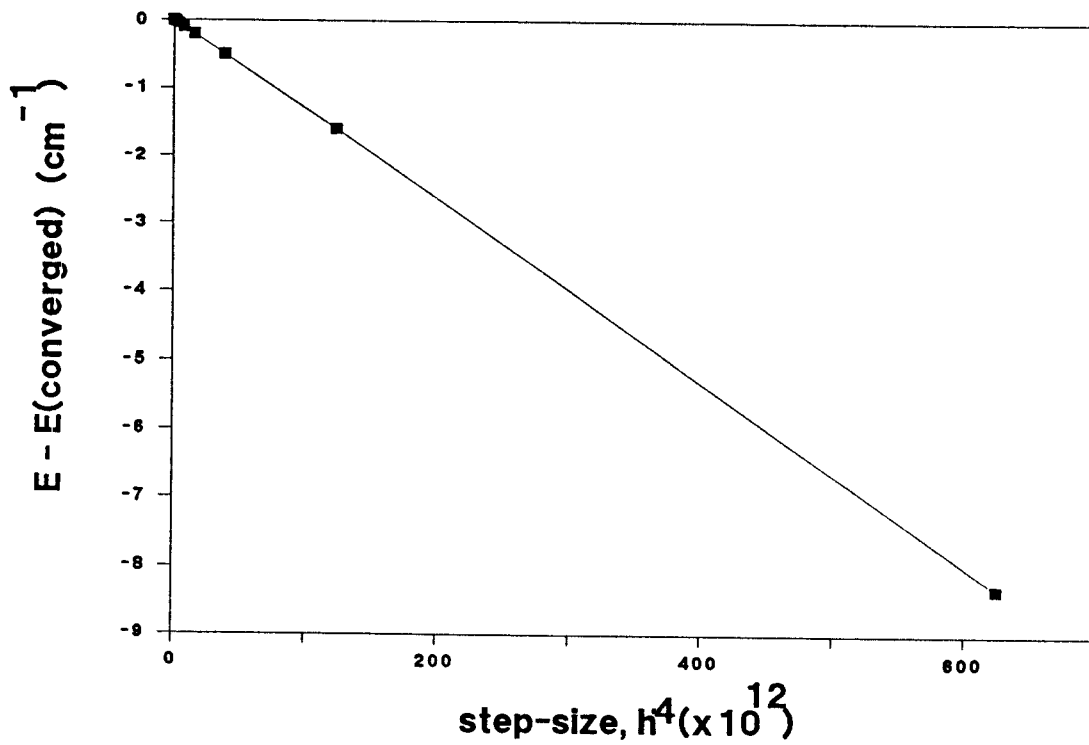
Figure II

As for Figure I for levels v = 19 (upper) and v = 27.

19
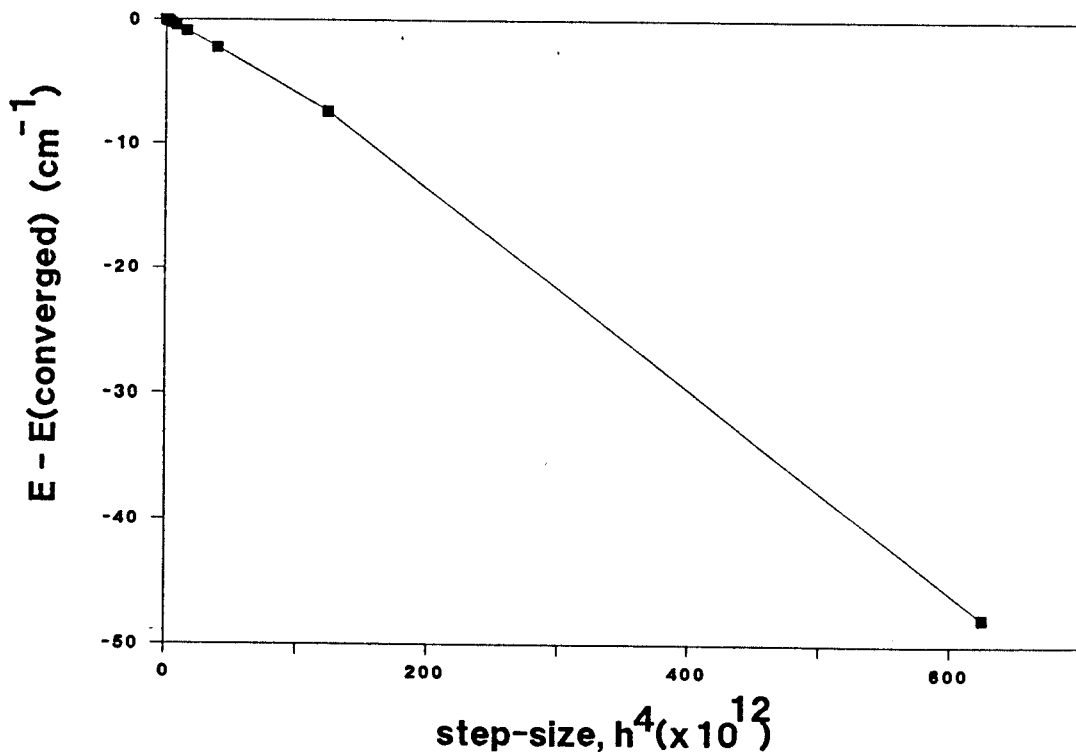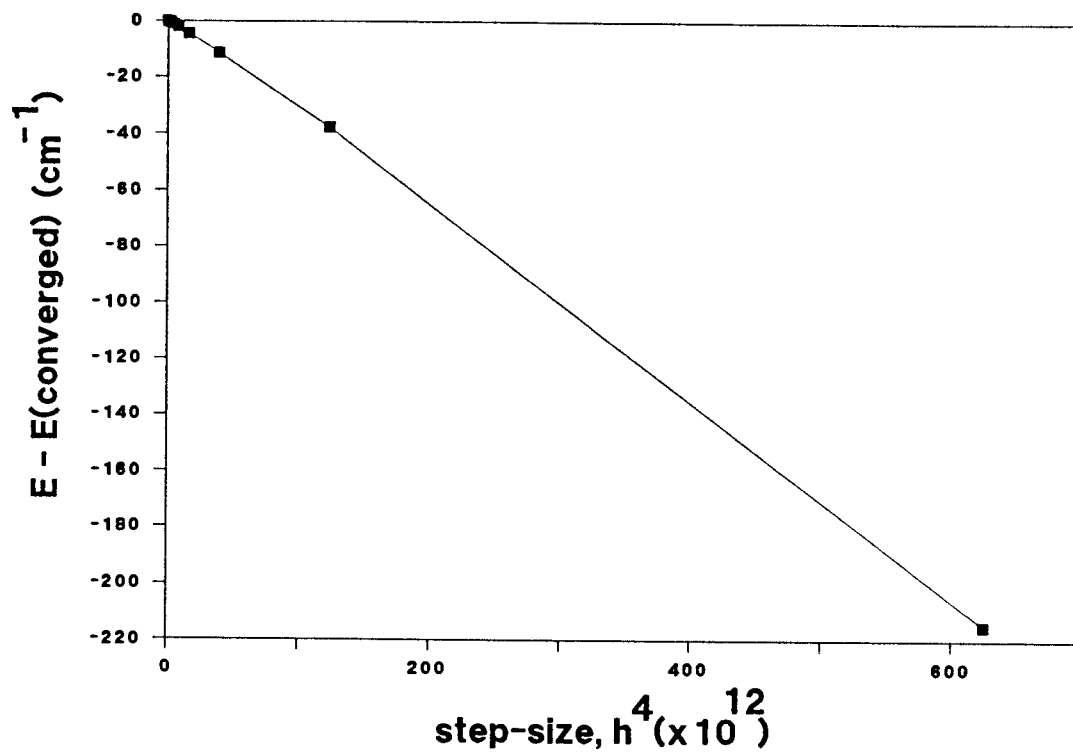
B. A Linear Inhomogeneous Differential Equation

In their work on the use of perturbation theory to correct for the breakdown of the Born-Oppenheimer approximation, Hutson and Howard [5] use an approach analogous to Numerov integration to solve equations of the form

$$2.2.12 \qquad \frac{d^2\Psi}{dr^2} = V(r)\Psi(r) + g(r)$$

The functions $V(r)$ and $g(r)$ have been pre-multiplied by the scaling factor $(2\mu/\hbar^2)$. The problem of solving this linear inhomogeneous differential equation is now a boundary value problem and not an eigenvalue problem. As before, $V(r)$ and $g(r)$ are defined on a radial grid and the finite-difference approximation produces

$$2.2.13 \qquad \Psi_{i+1} - 2\Psi_i + \Psi_{i-1} = V(r)\Psi(r) + g(r)$$

In this case, the values Y_i take the form

$$2.2.14 \qquad Y_i = [1 - (h^2/12)V_i]\Psi_i - (h^2/12)g_i$$

The final equation is

$$2.2.15 \qquad Y_{i-1} - 2Y_i + Y_{i+1} = h^2\frac{V_iY_i}{F_i} + h^2\frac{g_i}{F_i}$$

$$F_i = 1 - (h^2/12)V_i$$

Equation (2.2.14) is a set of N simultaneous equations and can be readily solved by guassian elimination. Equation (2.2.14) may be conveniently written in matrix form

$$2.2.16 \qquad AY = G$$

where A is an N by N tridiagonal matrix with non-zero elements given by

2.2.17 $\qquad A_{ii} = -2 - h^2\dfrac{V_i}{F_i}$

$$A_{i,i-1} = A_{i,i+1} = 1.0$$

and the elements of G are

2.2.18 $\qquad G_i = h^2\dfrac{g_i}{F_i}$

A FORTRAN subroutine (LIDE) has been made available by Hutson and Howard [5] that solves such a system of one-dimensional equations. An example of the use of this type of differential equation is given in the next section on the method of inverse iteration.

2.3 Inverse Iteration

The technique of inverse iteration [6] is used primarily to improve approximations to eigenvector/eigenvalue pairs from initial guesses. The linear equation at the root of the inverse iteration scheme has the form

2.3.1 $\qquad (A - \tau I).y = b$

where A is the hamiltonian for the system in matrix form, τ is the initial eigenvalue guess (close to the eigenvalue λ of A), I is the identity matrix and b is the initial guess for the eigenvector. The solution to equation (2.3.1), y will be close to the eigenvector corresponding to λ. The procedure is then iterated, replacing b by y and solving for a new y. Successive solutions y will be even closer to the true eigenvector. The vectors y and b may be expanded as linear combinations of the eigenvectors x_j of A

2.3.2 $\qquad y = \sum_j \alpha_j x_j \qquad b = \sum_j \beta_j x_j$

Substituting for y and b from equation (2.3.2) into equation (2.3.1) gives

21

2.3.3 $\sum_j \alpha_j (\lambda_j - \tau) x_j = \sum_j \beta_j x_j$

such that

2.3.4 $\alpha_j = \dfrac{\beta_j}{\lambda_j - \tau}$ $y = \sum_j \dfrac{\beta_j x_j}{\lambda_j - \tau}$

Thus, if τ is close to an eigenvalue, λ_n, y will be approximately equal to x_n. Each iteration step introduces another power of $\lambda_j - \tau$ in the denominator of (2.3.4). This results in rapid convergence for well-behaved systems. The corrected eigenvalue after each iteration is given by

2.3.5 $\lambda_{corr} = \lambda_i + \dfrac{\langle y_{i+1} | y_i \rangle}{\langle y_{i+1} | y_{i+1} \rangle}$

where y_i and λ_i are the former eigenvector and eigenvalue combination and y_{i+1} is the new eigenvector. Having obtained the first eigenvalue correction, there are two possible courses of action. One possibility is to add λ_{corr} to λ_i to form a new eigenvalue guess, λ_{i+1} which along with y_{i+1} will form the next λ_i/y_i pairing. Alternatively, it is not strictly necessary to update the input value of λ after each iteration. In this case, the iterative process is continued until the value for λ_{corr} has achieved a suitable convergence. In both cases, the stopping criterion for the procedure is determined by a user-supplied tolerance for the convergence of the eigenvalue. The use of these two slightly different approaches will be investigated further in the following one dimensional example.

The One Dimensional Harmonic Oscillator Problem
Using Inverse Iteration

The hamiltonian for the one dimensional harmonic oscillator has the form,

2.3.6 $H = -(1/2)\dfrac{d^2}{dx^2} + (1/2)x^2$

where the units are the reduced energy units denoted by u. For simplicity, the vibrational frequency is assigned a value of 1u. Following the method of inverse iteration, the equation to be solved is

$$2.3.7 \qquad (H - E)\Psi_{new} = \Psi_{old}$$

where Ψ_{old} is the initial guess or previously calculated function and E is the original eigenvalue guess or possibly the value updated from the calculation of Ψ_{old}. Equation (2.3.7) can be directly incorporated into LIDE and the energy correction is given by

$$2.3.8 \qquad E_{corr} = \frac{\langle\Psi_{new}|\Psi_{old}\rangle}{\langle\Psi_{new}|\Psi_{new}\rangle}$$

The initial wavefunction guesses were either symmetric or antisymmetric functions and a range of input eigenvalues was used. A maximum number of iterations was also specified since there is no guarantee that certain combinations of eigenvalues and eigenvectors will converge. For a fixed radial range, the number of intervals was varied and comparisons were made at each level with results obtained from the Numerov-Cooley method. The exact values for the harmonic oscillator energy levels are

$$2.3.9 \qquad E_n = n + 0.5u,$$

$$n = 0,1,2....$$

Table I lists some of the results of the inverse iteration calculations together with the corresponding Numerov-Cooley energies. The radial grid range employed was from 0.0 to 16.0 u and the precision required for the convergence of both iteration schemes was $\pm 1.0 \times 10^{-06}u$. A comparison of energy values calculated from the two methods indicates that the level of accuracy obtained from the Numerov-Cooley process is consistently achieved by the method of inverse iteration. As expected, the overall precision of the eigenvalues increases as a function of decreasing step-size, h. The

inverse iteration scheme is seen to converge quickly in all cases
(that is within 10 iteration cycles). The maximum allowed number of
iterations, set at 20 for both methods, was not exceeded in the test
case presented here. The results indicated that an update of the
energy after each iteration of the inverse iteration process lead to
a faster convergence of the scheme. In more general applications of
this method, updating the eigenvalue in this manner may lead to
instabilities in the inverse iteration scheme. This will become
apparent in later work involving multigrid methods.

2.4   The Method of Secular Equations

In many of the calculations to follow in this work, the test of
the accuracy of the calculation method was made by comparison with
results obtained by the matrix secular equation scheme. The setting
up of the secular equations and the solution of the resulting secular
determinant is a much tried and tested means of solving systems to
which a perturbation has been applied. The method in general is
outlined by many quantum mechanical texts, see for example Atkins
[7]. In the recurring problem of a pair of coupled oscillators, the
wavefunction for the new, perturbed system is expanded as a linear
combination of the known, uncoupled two-dimensional functions.

The method as applied to this problem is outlined below. The
hamiltonian for the system has the form

$$2.4.1 \qquad H = h_x + h_y + \alpha x^2 y^2$$

where h_x and h_y are the unperturbed harmonic oscillator hamiltonians

$$h_x = -(1/2)\frac{\partial^2}{\partial x^2} + (1/2)\omega_x^2 x^2$$

$$h_y = -(1/2)\frac{\partial^2}{\partial y^2} + (1/2)\omega_y^2 y^2$$

and α determines the magnitude of the coupling (the magnitude of the

perturbation). The two oscillators x and y have harmonic frequencies ω_x and ω_y chosen to satisfy the condition

2.4.2 $\omega_x + \omega_y = 2.0u$

The units are chosen such that $\mu = \hbar = 1u$. The orthonormal basis is given by

2.4.3 $|nm\rangle = \Psi_n(x)\Psi_m(y)$

where $\Psi_n(x)$ and $\Psi_m(y)$ are the solutions of h_x and h_y respectively and have the general form

2.4.4 $\Psi_v = N_v H_v(z)\exp(-\tfrac{1}{2}z^2)$

where N_v is the normalisation and H_v are the hermite polynomials. In accordance with the matrix secular equation method, the hamiltonian (2.4.1) is diagonalised in the basis formed by the functions given in expression (2.4.3)

2.4.5 $\langle n_1 m_1 | H | nm \rangle$

The solutions of the unperturbed system factorise out to leave equation (2.4.5) in the form

2.4.6 $\{(n+\tfrac{1}{2})\omega_x + (m+\tfrac{1}{2})\omega_y\}\delta_{n_1 n}\delta_{m_1 m} + \alpha\langle n_1 m_1 | x^2 y^2 | nm \rangle$

Thus, in order to set up the secular matrix, it is necessary to calculate the elements of $\langle n_1 | x^2 | n \rangle$ and $\langle m_1 | y^2 | m \rangle$. Fortunately, because of the simple known form of the harmonic functions, this calculation is analytically possible and the non-zero elements are,

2.4.7 $n = n_1 - 2$; $\tfrac{1}{2}\{n(n-1)\}^{\frac{1}{2}}\omega$

          $n = n_1$; $(n+\tfrac{1}{2})\omega$

          $n = n_1 + 2$; $\tfrac{1}{2}\{(n+1)(n+2)\}^{\frac{1}{2}}\omega$

Sufficient functions were included in the basis set to converge the levels of interest in each calculation to an accuracy of $\pm 1.0 \times 10^{-06}$u. Some results for the three systems used in this study with varying degrees of perturbation are given in Table II. The range of α was taken as 0.1 to 1.0 for each of the three studied cases, which were

2.4.8   Case A; $\omega_x^2 = 1.69$u, $\omega_y^2 = 0.49$u

            Case B; $\omega_x^2 = 1.21$u, $\omega_y^2 = 0.81$u

            Case C; $\omega_x^2 = \omega_y^2 = 1.0$u

The number of basis functions used in a typical calculation to diagonalise the hamiltonian (2.4.5) was 34×34. The diagonalisation was carried out using the Fortran NAG (version 11) routine F01AGF. The eigenvector calculation which was used to assign quantum numbers to the obtained eigenvalues used NAG routines F02BEF and F01AHF.

The method itself is very efficient for systems where a relatively small perturbation has been applied. It is also much more reliable for the eigenvalues near the ground state energy - it becomes increasingly more difficult to converge and assign eigenvalues for the higher energy levels. This will be discussed further in the following chapter.

2.5   Brillouin-Wigner Perturbation Theory

<u>Theory</u>

As with the standard Rayleigh-Schrödinger perturbation theory, the effect of a small extra potential, H_1 acting on a system governed by a dominant hamiltonian, H_0 is to be considered. The zeroth order solution of the unperturbed hamiltonian H_0 is given by

2.5.1 $H_0 |\psi_0\rangle = E_0 |\psi_0\rangle$

where the functions $|\psi_0\rangle$ are normalised to unity. On introduction of

the perturbation H_1, the exact solution of the problem may be written in the form

2.5.2 $H|\psi> = E|\psi>$

where $H = H_0 + H_1$

The substitution of the total hamiltonian H into equation (2.5.2) and appropriate rearrangement produces the perturbation equation

2.5.3 $(E - H_0)|\psi> = H_1|\psi>$

If no condition is made on the normalisation of the eigenfunction $|\psi>$, it may be split into two terms

2.5.4 $|\psi> = |\psi_0> + |\phi>$

where the correction term due to the perturbation, $|\phi>$ is to be orthogonal to the unperturbed solution, i.e.

2.5.5 $<\psi_0|\phi> = 0$

This orthogonality condition may be conveniently defined in terms of a projection operator, P which has the form

2.5.6 $P = 1 - M$

where $M = |\psi_0><\psi_0|$

Further details on projection operators are given in the book by Ziman [8]. The action of the operator M on a function, $|\psi>$ serves to project out the component of that function along the direction of $|\psi_0>$. Thus, the projection operator that is complementary to M, P leaves the component of $|\psi>$ that is orthogonal to $|\psi_0>$. The action of P on $|\psi>$ may be written explicitly as follows

2.5.7 $\quad P|\psi> = (1 - |\psi_0><\psi_0|)|\psi>$

$\quad = |\psi> - |\psi_0><\psi_0|\psi>$

$\quad = |\psi> - M|\psi>$

But, from the definition of the operator M and the definition of $|\psi>$ given in equation (2.5.4), the action of M will project out $|\psi_0>$. Therefore, the application of P on $|\psi>$ simply produces the orthogonal term, $|\phi>$

2.5.8 $\quad P|\psi> = |\psi> - |\psi_0>$

$\quad = |\phi>$

On application of the hamiltonian H_0 to equation (2.5.8), it can be shown that P commutes with H_0

2.5.9 $\quad P.H_0|\phi> = H_0|\phi> - |\psi_0><\psi_0|H_0\phi>$

$\quad = H_0|\phi> - |\psi_0>E_0<\psi_0|\phi>$

$\quad = H_0|\phi>, \quad \text{since } <\psi_0|\phi> = 0$

This scheme is equivalent to projecting on $|\phi>$ with P and then operating on the solution with H_0. The Brillouin-Wigner perturbation scheme may now be completed with the aid of the projection operator P. Firstly, the left hand side of equation (2.5.3) is expanded by the substitution of $|\psi>$ from (2.5.4), which gives

2.5.10 $\quad (E - H_0)|\psi_0> + (E - H_0)|\phi> = H_1|\psi>$

or on rearrangement,

$\quad (E - H_0)|\phi> = H_1|\psi> - (E - E_0)|\psi_0>$

The projection of both sides of equation (2.5.10) by P eliminates the

term involving $|\psi_0\rangle$ whilst having no effect on the $|\phi\rangle$ term (this was seen in the above description) and produces

2.5.11 $(E - H_0)|\phi\rangle = P.H_1|\psi\rangle$

For the energy correction, equation(2.5.3) is operated on by **M** to give

2.5.12 $|\psi_0\rangle\langle\psi_0|(E - H_0)|\psi\rangle = |\psi_0\rangle\langle\psi_0|H_1|\psi\rangle$

From the commutation property of **M** with H_0, equation (2.5.12) may be written

2.5.13 $(E - H_0)|\psi_0\rangle = |\psi_0\rangle\langle\psi_0|H_1|\psi\rangle$

or

$(E - E_0)|\psi_0\rangle = |\psi_0\rangle\langle\psi_0|H_1|\psi\rangle$

Finally, premultiplying by $|\psi_0\rangle$ and integrating produces the required energy correction,

2.5.14 $E = E_0 + \langle\psi_0|H_1|\psi\rangle$

Equations (2.5.11) and (2.5.14) are exact but must be solved approximately; their solutions are affected by means of an iterative process. Equation (2.5.11) is another example of a linear inhomogeneous differential equation and may be solved by means discussed earlier. In order to solve for the orthogonal correction $|\phi\rangle$, an initial guess must be provided for the energy E and wavefunction $|\psi\rangle$. The energy guess E must not be equal to the known solution to the unperturbed problem, E_0 but the function $|\psi\rangle$ may be set equal to $|\psi_0\rangle$. The equation may now be solved by a guassian elimination technique (if numerically feasible) or, as is the case in Chapter 4, by multigrid means. Gaussian elimination techniques were adequate in the one-dimensional calculations but are limited by computational size in higher dimensional problems. In all of the

calculations, the action of the perturbation hamiltonian on the function $|\psi\rangle$ is evaluated and stored in the form of an equally-spaced grid. The resulting vector is then operated on by P to ensure its orthogonality to the solution of the unperturbed problem. Once the function $|\phi\rangle$ has been obtained, its orthogonality with $|\psi_0\rangle$ is also ensured. The 'new' wavefunction, $|\psi\rangle$ is now formed from equation (2.5.4) and the energy E is calculated from equation (2.5.14). The process is then repeated with the new updated values for E and $|\psi\rangle$. The iteration scheme is continued until a preset convergence tolerance for E is attained.

Example Problem

The test system to be considered is that of a pair of oscillators, h_x and h_y, coupled by a term involving x^2y^2, as described above in equation (2.4.1). The perturbation equation to be solved by means of gaussian elimination has the form

2.5.15 $\qquad (E - H_0)|\phi\rangle = P.H_1|\psi\rangle$

where $\qquad H_0 = h_x + h_y$

and $\qquad H_1 = \alpha x^2 y^2$

In order to solve this equation accurately, a very large amount of computer storage is required. The one-dimensional linear inhomogeneous differential equation solved by LIDE [5] required the set up and storage of an (N by N) tridiagonal matrix. In two dimensions, the corresponding band matrix has dimension (N^2 by N^2). The value of N can often exceeded one thousand without creating major difficulties in one-dimensional problems. For the current problem however, even the use of Supercomputers could not cope for the demand of accurate, converged solutions. The calculations performed here were limited to the allowed storage on the University of London Computing Centre Cray XMP-48.

Unfortunately, the extent of the problem is such that there is

30

not enough available memory on the Cray to produce any meaningful results. Results could only be obtained for a maximum grid of approximately (50 by 50) points. Thus, it is not possible to use brute-force finite difference grid techniques to solve even the most simple of two-dimensional problems. There is therefore a need for more subtle direct approaches to calculations of multi-dimensional problems. Attempts were made to achieve this by using multigrid techniques and these are outlined in Chapter 4.

Table I

Comparison between results obtained from the methods of inverse
iteration and Numerov-Cooley as applied to a one-dimensional harmonic
oscillator. The radial grid range is from 0.0 to 16.0 u and the
required precision for convergence is $1.0 \times 10^{-06} u$.

<u>Calculations for a grid of 64 points</u>

ENERGY LEVELS FROM THE NUMEROV COOLEY METHOD

ENERGY	EXACT	ERROR		ENERGY	EXACT	ERROR
0.499985	0.50000	0.000015		3.499021	3.50000	0.000979
1.499892	1.50000	0.000108		4.497987	4.50000	0.002013
2.499613	2.50000	0.000387		5.496379	5.50000	0.003621

ENERGY LEVELS FROM INVERSE ITERATION

No E_{shift}, Ψ_{old} symmetric

N_{it}	E_{guess}	E_{iter}	ERROR
5	0.000	0.499985	0.000015
2	1.000	0.499985	0.000015
7	2.000	0.499985	0.000015
6	3.000	1.499892	0.000108
8	4.000	2.499613	0.000387
2	5.000	2.499613	0.000387

No E_{shift}, Ψ_{old} antisymmetric

N_{it}	E_{guess}	E_{iter}	ERROR
9	0.000	1.499893	0.000107
5	1.000	0.499985	0.000015
6	2.000	1.499892	0.000108
2	3.000	1.499892	0.000108
8	4.000	1.499892	0.000108
6	5.000	2.499613	0.000387

E_{shift} on, Ψ_{old} symmetric

4	0.000	0.499985	0.000015
2	1.000	0.499985	0.000015
4	2.000	0.499985	0.000015
6	3.000	0.499985	0.000015
4	4.000	2.499613	0.000387
2	5.000	2.499613	0.000387

E_{shift} on, Ψ_{old} antisymmetric

7	0.000	5.496379	0.003621
4	1.000	3.499021	0.000979
5	2.000	1.499892	0.000108
2	3.000	1.499892	0.000108
5	4.000	1.499892	0.000108
4	5.000	3.499021	0.000979

32

Table I continued

Calculations for a grid of 128 points

ENERGY LEVELS FROM NUMEROV COOLEY METHOD

ENERGY	EXACT	ERROR
0.499999	0.500000	0.000001
1.499993	1.500000	0.000007
2.499976	2.500000	0.000024
3.499940	3.500000	0.000060
4.499876	4.500000	0.000124
5.499778	5.500000	0.000222

ENERGY LEVELS FROM INVERSE ITERATION

No E_{shift}, Ψ_{old} symmetric

N_{it}	E_{guess}	E_{iter}	ERROR
5	0.000	0.499999	0.000001
1	1.000	0.499999	0.000001
7	2.000	1.499999	0.000001
5	3.000	1.499993	0.000007
8	4.000	2.499976	0.000024
2	5.000	2.499976	0.000024

No E_{shift}, Ψ_{old} antisymmetric

N_{it}	E_{guess}	E_{iter}	ERROR
9	0.000	1.499994	0.000006
4	1.000	0.499999	0.000001
6	2.000	1.499993	0.000007
2	3.000	1.499993	0.000007
8	4.000	1.499993	0.000007
5	5.000	2.499976	0.000024

E_{shift} on, Ψ_{old} symmetric

4	0.000	0.499999	0.000001
1	1.000	0.499999	0.000001
4	2.000	0.499999	0.000001
6	3.000	0.499999	0.000001
4	4.000	2.499976	0.000024
2	5.000	2.499976	0.000024

E_{shift} on, Ψ_{old} antisymmetric

7	0.000	5.499778	0.000222
4	1.000	3.499940	0.000060
5	2.000	1.499993	0.000007
2	3.000	1.499993	0.000007
5	4.000	1.499993	0.000007
4	5.000	3.499940	0.000060

Table I continued

<u>Calculations for a grid of 256 points</u>

ENERGY LEVELS FROM NUMEROV COOLEY METHOD

ENERGY	EXACT	ERROR
0.500000	0.500000	0.000000
1.500000	1.500000	0.000000
2.499999	2.500000	0.000001
3.499996	3.500000	0.000004
4.499992	4.500000	0.000008
5.499986	5.500000	0.000014

ENERGY LEVELS FROM INVERSE ITERATION

No E_{shift}, Ψ_{old} symmetric

N_{it}	E_{guess}	E_{iter}	ERROR
5	0.000	0.500000	0.000000
1	1.000	0.500000	0.000000
7	2.000	0.500000	0.000000
4	3.000	1.500000	0.000000
8	4.000	2.499998	0.000002
1	5.000	2.499999	0.000001

No E_{shift}, Ψ_{old} antisymmetric

N_{it}	E_{guess}	E_{iter}	ERROR
9	0.000	1.500000	0.000000
4	1.000	0.500000	0.000000
6	2.000	1.500000	0.000000
1	3.000	1.500000	0.000000
8	4.000	1.500000	0.000000
4	5.000	2.499999	0.000001

E_{shift} on, Ψ_{old} symmetric

4	0.000	0.500000	0.000000
1	1.000	0.500000	0.000000
4	2.000	0.500000	0.000000
6	3.000	0.500000	0.000000
4	4.000	2.499999	0.000001
1	5.000	2.499999	0.000001

E_{shift} on, Ψ_{old} antisymmetric

8	0.000	5.499986	0.000014
4	1.000	3.499996	0.000004
5	2.000	1.500000	0.000000
1	3.000	1.500000	0.000000
5	4.000	1.500000	0.000000
4	5.000	3.499996	0.000004

Table II

Results obtained from the diagonalisation of the hamiltonian for a pair of coupled oscillators for the three cases described in Section 2.4. The magnitude of the perturbation is given by α. The x quantum number is labelled n and the y quantum number is given by m. All values presented are converged to $\pm 1.0 \times 10^{-06}$u.

$$\alpha = 0.1$$

Case A			Case B			Case C		
n	m	E_{nm}	n	m	E_{nm}	n	m	E_{nm}
0	0	1.025451	0	0	1.023610	0	0	1.023398
0	1	1.773965	0	1	1.968369	0	1	2.067541
0	2	2.517722	0	2	2.905966	0	2	3.068870
1	0	2.372089	1	0	2.167856	1	0	2.067541
1	1	3.210373	1	1	3.197190	1	1	3.195646
1	2	4.036081	1	2	4.201162	1	2	4.336284
2	0	3.715129	2	0	3.312286	2	0	3.147662
2	1	4.634669	2	1	4.423253	2	1	4.336284
2	2	5.544587	2	2	5.461104	2	2	5.547657

$$\alpha = 0.2$$

0	0	1.047888	0	0	1.044704	0	0	1.044334
0	1	1.836365	0	1	2.026464	0	1	2.124766
0	2	2.611361	0	2	2.987883	0	2	3.128909
1	0	2.430941	1	0	2.224936	1	0	2.124766
1	1	3.376439	1	1	3.356446	1	1	3.354071
1	2	4.287192	1	2	4.396501	1	2	4.591870
2	0	3.804264	2	0	3.405678	2	0	3.261985
2	1	4.861259	2	1	4.675054	2	1	4.591870
2	2	5.925207	2	2	5.979183	2	2	5.946038

Table II continued

$$\alpha = 0.4$$

Case A				Case B				Case C		
n	m	E_{nm}		n	m	E_{nm}		n	m	E_{nm}
0	0	1.086960		0	0	1.081880		0	0	1.081282
0	1	1.941156		0	1	2.124576		0	1	2.221196
0	2	2.762138		0	2	3.117594		0	2	3.232684
1	0	2.527541		1	0	2.320610		1	0	2.221196
1	1	3.642456		1	1	3.615290		1	1	3.612016
1	2	4.668886		1	2	4.964332		1	2	4.990230
2	0	3.945327		2	0	3.559923		2	0	3.441076
2	1	5.317310		2	1	5.069326		2	1	4.990230
2	2	6.434058		2	2	6.559770		2	2	6.547221

$$\alpha = 0.6$$

0	0	1.120859		0	0	1.114469		0	0	1.113710
0	1	2.029358		0	1	2.207551		0	1	2.302623
0	2	2.885143		0	2	3.222738		0	2	3.583461
1	0	2.607577		1	0	2.401082		1	0	2.302623
1	1	3.858434		1	1	3.827577		1	1	3.823828
1	2	4.957197		1	2	5.266472		1	2	5.306586
2	0	4.059327		2	0	3.687418		2	0	3.322297
2	1	5.634917		2	1	5.381773		2	1	5.306586
2	2	7.217413		2	2	6.995722		2	2	7.007004

Table II continued

$$\alpha = 0.8$$

Case A			Case B			Case C		
n	m	E_{nm}	n	m	E_{nm}	n	m	E_{nm}
0	0	1.151197	0	0	1.143833	0	0	1.142954
0	1	2.106762	0	1	2.280610	0	1	2.374266
0	2	2.991175	0	2	3.313462	0	2	3.704088
1	0	2.677265	1	0	2.471730	1	0	2.374266
1	1	4.043928	1	1	4.010897	1	1	4.006863
1	2	5.183568	1	2	5.529746	1	2	5.574384
2	0	4.157385	2	0	3.797805	2	0	3.402341
2	1	5.904609	2	1	5.645029	2	1	5.574384
2	2	7.573395	2	2	7.308784	2	2	7.378585

$$\alpha = 1.0$$

Case A			Case B			Case C		
0	0	1.178878	0	0	1.170756	0	0	1.169783
0	1	2.176393	0	1	2.346499	0	1	2.438855
0	2	3.085442	0	2	3.394393	0	2	3.475318
1	0	2.739686	1	0	2.535340	1	0	2.438855
1	1	4.208344	1	1	4.173942	1	1	4.169725
1	2	5.363632	1	2	5.763378	1	2	5.809133
2	0	4.244638	2	0	3.896107	2	0	3.810017
2	1	6.141313	2	1	5.874460	2	1	5.809133
2	2	7.891645	2	2	7.893393	2	2	7.683470

2.6 Appendix - Two-Dimensional Numerov Correction

The derivation of the Numerov correction in two dimensions begins with the Taylor series expansion of the kinetic energy operator, $(D_x^2+D_y^2)$ in terms of the finite difference grid. For simplicity, all cases studied in this work consisted of equally spaced square grids, such that $h_x = h_y = h$. The required expansions are of the form

$$2.6.1 \qquad f(x\pm h,y) = \{1 \pm hD_x + \frac{h^2}{2!}D_x^2 \pm \frac{h^3}{3!}D_x^3 + \frac{h^4}{4!}D_x^4 + \ldots\}f(x,y)$$

and similarly for $f(x,y\pm h)$, and

$$2.6.2 \qquad f(x\pm h,y\pm h) = \{1 \pm h(D_x+D_y) + \frac{h^2}{2!}(D_x+D_y)^2 \pm \frac{h^3}{3!}(D_x+D_y)^3$$

$$+ \frac{h^4}{4!}(D_x+D_y)^4 + \ldots\}f(x,y)$$

The usual five-point finite difference grid is obtained by the sum

$$2.6.3 \qquad f(x+h,y) + f(x-h,y) + f(x,y+h) + f(x,y-h)$$

$$= \{4 + h^2(D_x^2+D_y^2) + \frac{h^4(D_x^4+D_y^4)}{12} + \ldots\}f(x,y)$$

$$= A$$

If the terms after and including the term in h^4 are dropped, this expansion has an accuracy of $O(h^2)$ for $(D_x^2+D_y^2)$ on the five-point grid

$$2.6.4 \qquad (D_x^2+D_y^2) = \frac{1}{h^2}\begin{bmatrix} 0 & 1 & 0 \\ 1 & -4 & 1 \\ 0 & 1 & 0 \end{bmatrix}$$

An alternative, nine-point grid may be formed with the help of the following summation

2.6.5 $\quad$ $f(x+h,y+h) + f(x-h,y-h) + f(x+h,y-h) + f(x-h,y+h)$

$$= \{4 + 2h^2(D_x^2+D_y^2) + \frac{h^4}{6}(D_x^4+6D_x^2D_y^2+D_y^4) + \ldots\}f(x,y)$$

$$= B$$

Taking the combination $(4A + B)$, will give the required result

2.6.6 $\quad$ $4A + B =$
$$\{20 + 6h^2(D_x^2+D_y^2) + \frac{h^4}{2}(D_x^4+2D_x^2D_y^2+D_y^4) + \ldots\}f(x,y)$$

Truncating before the term in h^4 leaves the nine-point scheme, again with an accuracy of $O(h^2)$;

2.6.7 $\quad$ $(D_x^2+D_y^2) = \dfrac{1}{h^2}\begin{bmatrix} 1 & 4 & 1 \\ 4 & -20 & 4 \\ 1 & 4 & 1 \end{bmatrix}$

Equation (2.6.7) may be rewritten as follows

2.6.8 $\quad$ $(D_x^2+D_y^2) = [4\{f(1,0)+f(-1,0)+f(0,1)+f(0,-1)\}$

$$+ \ f(1,1)+f(-1,-1)+f(1,-1)+f(-1,1)-20f(0,0)]/6h^2$$

$$- \ \frac{h^2}{12}(D_x^4+2D_x^2D_y^2+D_y^4)$$

where the term in h^4 has now been included and $f(i,j)$ is given by

2.6.9 $\quad$ $f(i,j) = f(x+ih,y+jh)$

The term in h^4 is now in a form which will come directly from the two-dimensional Schrödinger equation

2.6.10 $\quad$ $(D_x^2+D_y^2)\psi = (V-E)\psi$

The approach now to be adopted is exactly analogous to the one-

dimensional development described in Section 2.2. In particular, the relevant equations are numbered (2.2.3) to (2.2.5) and give the Numerov correction for the radial Schrödinger equation. Equation (2.6.10) is operated on both sides by $(D_x^2+D_y^2)$ to give

2.6.11 $\qquad (D_x^2+D_y^2)^2\psi \quad = \quad (D_x^2+D_y^2)(V-E)\psi$

or

$$(D_x^4+2D_x^2D_y^2+D_y^4) \quad = \quad (D_x^2+D_y^2)(V-E)\psi$$

Thus, the fourth order term may be expressed as a second order expansion of the right hand side of equation (2.6.11). The inclusion of this term in the original expansion of $(D_x^2+D_y^2)$ (the nine-point scheme given by expression (2.6.7)) produces the two-dimensional Numerov correction

2.6.12 $\qquad Y_{ij} \quad = \quad \psi_{ij} \, - \, \dfrac{h^2}{12}(V_{ij}-E)\psi_{ij}$

Note, this correction term is only valid when the nine-point finite difference scheme as described above is employed.

2.7 References

1. J. K. Cashion, J. Chem. Phys. **39**, 1872, (1963).

2. B. Numerov, Publ. Observatoire Central Astroph. Russ., 2, 188, (1933).

3. J. W. Cooley, Math. Computation, **XV**, 363, (1961).

4. K. P. Huber and G. Herzberg, Constants of Diatomic Molecules, Litton Educational Publishing, (1979).

5. J. M. Hutson and B. J. Howard, Mol. Phys., 41, 1113, (1980).

6. W. H. Press, B. P. Flannery, S. A. Teukolsky, W. T. Vetterling, "Numerical Recipes - The Art of Scientific Computing", Cambridge University Press, (1988).

7. P. W. Atkins, "Molecular Quantum Mechanics", Second Edition, Oxford University Press, (1986).

8. J. M. Ziman, "Elements of Advanced Quantum Theory", Cambridge University Press, (1980).22

3. Non-Adiabatic Corrections for Coupled Oscillators Using Rayleigh-Schrödinger Perturbation Theory

3.1 Introduction

The system of a pair of coupled oscillators has been used to investigate approximate methods of solving quantum mechanical problems applicable to more than one dimension and classical chaos [1,2]. Ezra has shown for the generalised Henon-Heiles (GHH) hamiltonian that, when the harmonic frequencies are non-degenerate, a Born-Oppenheimer separation of the motion in the two coordinates (x and y in this case), analogous to the separation of electronic and nuclear motion in molecules, may be applied to calculate the quantum states of the system [3]. The approximation proved to be quite accurate for low energies. Using a hamiltonian with the coupling described by a term in x^2y^2 (as well as the GHH), it is demonstrated that by including the appropriate non-adiabatic terms (neglected in the Born-Oppenheimer separation) by perturbation theory, eigenvalues accurate to one part in 10^6 can be obtained.

In this work, the x-coordinate is taken to have the highest harmonic frequency. After making the Born-Oppenheimer separation, an effective, y dependent, harmonic frequency results for motion along the x coordinate. The wavefunction describing this motion will be written as $X(x;y)$, where the parametric dependence on y is shown explicitly. The energy levels are obtained by solving a one-dimensional Schrödinger equation for motion along the y coordinate in an effective potential well defined by the eigenvalues $U(y)$ corresponding to $X(x;y)$. These eigenvalues are solutions of the fixed y hamiltonian, obtained by neglecting all derivatives with respect to y. This approach has been used a number of times in previous works [5].

The Born-Oppenheimer method ignores the non-diagonal terms arising from the kinetic energy operator ($\partial^2/\partial y^2$) acting on $X(x;y)$. The adiabatic approximation derives from the inclusion of these diagonal terms. In this work, the Rayleigh-Schrödinger perturbation theory approach of Hutson and Howard [4] was used to include the effect of the off-diagonal, non-adiabatic corrections starting from the adiabatic approximation. The convergence properties of the

perturbation series were examined for different harmonic frequencies and magnitude of perturbation. The order in which the adiabatic separation is made is shown to have little effect on the accuracy of the energy levels. The convergence of the perturbation series was explored for the degenerate as well as the non-degenerate case.

The two hamiltonians used in this work were

3.1.1 $\qquad H_a = hx + hy + \alpha x^2 y^2$

and

3.1.2 $\qquad H_b = hx + hy + \alpha(yx^2 + \beta y^3);$ $\qquad$ the GHH

where hx and hy represent unperturbed harmonic oscillators in the x and y coordinates respectively, and α and β are the anharmonic coupling constants. The term "Born-Oppenheimer approximation" used throughout this work is referred to as the "adiabatic approximation (AA)" by Ezra and the "adiabatic approximation" is referred to as the "diagonally corrected adiabatic approximation (CA)".

3.2 Theory

The adiabatic approximation has been described in detail in past works, therefore only a brief outline of its use in the present problem is given here. Including only the diagonal adiabatic coupling $\tau^{(2)}_{jj}$, results in the multi-dimensional Schrödinger equation being reduced to a set of uncoupled one-dimensional differential equations which can be solved by using the Numerov-Cooley method [6], as outlined in the previous chapter.

3.2.1 $\qquad \{-\partial^2/\partial y^2 + U_j(y) + \tau_{jj}^{(2)} - E_{nj}\}Y_{nj}(y) = 0$

$U_j(y)$ is the eigenvalue corresponding to the channel function $X_j(x;y)$ and for H_b,

3.2.2 $\qquad \tau(2)jj = (j^2 + j + 1)\{\alpha/4w_x(y)^2\}^2$

where the effective x frequency is

3.2.3 $\qquad w_x^2 (y) = w_x^2 + 2\alpha y$

The units chosen correspond to those of Ezra [3], $\hbar = \mu = 1$ and the frequencies are such that $(w_x + w_y) = 2.0$. The corresponding expressions for H_a are

3.2.4 $\qquad \tau^{(2)}_{jj} = (j^2 + j + 1)\{\alpha y/2w_x(y)^2\}^2$

3.2.5 $\qquad w_x^2 (y) = w_x^2 + 2\alpha y^2$

The non-adiabatic perturbation, H' is best defined by the matrix elements in the adiabatic basis, $X_j(x;y)$ [4,7]

3.2.6 $\qquad \langle X_i(x;y) \mid H' \mid X_j(x;y)\rangle = \tau^{(1)}_{ij} / y + \tau^{(2)}_{ij}(1-\delta_{ij})$

$$= H'_{ij}(y)$$

The momentum and kinetic coupling terms are

3.2.7 $\qquad \tau^{(1)}_{ij} = \langle X_i(x;y) \mid \quad -\partial/\partial y \quad \mid X_j(x;y)\rangle x$

$\qquad\qquad \tau^{(2)}_{ij} = \langle X_i(x;y) \mid -\tfrac{1}{2}\partial^2/\partial y^2 \mid X_j(x;y)\rangle x$

where $\langle \;\mid\mid\; \rangle x$ implies integration over the x coordinate only. All the non-zero elements of the coupling matrices are given for both hamiltonians in the appendix to this chapter.

The Rayleigh-Schrödinger perturbation theory used in these calculations follows that of Hutson and Howard [4]. The perturbation correction of order k from channel 1 to the particular state of interest (level n of channel j) designated by $Y_1^{(k)}$, was obtained by solving the appropriate linear, inhomogeneous differential equations as described in reference [4]. The method of solving such equations has already been described in Chapter 2. The expressions for the energy corrections to the fifth order are given here (up to the third

44

order have been given previously [4]. Knowledge of the second order correction to the wavefunction is sufficient to determine energy corrections up to the fifth order. The integrals are over the y coordinate only as the x integration has already been performed in obtaining $H'_{jk}(y)$.

3.2.8
$$E(2) = \sum_k \langle Y_{nj}^{(0)} \mid H'_{jk} \mid Y_k^{(1)} \rangle$$

$$E(3) = \sum_k \sum_l \langle Y_k^{(1)} \mid H'_{kl} \mid Y_l^{(2)} \rangle$$

$$E(4) = \sum_k \sum_l \langle Y_k^{(1)} \mid H'_{kl} \mid Y_l^{(2)} \rangle$$
$$- E(2) \sum_k \sum_l \langle Y_k^{(1)} \mid Y_l^{(2)} \rangle$$

$$E(5) = \sum_k \sum_l \langle Y_k^{(2)} \mid H'_{kl} \mid Y_l^{(2)} \rangle$$
$$- 2E(2) \sum_k \sum_l \langle Y_k^{(1)} \mid Y_l^{(2)} \rangle$$
$$- E(3) \sum_k \sum_l \langle Y_k^{(1)} \mid Y_l^{(2)} \rangle$$

The sums in the above expressions range over all the adiabatic channels. However, for the systems studied in this work, there are a limited number of strongly interacting channels for a given state and the summations can be truncated.

3.3 Computational Details

The adiabatic energy levels and wavefunctions were calculated using the Numerov-Cooley method on a grid of 3200 points and a step-size of 0.005 units. The range of y was from -8.0 units to +8.0 units. This grid size was sufficient to ensure the convergence of all energy levels studied to 1 part in 10^6. The most laborious computational tasks in the calculation involve the evaluation of the many integrals required to produce the increasing orders of energy correction. The higher the level of correction, the greater the

number of integrals involved. Each integral was solved by a reduction to a single function of y and an integration over this function. As such a fine grid was chosen, the integrations simply involved summing the function at each point and multiplying by the step size (essentially the trapezoidal rule for numerical integration). Integrals of the form $\langle Y_{nj}^{(0)} \mid H'jk \mid Y_k^{(1)} \rangle$ are calculated in three stages. Firstly, the appropriate j,k elements of the non-adiabatic matrices ($\tau^{(1)}$ and $\tau^{(2)}$) are selected and evaluated as functions of y. Next the perturbation hamiltonian H' is used to operate on the appropriate wavefunction or wavefunction correction. Once the required differentiations have been performed by a second order finite difference technique, the integral is evaluated in the manner already described.

The calculations were simplified in some places by making use of the hermitian properties of the total perturbation matrix, H'

3.3.1 $\qquad \langle Y_{nj}^{(0)} \mid H'_{jk} \mid Y_k^{(1)} \rangle = \langle Y_k^{(1)} \mid H'_{kj} \mid Y_{nj}^{(0)} \rangle$

The accuracy of the integrations and the differentiation implicit in H' can be illustrated by evaluating all of the terms explicitly and comparing the calculated energies with those obtained using the hermitian properties. When the energies have been converged and are thus well behaved, the integrals are accurate to $\pm 1.0 \times 10^{-6}$. When convergence has not quite been attained, the same accuracy still results, but for higher levels where the perturbation series oscillates, this difference can rise to as much as $\pm 4.0 \times 10^{-5}$.

Figure I

Plot of the adiabatic energies against magnitude of perturbation (α) for case A of the H_a hamiltonian. The top plot refers to the even channels, 0,2 and 4 and the bottom plot refers to channels 1,3 and 5.
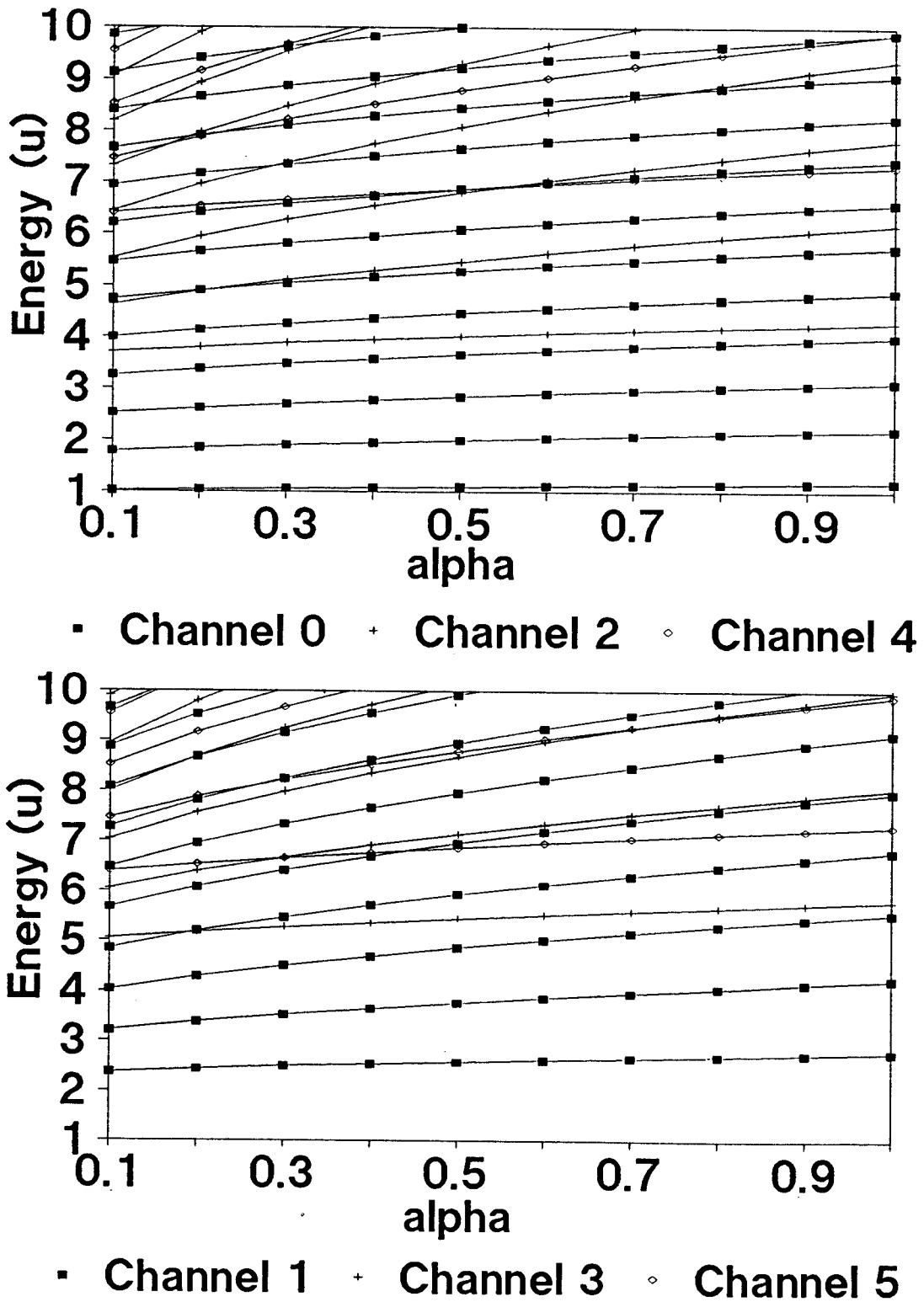
Figure II

Plot of the adiabatic energies against magnitude of perturbation (α) for case B of the H_a hamiltonian. The top plot refers to the even channels (0,2,4) and the bottom plot refers to channels (1,3,5).

- Channel 0   + Channel 2   ◦ Channel 4

- Channel 1   + Channel 3   ◦ Channel 5
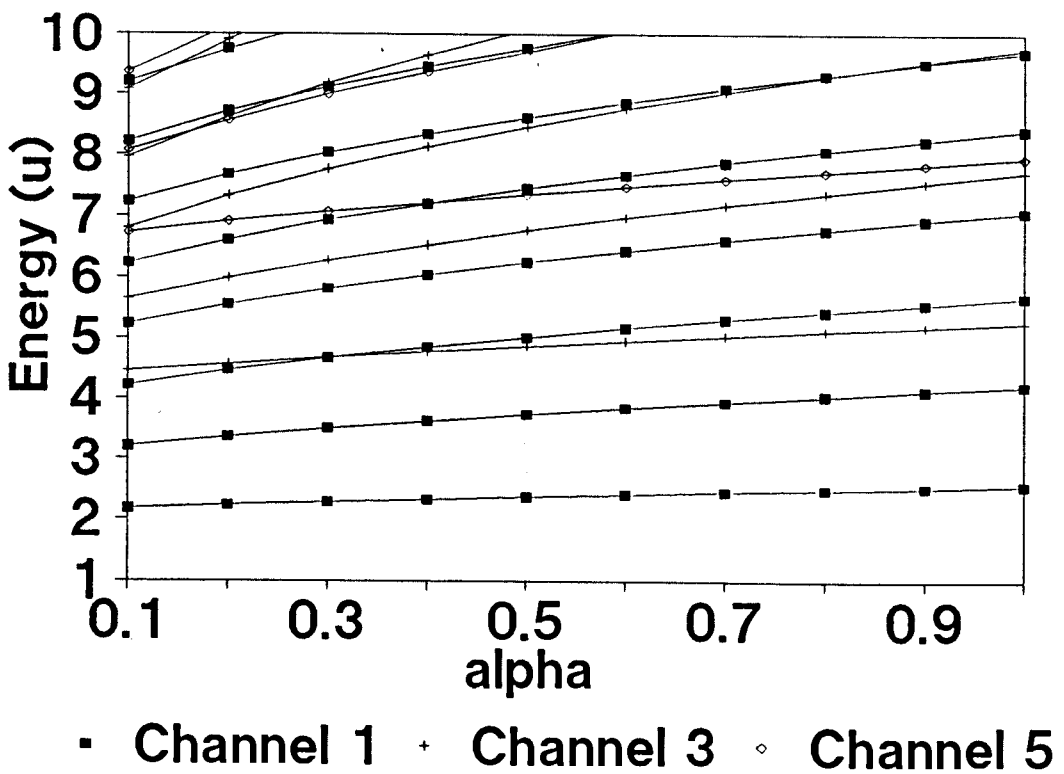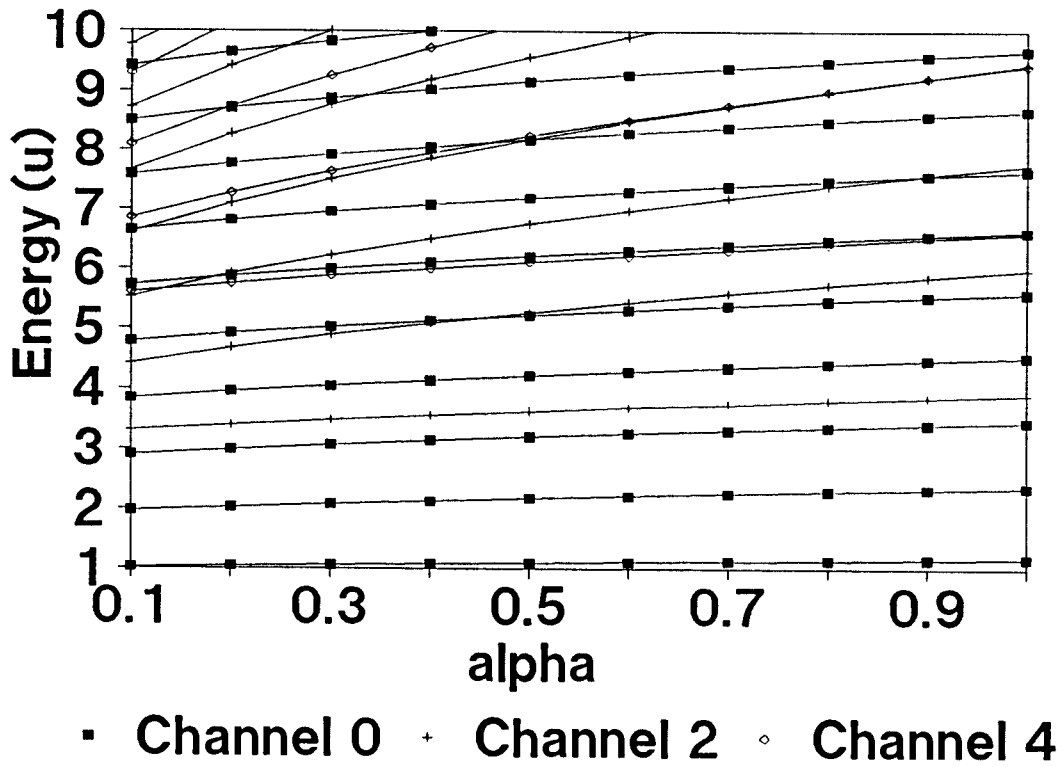
3.4   Results and Discussion

A. <u>The H_a hamiltonian</u>

The majority of the calculations were performed on the H_a hamiltonian. To illustrate the effectiveness of the adiabatic separation, three sets of harmonic frequencies were chosen

Case A: $w_x^2 = 1.69$ $w_y^2 = 0.49$

Case B: $w_x^2 = 1.21$ $w_y^2 = 0.81$

Case C: $w_x^2 = w_y^2 = 1.0$

The two cases A and B are discussed in this section, with the degenerate case C appearing in a later section. The behaviour of the adiabatic energy levels and the perturbation series were investigated as a function of α for each case. All the energy levels rise monotonically with increasing α, but not at the same rate which leads to crossings occurring between the energy levels of different adiabatic channels. Figures I and II which show plots of all eigenvalues with energy less than or equal to 10.0 against α, illustrate this point. Each figure is divided into two parts because the non-adiabatic perturbation matrix elements do not couple between even and odd adiabatic channels. The nth level within adiabatic channel m will be designated by [n,m].

Tables I and II show examples of the effect on the convergence of the perturbation series of increasing α on selected energy levels. For $\alpha \geq 1$ the perturbation begins to dominate the harmonic terms and the perturbation series loses stability. For comparison, the hamiltonian was diagonalised in a basis of the unperturbed two dimensional harmonic oscillator functions; the method of secular equations as discussed in Chapter 2. This basis will be referred to as the Diabatic Basis and the functions labelled by the eigenvalues of hx and hy as (nx,ny). The eigenvalues and selected eigenvectors were obtained using Fortran NAG (version 11) routines F01AGF, F02BEF and F01AHF. A basis set of 34×34 functions proved to be sufficient to converge most of the levels used in the discussion here to an

Figure III

Plot of the perturbed [0,0] energies against the magnitude of the perturbation (α) for case A (top) and case B of H_a. E_d is the value obtained by the method of secular equations.

| ■ | Ebo - Ed | + | Eadb - Ed | ◇ | E(1) - Ed |
| △ | E(2) - Ed | × | E(3) - Ed | ▽ | E(4) - Ed |
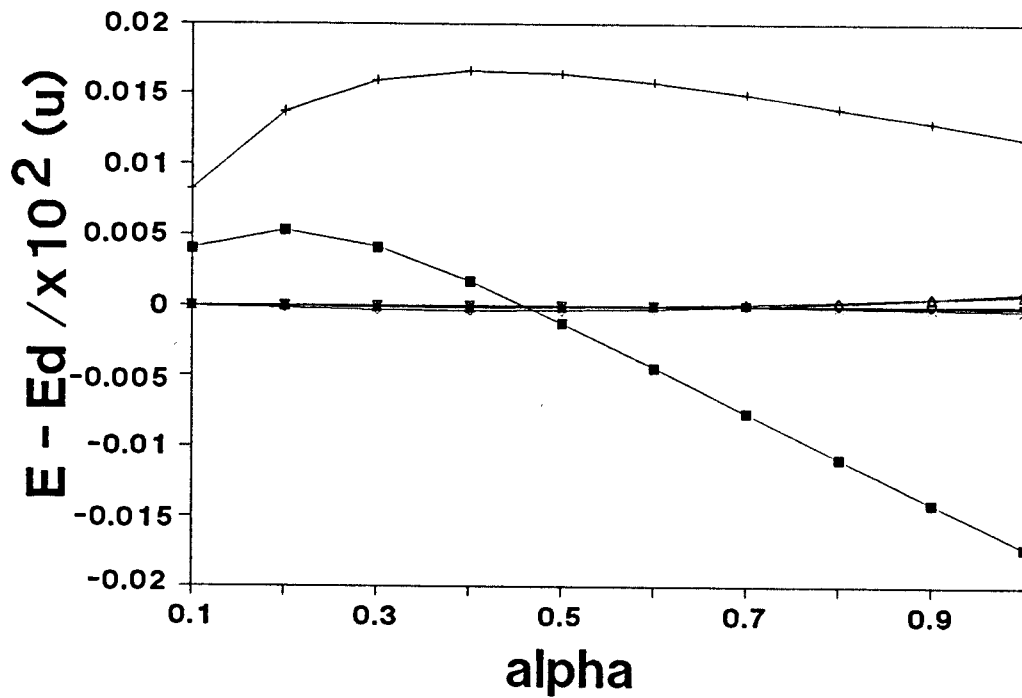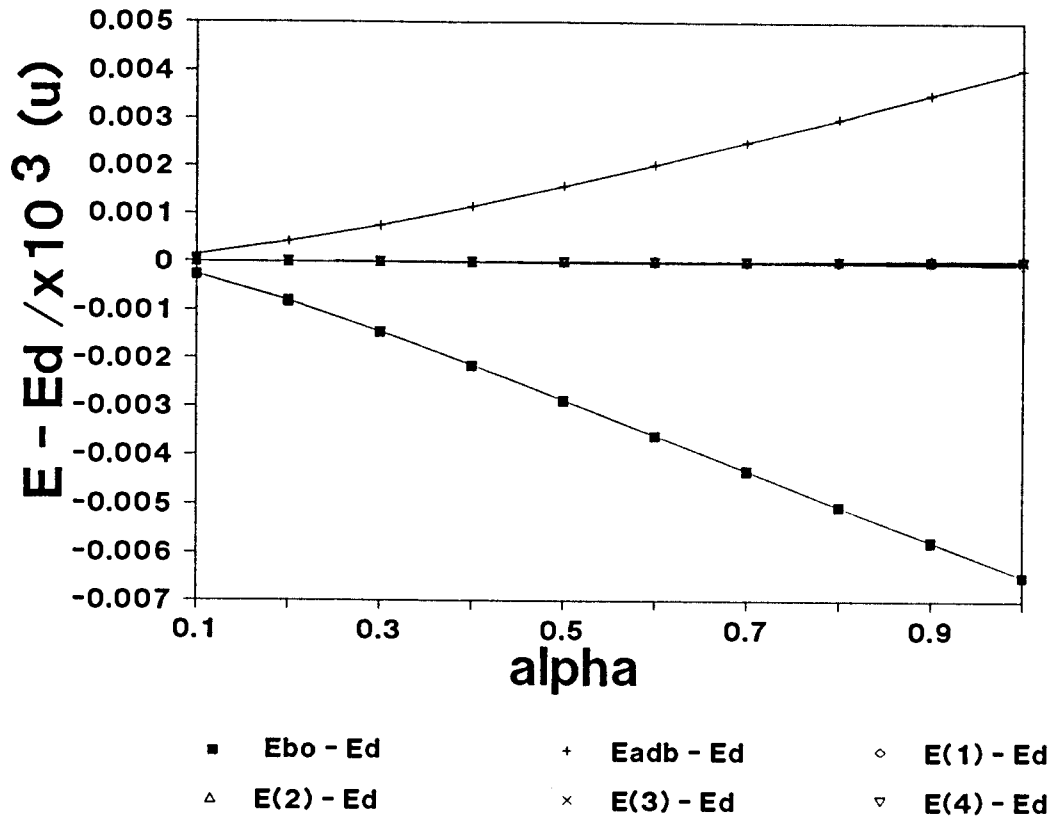
Figure IV

As for Figure III but showing the [1,5] level for case A (top) and case B.
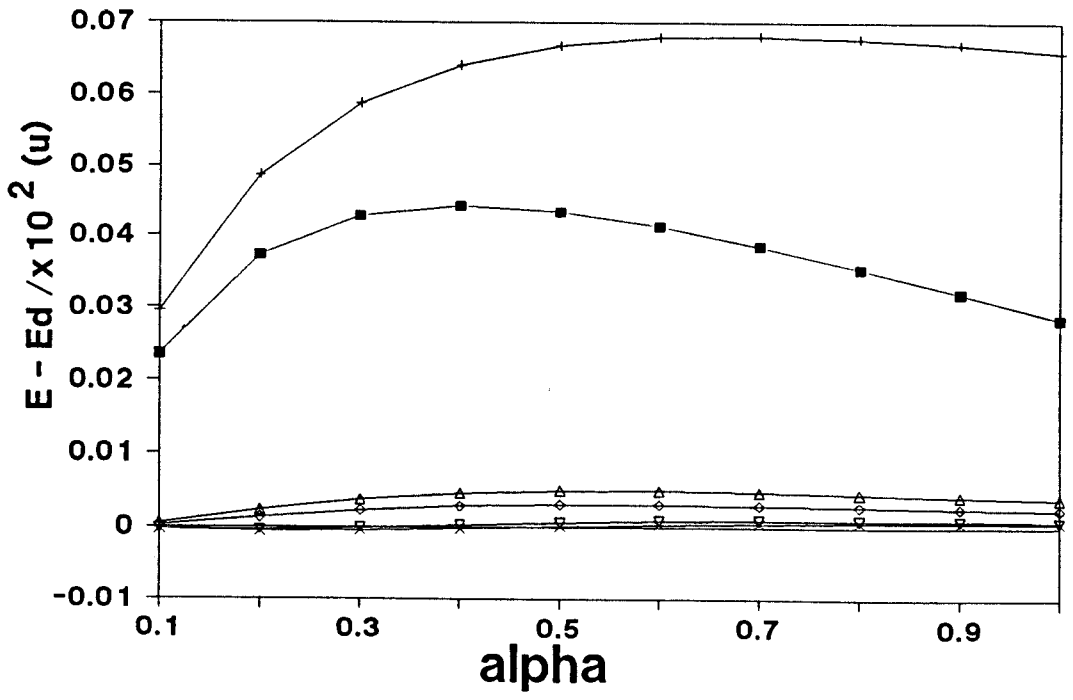
Figure V

As for Figure III but showing the [3,1] level for case A (top) and case B.
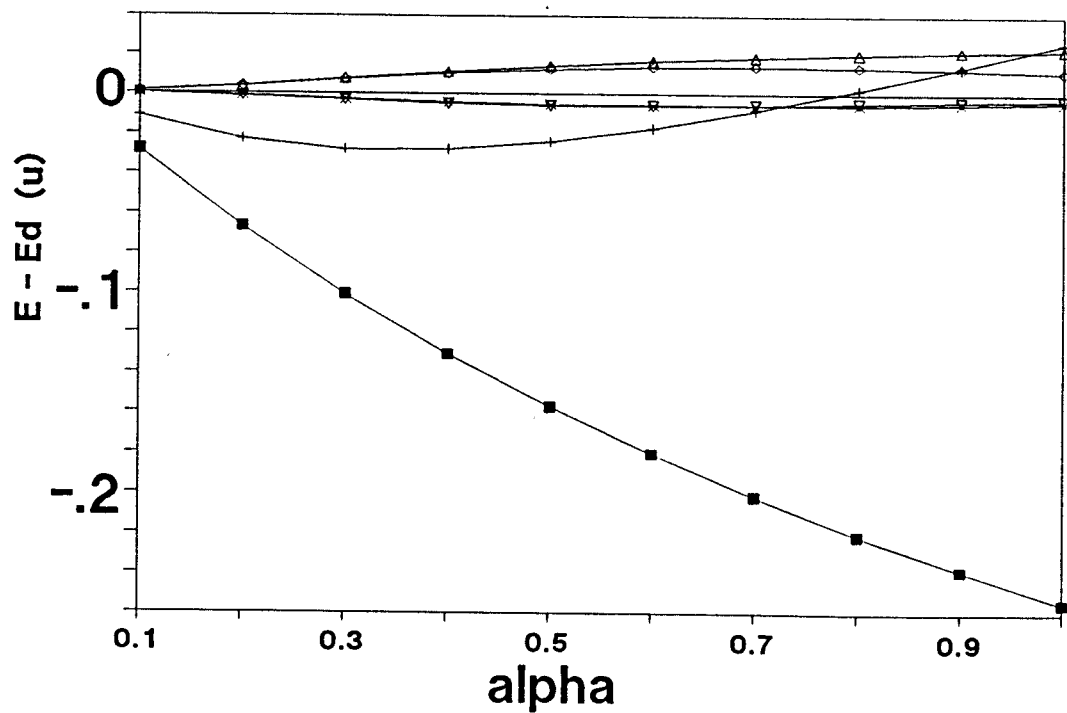
accuracy of 1 in 10^5. The diagonalisation of a matrix of this magnitude took approximately 250 seconds on the Southampton University IBM 3090-150 mainframe with compiler (FORTVS2) optimization level 3.

The well behaved nature of the perturbation series away from any intersections of the adiabatic energy levels is illustrated in Figures III, IV and V. The plots show as a function of α, both the Born-Oppenheimer (E_{bo}) and adiabatic (E_{adb}) approximations as well as the four orders of energy corrections to each adiabatic energy level (E_{ncorr}). The ground state plots show the adiabatic approximation is an upper bound to the exact value while the Born-Oppenheimer approximation is a lower bound. For excited levels the two approximations do not necessarily envelope the exact values.

The diagrams in Figures I and II show various intersecting levels and in the region around these crossing points the largest non-adiabatic interactions would be expected. The [0,5] and [2,1] levels of the case A, which cross at $\alpha = 0.2$, and the [0,6] and [2,2] levels of the case B, crossing at $\alpha = 0.9$, are two such examples. Figures VI and VII show plots of the different levels of approximation for these strongly interacting levels. The fourth- and fifth- order corrections for the second example are very strongly effected by the interaction and could not be displayed. It is in these regions of near degeneracy of the adiabatic approximate solutions that the perturbation series fails to converge.

There are examples in Figures I and II of intersecting levels which should, in the light of the adiabatic approximation, be strongly interacting, for instance the [2,1]/[0,4] levels in Figure II which cross at $\alpha = 0.5$. However, for small perturbations, the states may also be approximated by a predominant single basis term in the diabatic basis, in this case (2,1)/(0,4). In the diabatic basis, coupling only occurs between states differing by 2 in both nx and ny, so these states are only coupled by the extent that the single diabatic basis function does not completely describe the wavefunction. The crossing of the [2,4] and [4,1] levels in Figure I

53

Figure VI

As for Figure III but showing the interactions between the [2,1] and [0,5] levels for case A.
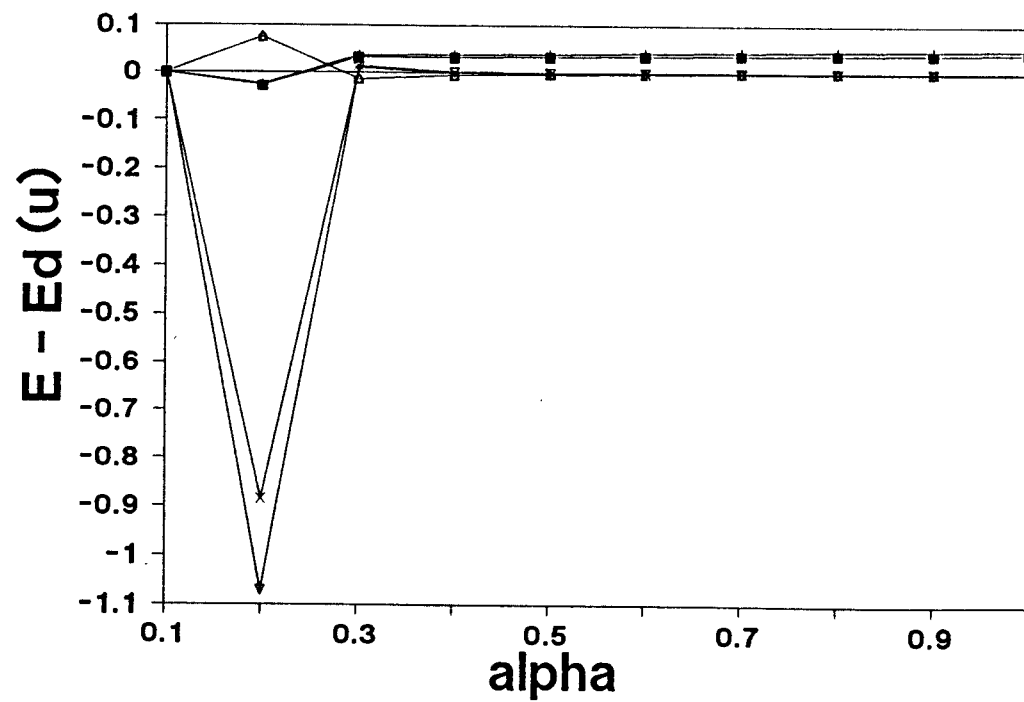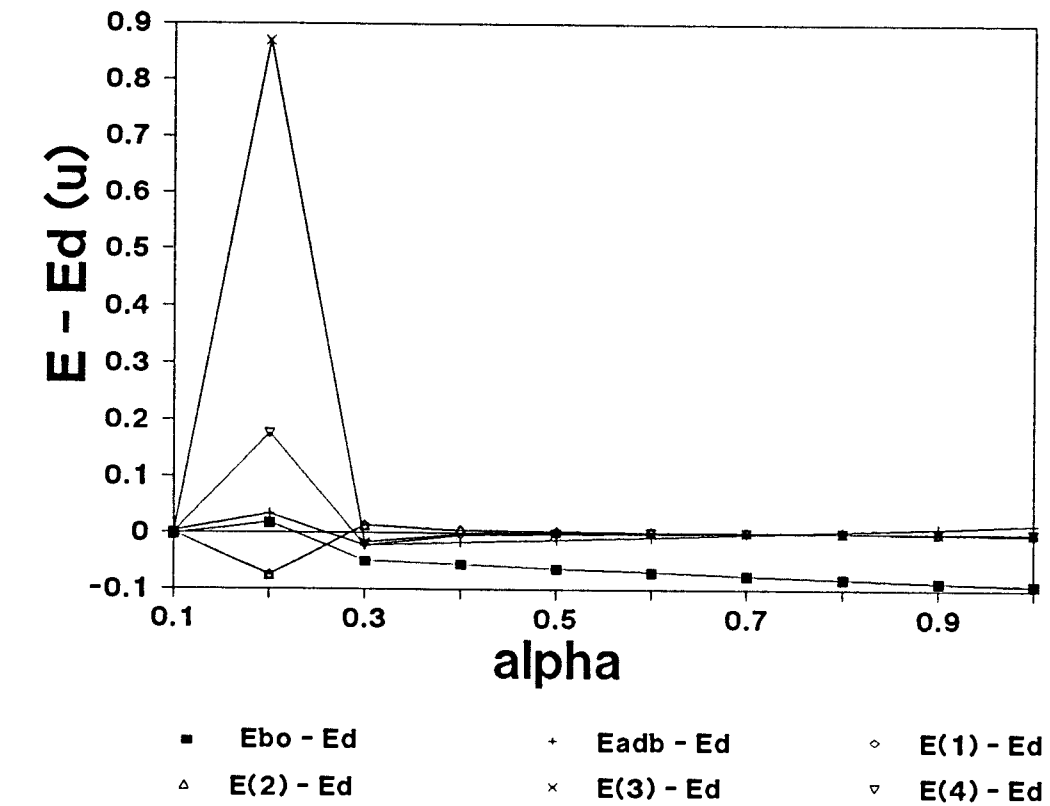
Figure VII

As for Figure III but showing the interactions between the [2,2] and [0,6] levels for case B.

Legend:
- ■ Ebo - Ed
- ⊣ Eadb - Ed
- ◇ E(2) - Ed
- △ E(3) - Ed
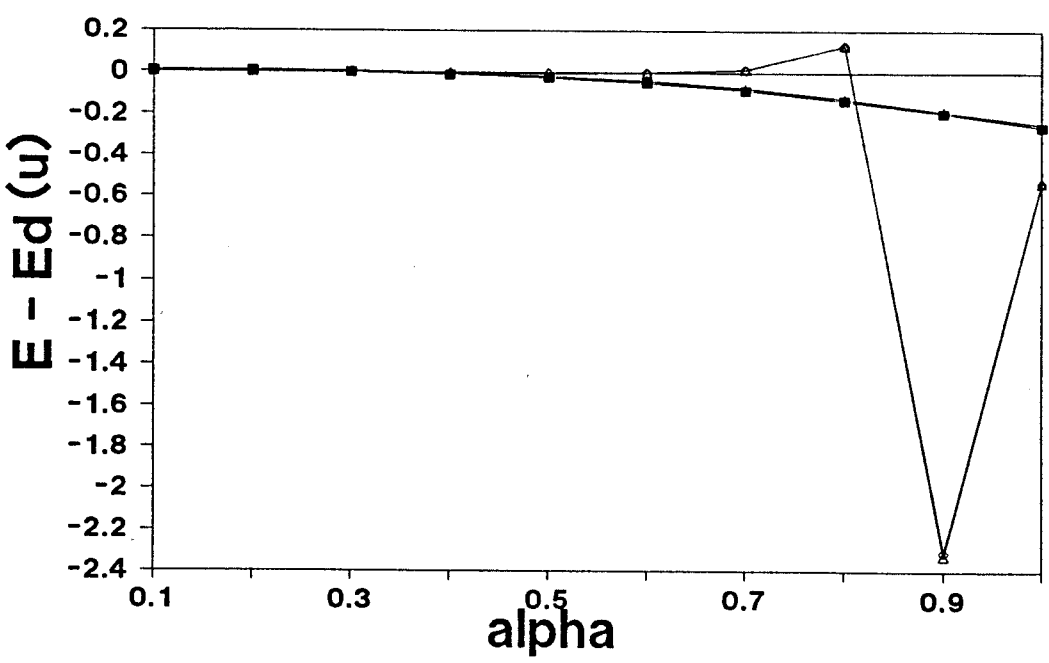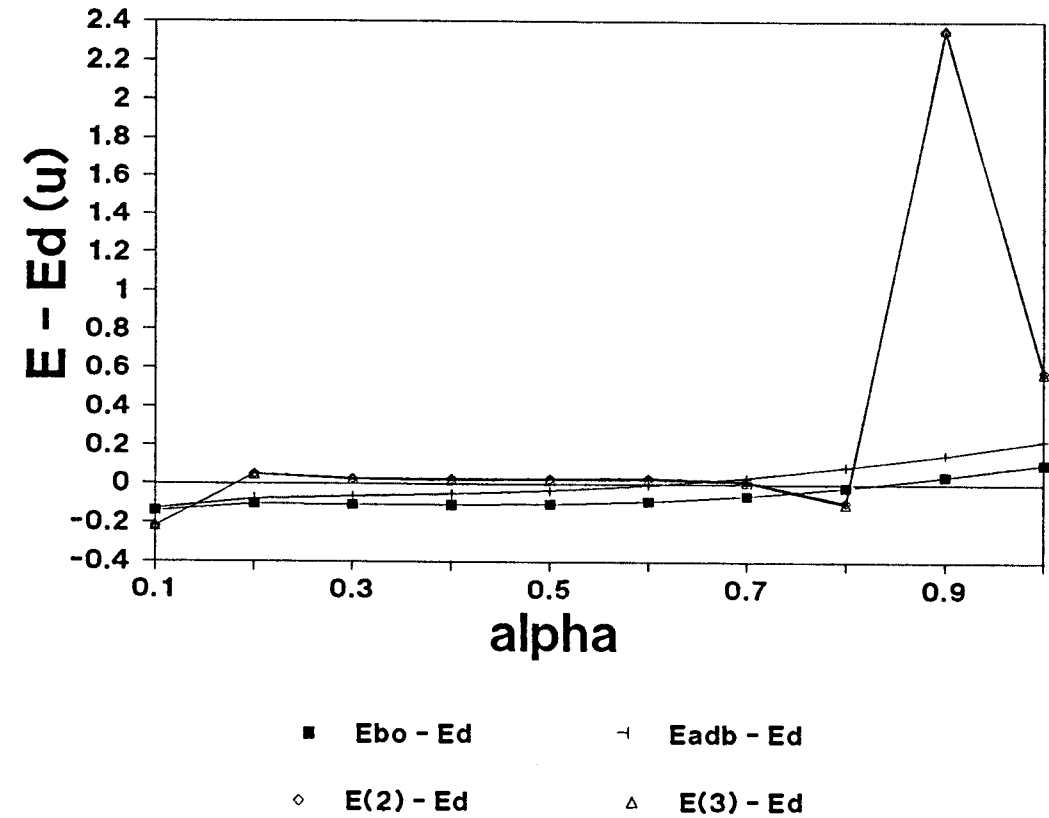
is another example of this sort. For higher eigenvalues and larger perturbations, such a characterisation in terms of a single (nx,ny) basis function becomes less and less meaningful and the extent of coupling between the levels rises accordingly. At high energies, the y grid used was not sufficient to converge the adiabatic energies to the same accuracy as the lower levels. Despite this the perturbation series is still stable for small α.

Overall, the perturbation series is seen to be stable and converging when the initial adiabatic approximation is reliable. As a further test of the stability of the scheme, the x and y frequencies were exchanged and results were taken at various levels of perturbation. The calculation showed only minor differences at higher energies; the use of the "fastest" motion in the approximation did not prove to be crucial.

B. The H_b hamiltonian

For comparison with previous work on the use of the adiabatic separation for coupled oscillators, the Generalised Henon-Heiles hamiltonian was investigated for selected values of the perturbation parameters. The values of the parameters used were, $w_x^2 = 1.69$, $w_y^2 = 0.49$, $\alpha = -0.1$, $\beta = 0.1$. As the value of the y distance increases to about 8.45, the effective frequency $w_x(y)$ becomes zero and the diagonal coupling term, $\tau^{(2)}_{jj}$, tends to infinity. At larger values of y, the effective frequency becomes imaginary. This corresponds to the lack of a minimum along the x direction. This is illustrated in Figure VIII, which shows an isometric plot of the potential V(x;y). The surface has been cut at a maximum value of V = 10.0 so that both the central well region and the surrounding regions where the potential tends to negative infinity can be seen. True bound states can only be obtained if the range of the potential is restricted to encompass just the central well region (y < 8.45). Thus, the Numerov-Cooley procedure could only be used to obtain the lower adiabatic energy levels (E < 10.0) with any real accuracy. This explains why this hamiltonian was not suitable for an extensive study of the perturbation scheme.

Figure VIII

A three-dimensional plot of the potential V(x,y) for the generalized Henon-Heiles hamiltonian H_b, with parameters $\omega_x^2 = 1.69$ and $\omega_y^2 = 0.49$, $\alpha = -0.1$ and $\beta = 0.1$.

HENON-HEILES POTENTIAL CUTOFF AT E=10

Table III shows the good agreement between the "corrected" energy levels and the exact quantum values of Noid [8], especially at the lower energies. The adiabatic potentials rise very steeply as the enforced cut-off is approached and this causes instabilities in the Numerov-Cooley technique at higher energies. In spite of the resulting convergence problems with the adiabatic levels, the perturbation calculation is still seen to be stable.

C. Degenerate Frequencies

Table IV shows the results of a calculation for the degenerate oscillator for the H_b hamiltonian, using the parameters of Noid and Marcus [9] ($w_x^2 = w_y^2 = 1$, $\alpha = 0.1118$, $\beta = -1/3$). The adiabatic approximation is not expected to be very good for such a system. Nevertheless, the perturbation series does converge for the lowest few levels, and indeed the [0,1] and [1,0] levels are found to be degenerate. A more extensive study of the degenerate system for the H_a hamiltonian illustrates that the equal frequency case has all the attributes and faults of the non-degenerate systems, except that the problems are magnified by the complete symmetry of the problem.

Figure IX contains plots of adiabatic energy against α for even and odd channels. Once again, the lower levels are free from intersection which results in well-behaved and largely converged energies. Some of these are shown in Table V. The perturbation scheme is seen to be stable for degenerate levels from non-intersecting channels.

Figure IX

Plot of the adiabatic energies against magnitude of perturbation (α) for the degenerate case C of the hamiltonian H_a. The upper plot is for the even channels (0,2,4,6) and the lower plot is for (1,3,5,7).
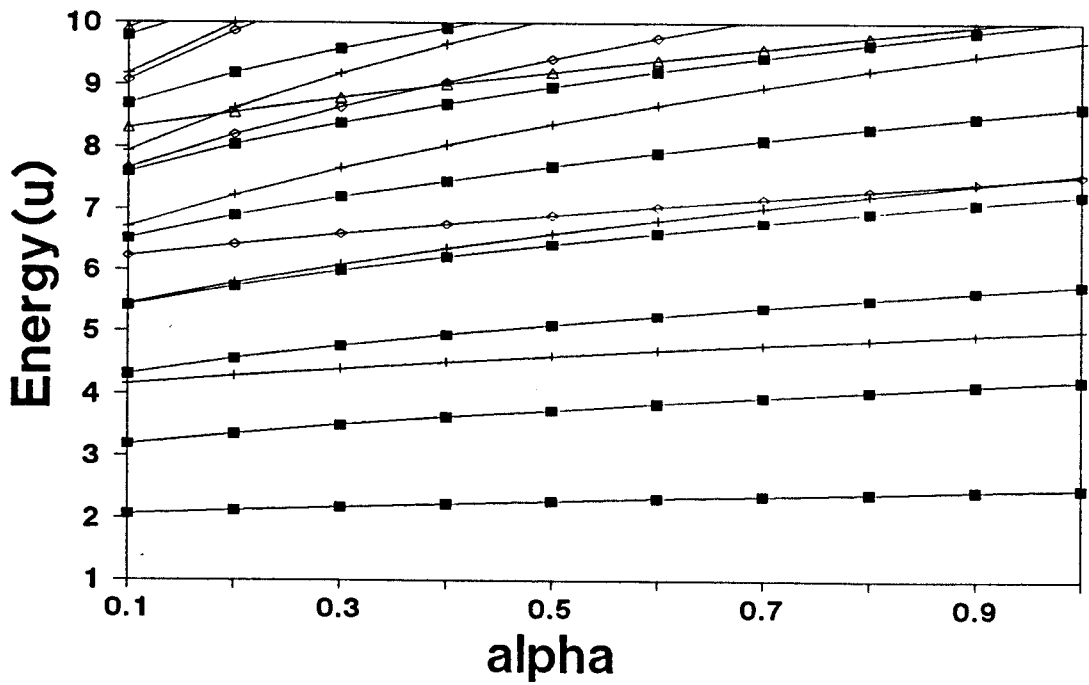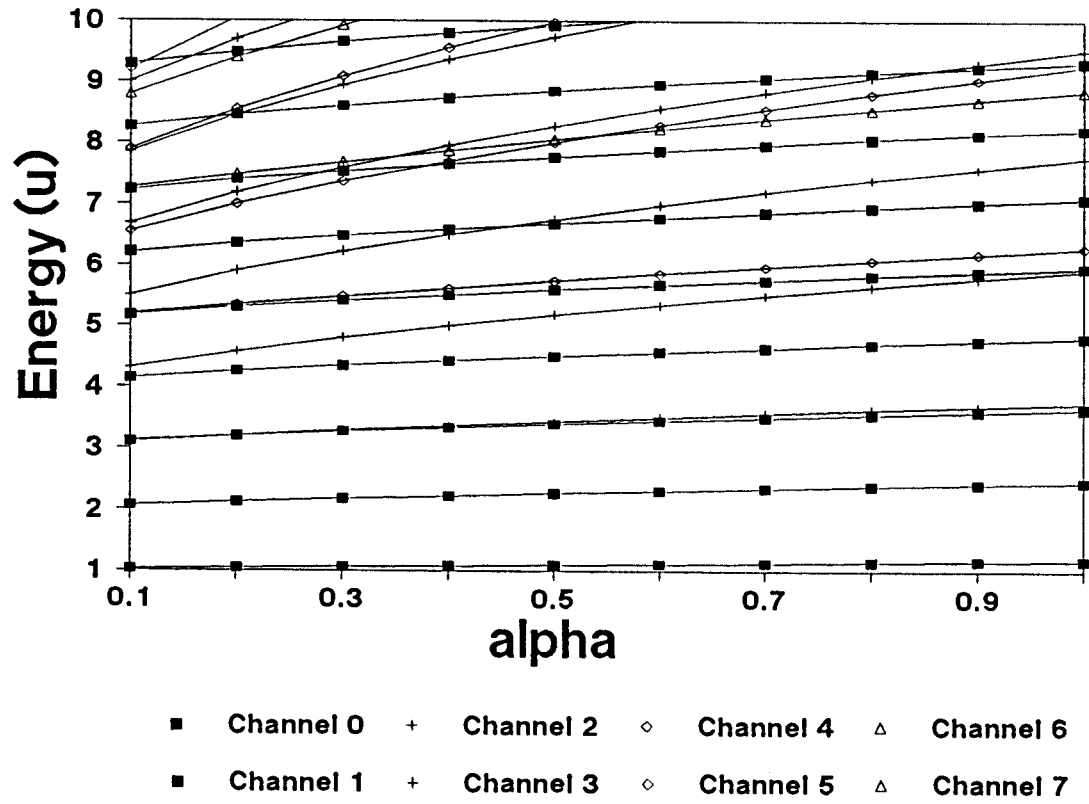
3.5 Conclusion

Having obtained the adiabatic energy levels, an alternative approach to the calculation of the non-adiabatic energies is to diagonalise the non-adiabatic coupling matrix in a basis formed by the adiabatic approximate solutions. This requires a large number of the complete adiabatic solutions to be found, that is all the $Y_{nj}(y)$ as well as the $X_j(x;y)$, which involves a large computational effort [10]. Indeed, in many cases this is further complicated by the contribution of repulsive channels which support no bound states.

The perturbation procedure presented requires all the $X_j(x;y)$ and the non-adiabatic interactions just as for the diagonalisation procedure, but only the $Y_{nj}(y)$ for the state of interest is needed. Furthermore, repulsive channels can be included without any modification in the perturbation calculation. Convergence of the perturbation series does not vary uniformly with energy. There is a trend to poorer convergence at higher energies but the variations due to accidental degeneracies of the adiabatic levels are much more significant.

Table I

Energy corrections up to the fifth order at increasing values of α
for selected energy levels of the H_a hamiltonian for case A.

α	EADB	E2CORR	E3CORR	E4CORR	E5CORR	ED
[0,0]						
0.1	1.025588	1.025451	1.025451	1.025451	1.025451	1.025451
0.3	1.068981	1.068218	1.068223	1.068220	1.068221	1.068221
0.5	1.106009	1.104422	1.104440	1.104431	1.104431	1.104432
0.7	1.138908	1.136384	1.136426	1.136404	1.136405	1.136406
0.9	1.168828	1.165287	1.165365	1.165323	1.165325	1.165329
[0,5]						
0.1	4.735483	4.734974	4.734979	4.734971	4.734972	4.734972
0.3	5.048080	4.998167	4.998518	5.025933	5.022387	5.011602
0.5	5.281795	5.239293	5.239763	5.242807	5.242389	5.242559
0.7	5.476197	5.431411	5.432056	5.432270	5.432192	5.432780
0.9	5.645790	5.598533	5.599359	5.598063	5.598201	5.598812
[1,5]						
0.1	6.479802	6.471488	6.471532	6.471516	6.471515	6.471534
0.3	7.340155	7.323884	7.324102	7.324153	7.324146	7.324194
0.5	7.964967	7.948194	7.948451	7.948508	7.948506	7.948529
0.7	8.475420	8.460432	8.460592	8.460412	8.460444	8.460434
0.9	8.914825	8.902456	8.902422	8.901715	8.901826	8.901793
[2,1]						
0.2	4.895154	4.786049	4.786562	5.731124	5.036818	4.861259
0.4	5.300303	5.322585	5.322631	5.314243	5.313557	5.317310
0.6	5.627242	5.636624	5.637173	5.634327	5.634255	5.634916
0.8	5.908113	5.904576	5.905920	5.904599	5.904547	5.904603
1.0	6.157669	6.139841	6.142256	6.141481	6.141311	6.141289

Table I continued

α	EADB	E2CORR	E3CORR	E4CORR	E5CORR	ED
[2,4]						
0.2	7.959715	7.921583	7.922175	7.922054	7.921945	7.922121
0.4	8.912583	8.775185	8.779725	8.811571	8.778251	8.794692
0.6	9.650988	9.546694	9.568589	9.515635	9.527016	9.509321
0.8	10.269217	10.095625	10.073114	10.180926	10.174761	10.137974
1.0	10.808156	10.571190	10.563224	10.633861	10.607102	10.612224
[3,1]						
0.1	6.056753	6.055496	6.055502	6.055454	6.055454	6.055452
0.3	6.673762	6.660412	6.660778	6.660071	6.660081	6.660083
0.5	7.139683	7.107744	7.109210	7.107412	7.107378	7.107579
0.7	7.530120	7.476317	7.479638	7.476507	7.476240	7.477033
0.9	7.872941	7.795212	7.801085	7.796416	7.795598	7.797529
[3,6]						
0.1	10.820990	10.804455	10.804730	10.805108	10.805047	10.804897
0.3	12.819908	12.713117	12.716551	12.716556	12.714737	12.715720
0.5	14.218420	13.964226	13.972909	14.015069	13.961534	14.006288
0.7	15.340558	14.530954	14.550948	19.089653	9.583417	14.991820
0.9	16.295537	16.662330	16.665762	14.404597	12.914194	15.804499
[4,1]						
0.2	7.879303	7.886423	7.886411	7.885451	7.885457	7.885535
0.4	8.516570	8.544918	8.545424	8.538130	8.537960	8.539235
0.6	9.031334	9.097040	9.098028	9.067712	9.066262	9.076635
0.8	9.476662	9.595729	9.596809	9.507187	9.498474	9.545133
1.0	9.875584	10.062669	10.063153	9.851611	9.817131	9.963761

EADB is the diagonally corrected Born-Oppenheimer approximation, ED
is the value obtained by diagonalisation in the (n_x, n_y) basis, Encorr
is the energy up to the nth order energy correction and alpha is the
coupling constant.

Table II

As for Table I for case B.

α	EADB	E2CORR	E3CORR	E4CORR	E5CORR	ED
[0,0]						
0.1	1.023871	1.023610	1.023610	1.023610	1.023610	1.023610
0.3	1.065394	1.063984	1.063998	1.063989	1.063990	1.063990
0.5	1.101487	1.098617	1.098670	1.098639	1.098641	1.098643
0.7	1.133926	1.129434	1.129556	1.129485	1.129490	1.129496
0.9	1.163672	1.157452	1.157670	1.157542	1.157554	1.157564
[0,4]						
0.2	4.917991	4.905908	4.906047	4.905739	4.905753	4.905792
0.4	5.130143	5.114218	5.114553	5.113994	5.114042	5.114059
0.6	5.300866	5.284251	5.284689	5.284132	5.284196	5.284191
0.8	5.447446	5.431303	5.431762	5.431291	5.431355	5.431347
1.0	5.577675	5.562508	5.562931	5.562536	5.562587	5.562585
[0,6]						
0.1	6.646911	6.638753	6.638798	6.638654	6.638658	6.638677
0.3	6.964388	6.959738	6.959840	6.960040	6.960026	6.960010
0.5	7.199821	7.216853	7.217044	7.219055	7.218957	7.218439
0.7	7.395348	7.485332	7.486010	7.471608	7.471506	7.471059
0.9	7.565924	5.441937	5.426344			7.749692
[1,5]						
0.2	7.671313	7.623887	7.624832	7.622039	7.622230	7.622567
0.4	8.342352	8.281059	8.282815	8.278108	8.278620	8.278273
0.6	8.870002	8.805167	8.807066	8.802498	8.803002	8.802105
0.8	9.316387	9.251488	9.253214	9.249373	9.249682	9.248646
1.0	9.708643	9.645128	9.646566	9.643375	9.643489	9.642564

Table II continued

α	EADB	E2CORR	E3CORR	E4CORR	E5CORR	ED
[2,1]						
0.1	4.422865	4.423267	4.423280	4.423252	4.423252	4.523253
0.3	4.896119	4.885651	4.886144	4.885825	4.885832	4.885813
0.5	5.264108	5.232259	5.234040	5.232859	5.232841	5.233111
0.7	5.574979	5.516049	5.519850	5.517268	5.516936	5.518365
0.9	5.848464	5.758288	5.764750	5.760792	5.759109	5.763330
[2,2]						
0.1	5.516222	5.423447	5.424199	5.531080	5.517646	5.461104
0.3	6.227391	6.316775	6.314221	6.274403	6.272637	6.290590
0.5	6.759249	6.819293	6.814907	6.785899	6.784930	6.793579
0.7	7.198404	7.183484	7.176504	7.154504	7.160781	7.167022
0.9	7.578496	9.775840	9.782859			7.426080
[3,1]						
0.2	5.983614	6.010199	6.010082	6.005197	6.004990	6.006546
0.4	6.529542	6.567621	6.568259	6.552954	6.552308	6.557410
0.6	6.975533	7.006351	7.009256	6.986818	6.986653	6.992675
0.8	7.362074	7.373734	7.380330	7.354539	7.355287	7.359969
1.0	7.707886	7.692853	7.704362	7.677478	7.678583	7.681617
[3,6]						
0.2	12.390234	12.079748	12.095720	12.053176	12.018243	12.095537
0.4	13.963707	14.189822	14.208629	12.184868	11.332992	13.378182
0.6	15.172284	14.854700	14.884605	14.475720	14.563881	14.393982
0.8	16.180153	15.725880	15.748359	15.251329	15.388852	15.102620
1.0	17.056786	16.497453	16.508072	15.990002	16.125636	15.714929

EADB is the diagonally corrected Born-Oppenheimer approximation, ED is the value obtained by diagonalisation in the (n_x,n_y) basis, Encorr is the energy up to the nth order energy correction and alpha is the coupling constant.

Table III

Corrected energy levels for the Generalized Henon-Heiles hamiltonian
(H_b) with parameters $\omega_x^2 = 1.69$, $\omega_y^2 = 0.49$, $\alpha = -0.1$, $\beta = 0.1$

[X,Y]	EADB	E2CORR	E3CORR	E4CORR	E5CORR	EQM
0,0	0.995569	0.995519	0.995519	0.995519	0.995519	0.9955
0,2	2.375389	2.375036	2.375037	2.375036	2.375036	2.3750
0,4	3.741193	3.740435	3.740436	3.740435	3.740435	3.7404
0,6	5.092192	5.090859	5.090861	5.090857	5.090857	5.0909
0,8	6.427464	6.425278	6.425283	6.425267	6.425268	6.4253
0,10	7.746016	7.742476	7.742489	7.742436	7.742437	7.7423
0,12	9.048678	9.042673	9.042723	9.042512	9.042528	9.0403
0,14	10.354356	10.343104	10.343409	10.342452	10.342632	10.3161
1,1	2.958949	2.958352	2.958353	2.958353	2.958353	2.9584
1,3	4.308606	4.306912	4.306914	4.306911	4.306911	4.3069
1,5	5.641764	5.638520	5.638528	5.638516	5.638517	5.6385
1,7	6.957053	6.951500	6.951520	6.951481	6.951481	6.9515
1,9	8.252809	8.243575	8.243628	8.243491	8.243494	8.2435
1,11	9.529041	9.513055	9.513263	9.512655	9.512714	9.5108
1,13	10.805743	10.775506	10.776748	10.773762	10.774575	10.7463
1,15	12.147797	12.092384	12.098093	12.088457	12.093295	
2,1	4.217152	4.216179	4.216180	4.216180	4.216180	4.2162
2,3	5.541836	5.538984	5.538991	5.538989	5.538989	5.5390
2,5	6.847445	6.841852	6.841876	6.841868	6.841868	6.8419
2,7	8.131909	8.122003	8.122073	8.122042	8.122037	8.1220
2,9	9.393133	9.375568	9.375820	9.375586	9.375565	9.3752
2,11	10.637864	10.604050	10.605463	10.603386	10.603668	10.5937
2,13	11.914997	11.851059	11.856691	11.848325	11.850181	

Table III continued

[X,Y]	EADB	E2CORR	E3CORR	E4CORR	E5CORR	EQM
3,0	4.804526	4.804263	4.804263	4.804263	4.804263	4.8043
3,2	6.112434	6.109885	6.109893	6.109892	6.109892	6.1099
3,4	7.399304	7.393429	7.393461	7.393464	7.393462	7.3935
3,6	8.662505	8.651220	8.651334	8.651334	8.651322	8.6513
3,8	9.899416	9.877858	9.878379	9.878082	9.878039	9.8776
3,10	11.118445	11.073819	11.076833	11.073130	11.073714	11.0612
3,12	12.375075	12.289661	12.300199	12.285854	12.289299	
4,1	6.689454	6.687822	6.687827	6.687826	6.687826	6.6878
4,3	7.957685	7.952384	7.952417	7.952416	7.952415	7.9524
4,5	9.199650	9.188148	9.188302	9.188281	9.188266	9.1882
4,7	10.412157	10.387988	10.388905	10.388255	10.388244	10.3877
4,9	11.605442	11.551633	11.556660	11.550223	11.551411	
4,11	12.841749	12.739114	12.754367	12.733094	12.734609	

Table IV

As for Table III for the case of degenerate frequencies;

$$\omega_x^2 = \omega_y^2 = 1, \quad \alpha^2 = 0.0125, \quad \beta = -1/3$$

NX	NY	EADB	E2CORR	E3CORR	E4CORR	E5CORR	EQM
0	0	0.998896	0.998595	0.998595	0.998595	0.998595	0.9986
0	1	1.991497	1.990075	1.990080	1.990076	1.990076	1.9901
1	0	1.991047	1.990076	1.990080	1.990076	1.990076	1.9901
1	1	2.989953	2.985314	2.985342	2.985316	2.985317	2.9853

EADB is the diagonally corrected Born-Oppenheimer approximation, EQM represents the exact quantum values of Noid [8] and [9] and EnCORR is the energy up to the nth order energy correction.

66

Table V

As for Tables 1 and 2 for case C of the H_a hamiltonian.

α	EADB	E2CORR	E3CORR	E4CORR	E5CORR	ED
[0,0]						
0.1	1.023770	1.023398	1.023399	1.023398	1.023398	1.023398
0.3	1.065447	1.063483	1.063509	1.063493	1.063493	1.063495
0.5	1.101861	1.097912	1.098009	1.097950	1.097954	1.097959
0.7	1.134691	1.128566	1.128782	1.128651	1.128663	1.128674
0.9	1.164866	1.156445	1.156824	1.156590	1.156618	1.156635
[0,1]						
0.1	2.068394	2.067539	2.067544	2.067541	2.067541	2.067541
0.3	2.178880	2.175329	2.175397	2.175357	2.175359	2.175364
0.5	2.269458	2.263282	2.263465	2.263351	2.263360	2.263372
0.7	2.347907	2.339309	2.339633	2.339420	2.339442	2.339462
0.9	2.417937	2.407108	2.407583	2.407255	2.407294	2.407322
[1,0]						
0.1	2.068645	2.067540	2.067545	2.067541	2.067541	2.067541
0.3	2.181272	2.175319	2.175439	2.175349	2.175354	2.175364
0.5	2.275418	2.263188	2.263637	2.263310	2.263339	2.263372
0.7	2.358346	2.339029	2.340043	2.339305	2.339395	2.339462
0.9	2.433499	2.406534	2.408343	2.407011	2.407213	2.407322
[0,2]						
0.1	3.108229	2.688427	2.690539	49.630831	-2.981709	3.068870
0.3	3.269024	2.898823	2.903953	9.049564	3.325396	3.183002
0.5	3.394543	3.054865	3.061471	5.426879	3.472954	3.278902
0.7	3.500766	3.183416	3.190889	4.402210	3.491146	3.363329
0.9	3.594350	3.294278	3.302350	4.004575	3.517157	3.439600
[2,0]						
0.1	3.111943	3.528119	3.526025			3.147662
0.3	3.289985	3.641810	3.637059	-2.698366		3.357673
0.5	3.437088	3.739423	3.734199	1.233005	-3.358517	3.515636
0.7	3.566604	3.825170	3.820801	2.507572	0.633425	3.645951
0.9	3.684359	3.902498	3.899970	3.118489	2.256597	3.756860

Table V continued

α	EADB	E2CORR	E3CORR	E4CORR	E5CORR	ED
[0,3]						
0.2	4.255456	4.224955	4.225247	4.225885	4.225762	4.226175
0.4	4.430571	4.392217	4.392856	4.391921	4.391963	4.392517
0.6	4.572646	4.530413	4.531397	4.529412	4.529629	4.530100
0.8	4.695233	4.650435	4.651769	4.649042	4.649414	4.649760
1.0	4.804523	4.757736	4.759420	4.756127	4.756640	4.756860
[3,0]						
0.2	4.281684	4.218513	4.219561	4.226204	4.222514	4.226175
0.4	4.497505	4.377672	4.381553	4.390132	4.377791	4.392517
0.6	4.683673	4.507286	4.515631	4.524127	4.498637	4.530100
0.8	4.851925	4.617999	4.632410	4.639288	4.595897	4.649860
1.0	5.007830	4.715134	4.737154	4.741123	4.674739	4.756860
[1,2]						
0.1	4.314893	4.340410	4.340200	4.334573	4.334471	4.336284
0.3	4.763328	4.816065	4.814741	4.799694	4.799398	4.804833
0.5	5.104475	5.174911	5.172210	5.147149	5.146659	5.155909
0.7	5.388676	5.473146	5.469020	5.432681	5.432042	5.445358
0.9	5.636125	5.732843	5.727328	5.678276	5.677627	5.695245
[2,1]						
0.1	4.323469	4.337816	4.337774	4.335715	4.335567	4.336284
0.3	4.803992	4.805208	4.805885	4.804764	4.804774	4.804833
0.5	5.179783	5.154712	5.157369	5.155930	5.155918	5.155909
0.7	5.497938	5.442374	5.447968	5.444615	5.444475	5.445358
0.9	5.778110	5.690089	5.699345	5.692897	5.692412	5.695245

EADB is the diagonally corrected Born-Oppenheimer approximation, ED is the value obtained by diagonalisation in the (n_x, n_y) basis, Encorr is the energy up to the nth order energy correction and alpha is the coupling constant.

3.6   Appendix

All of the matrix elements presented here were calculated both by direct differentiation of the adiabatic wavefunctions and by the formulae given by Child [11].

1. $\underline{H_a}$ - The hamiltonian with an $\alpha x^2 y^2$ Coupling

For the anti-symmetric $\tau^{(1)}$ the non-zero matrix elements are

$$\tau^{(1)}_{n,n-2} = \alpha y [n(n-1)]^{\frac{1}{2}} / \{ 2w_x(y)^2 \}$$

$$\tau^{(1)}_{n,n+2} = -\alpha y [(n+1)(n+2)]^{\frac{1}{2}} / \{ 2w_x(y)^2 \}$$

$$w_x^2(y) = w_x^2 + 2\alpha y^2$$

and for $\tau^{(2)}$,

$$\tau^{(2)}_{n,n-4} = -\alpha^2 y^2 [n(n-1)(n-2)(n-3)]^{\frac{1}{2}} / \{ 8w_x(y)^4 \}$$

$$\tau^{(2)}_{n,n-2} = - [n(n-1)]^{\frac{1}{2}} [\alpha^2 y^2 / \{w_x(y)^4\} - \alpha / \{4w_x(y)^2\}]$$

$$\tau^{(2)}_{n,n} = + \alpha^2 y^2 [n^2 + n + 1]^{\frac{1}{2}} / \{ 4w_x(y)^4 \}$$

$$\tau^{(2)}_{n,n+2} = + [(n+1)(n+2)]^{\frac{1}{2}} [\alpha^2 y^2 / \{w_x(y)^4\} - \alpha / \{4w_x(y)^2\}]$$

$$\tau^{(2)}_{n,n+4} = - \alpha^2 y^2 [(n+1)(n+2)(n+3)(n+4)]^{\frac{1}{2}} / \{ 8w_x(y)^4 \}$$

2 H_b - The GHH hamiltonian

For the anti-symmetric $\tau^{(1)}$ the only non-zero elements are

$$\tau^{(1)}_{n,n-2} = \alpha[n(n-1)]^{\frac{1}{2}}/\{4w_x(y)^2\}$$

$$\tau^{(1)}_{n,n+2} = -\alpha[(n+1)(n+2)]^{\frac{1}{2}}/\{4w_x(y)^2\}$$

$$w_x^2(y) = w_x^2 + 2\alpha y$$

and for $\tau^{(2)}$ the only non-zero matrix elements are

$$\tau^{(2)}_{n,n-4} = -\alpha^2[n(n-1)(n-2)(n-3)]^{\frac{1}{2}}/\{32w_x(y)^4\}$$

$$\tau^{(2)}_{n,n-2} = -\alpha^2[n(n-1)]^{\frac{1}{2}}/\{4w_x(y)^4\}$$

$$\tau^{(2)}_{n,n} = +\alpha^2[n^2+n+1]^{\frac{1}{2}}/\{16w_x(y)^4\}$$

$$\tau^{(2)}_{n,n+2} = +\alpha^2[(n+1)(n+2)]^{\frac{1}{2}}/\{4w_x(y)^4\}$$

$$\tau^{(2)}_{n,n+4} = -\alpha^2[(n+1)(n+2)(n+3)(n+4)]^{\frac{1}{2}}/\{32w_x(y)^4\}$$

These matrix elements for $\tau^{(2)}_{ij}$ do not agree with those published by T. Tung Nguyen Dang in his work on anharmonically coupled oscillators [12].

3.7 References

1. D. W. Noid, M.L. Kozykowski and R. A. Marcus, Ann. Rev. Phys. Chem., **32**, 267, (1981).

2. S. A. Rice, Advan. Chem. Phys., **47**, 117, (1981).

3. G. S. Ezra, Chem. Phys. Lett., **101**, 259, (1983).

4. J. M. Hutson and B. J. Howard, Mol. Phys., **41**, 1113, (1980).

5. S. L. Holmgren, M. Waldmen and W. Klemperer, J. Chem. Phys., **67**, 4414, (1977).
   D. K. Bondi, J. N. L. Connor, J. Manz and J. Römelt, Mol. Phys., **50**, 467, (1983).
   V. Aquilanti, G. Grossi and A. Lagana, Chem. Phys. Lett., **93**, 174, (1982).

6. J. K. Cashion, J. Chem. Phys., **39**, 1872, (1963).

7. J. G. Frey and B. J. Howard, Chem. Phys., **99**, 427, (1985)

8. R. T. Swimm and J. B. Delos, J. Chem. Phys., **71**, 1706, (1979).

9. D. W. Noid and R. A. Marcus, J. Chem. Phys., **67**, 559, (1977).

10. J. Manz and H. H. R. Schor, J. Phys. Chem., **90**, 2030, (1986).

11. M. S. Child, Molecular Collision Theory, page 89, Academic Press, (1974).

12. T. Tung Nguyen Dang, J. Chem. Phys., **83**, 5019, (1985).

4.   Multigrid Methods

4.1   Introduction

Multigrid methods have been applied in this work to one- and two-dimensional bound state problems which may all be described by second order differential equations. The general form of the equations studied is

4.1.1 $-\nabla^2 u(q) + c(q).u(q) = f(q)$

where q represents the coordinates ((x), or (x,y) in this case), $u(q)$ is the solution, $c(q)$ and $f(q)$ are known functions of the variables q (possibly constants) and ∇^2 represents the laplacian, operating on $u(q)$. Each bound state problem is characterised by known boundary conditions. For the cases under study here, the function $u(q)$ is required to be zero at each boundary point. In order to solve the equation (4.1.1) numerically, the method of finite difference (as introduced in Chapter 2) is used to discretise the problem on an equally spaced grid over the entire coordinate range. To this end, the exact solution, $u(q)$ is replaced by an approximate, discrete solution, $u_i(q)$ at each point on the grid and $f(q)$ and $c(q)$ are replaced by $f_i(q)$ and $c_i(q)$ respectively. The total number of points used to define the discrete solution is given by n and i refers to a specific point on the grid. The choice of appropriate finite difference schemes is discussed in the following section.

The discretisation process leaves a set of n simultaneous equations which may be conveniently expressed in matrix form

4.1.2 $\mathbf{A.u = f}$

A is a symmetric, sparse matrix with dimension (n×n). The system of linear equations denoted by equation (4.1.2) is in a form which may be treated using conventional iterative or relaxation methods [1]. The two iterative methods employed here were those of the Jacobi and Gauss-Seidel iteration schemes. Both schemes begin with an initial approximation, $v_i^{(0)}$ to the discrete solution u_i. In each case the solution vector after the jth iteration, $v_i^{(j)}$ is formed from the

73

previous approximation, $v_i^{(j-1)}$. The error vector, e_i between u_i and the current approximation, $v_i^{(j)}$ may be written in terms of the residual, r_i in the following residual equation (the subscript i is dropped for convenience)

4.1.3 $A.e = r^{(j)} = f - A.v^{(j)}$

The process of finding the residual from equation (4.1.3) is a crucial step in the multigrid method as it is necessary to overcome the shortcomings of the relaxation processes. It can be shown [1] that the standard iterative methods have the property of smoothing out the high frequency (oscillatory) error components of the approximate solution. In achieving this, they have little or no effect on the low frequency components. One way of combating this shortcoming of the relaxation methods is to move the problem onto a coarser grid and to relax on that grid; low frequency error modes appear less smooth, more oscillatory on a coarser grid. This implies that the relaxation methods should now act to smooth out these error components. At this point, it would be prudent to outline the procedure known as the coarse-grid correction scheme which incorporates a two-grid system:

4.1.4   (i)   Relax $\nu 1$ times on $A_k.v_k = f_k$ to obtain an approximation $v_k^{(\nu 1)}$;

           (ii)   Calculate the residual, $r_k = f_k - A_k.v_k^{(\nu 1)}$;

           (iii) Relax or solve $A_{k-1}.e_{k-1} = r_{k-1}$ to obtain the error term e_{k-1};

           (iv)   Correct $v_k^{(\nu 1)}$ via $v_k^{(\nu 1)} = v_k^{(\nu 1)} + e_{k-1}$;

           (v)   Relax $\nu 2$ times on $A_k.v_k = f_k$ to obtain the final approximate solution, $v_k^{(\nu 2)}$.

In the above scheme, the subscript k is now used to refer to the top, finest grid level and k-1 refers to the next coarsest grid. The k-1

grid level has half as many grid points as the level immediately above it. This is the usual convention in multigrid work [1,2]. The application of this procedure depends upon two inter-grid transfer processes. Firstly, the transfer of vectors from a fine grid to a coarse grid is carried out using restriction operators. The one used exclusively here is the injection operator. The process of transferring from coarse to fine grids is by way of interpolation or prolongation operators. Piece-wise linear interpolation was the chosen method in this work. The form of the injection and interpolation operators is outlined in the following section. The definition of these operators is simplified by using grid spacings with a ratio of 2 between adjacent grids.

The successful use of the coarse-grid correction scheme depends upon the ability to solve for the error vector at the coarse grid level, step (iii) of expression (4.1.4). This may not be possible since the problem at this level is akin to that on the finest grid, only with half the number of unknowns. Since the coarse grid problem is not much different from the original problem, it would seem natural to apply the above scheme (4.1.4) to the residual equation. The incorporation of such an idea requires a move from the above two-grid system to a system involving a multiple number of grids. To this end, the multigrid method requires a succession of grid levels, denoted by Ω_k, such that

4.1.5 $\qquad \Omega_k > \Omega_{k-1} > \Omega_{k-2} > \Omega_{k-3} \ldots \Omega_0$

$$\text{and} \quad h_k = \frac{h_{k-1}}{2} = \frac{h_{k-2}}{4} = \frac{h_{k-3}}{8} \ldots \text{etc}$$

where Ω_0 is the coarsest grid and may contain just one interior grid point. In practice, the size of coarsest grid is dependent on the nature of the problem in hand and must be chosen with great care to ensure the stability and convergence of the multigrid scheme. The basic aim of the multigrid procedure is to use standard relaxation techniques to approximate the problem in hand at the top grid level and to smooth out the error components of this approximation by the

judicious use of the coarser grids. The coarse-grid correction scheme can be repeated on successively coarser grids until a direct solution of the residual equation is possible. Once a sufficiently small grid has been reached (see later for details on how this is decided), the equation can be solved very efficiently using gaussian elimination. Having obtained a solution on the coarsest grid, the error/correction component is interpolated onto the next finer grid and is followed by further relaxation. The interpolation and relaxation process is continued until the top grid level is reached. This whole multigrid cycle is known as the V-cycle. The cycle is usually repeated a number of times until satisfactory convergence has been attained.

There are other 'types' of multigrid cycles, all using the same basic elements as the V-cycle described above. These elements are discussed in more detail in the next section. The other cycle used in this work was the full multigrid V-cycle (FMV), which is also known as nested iteration. Nested iteration begins with solving or relaxing on the coarsest grid to generate an improved initial guess for the next finer grid. The problem is then 'solved' at this level using the conventional V-cycle. This serves to generate a better approximation for the next finer grid, on which the V-cycle is once more applied. The FMV-cycle ends with a final V-cycle for the finest grid. The technique of nested iteration was applied to the direct solution of a two-dimensional Schrödinger equation.

Multigrid methods were applied to model problems in one and two dimensions involving perturbed and unperturbed harmonic oscillators. The method of inverse iteration, described in Chapter 2, was combined with the multigrid technique. Multigrid methods were used in place of the solver for the linear inhomogeneous differential equations that occur in this problem. In order to compare the one-dimensional results presented in Chapter 2, the Numerov correction was incorporated into the scheme. This meant that direct comparison with the results obtained using LIDE [3] was possible. In the two-dimensional case, direct comparison of this sort was not available. This is simply because gaussian elimination techniques would require

a large amount of computer storage and indeed cpu time for calculations at the chosen fine grid levels. However, the two-dimensional Numerov correction was derived and used in the calculations. The perturbed harmonic oscillator problem was tackled once more using an approach involving perturbation theory. In this case, Brillouin-Wigner perturbation theory (as outlined in Chapter 2) was the applied scheme. Once again, it was possible to compare the results obtained from the multigrid scheme in one dimension to those obtained using LIDE to solve the same equations. The two-dimensional cases are those presented in Chapters 2 and 3, thus comparisons could be made with these known solutions. The use of multigrid methods is concluded with a direct approach to calculations on the same harmonic oscillator systems. The nested iteration approach of Hackbusch [2] was the applied multigrid method. The efficiency and effectiveness of the multigrid schemes used in all of these applications is discussed. In particular, the key rôle played by the coarse grid level is highlighted. The effect of the number of relaxation iterations on the convergence of each scheme is also discussed.

4.2   The Elements of Multigrid

As outlined, there are only a few basic elements required for numerical analysis using multigrid methods. Firstly, there are the relaxation routines. For the one-dimensional cases, using the discretisation scheme which approximates u(x) to an accuracy of $O(h^2)$, equation(4.1.1) may be written

4.2.1 $-v_{i-1} + 2v_i - v_{i+1} + h_k^2.c_i.v_i = h_k^2 f_i$

where $1 \leq x_i \leq n-1$

with boundary conditions $v_0 = v_n = 0$

For the two-dimensional case, where the (x,y) coordinate system is represented as a square grid with equal spacing, the analogous equation is

4.2.2 $-v_{i-1,j} + 2v_{i,j} - v_{i+1,j} - v_{i,j-1} + 2v_{i,j} - v_{i,j+1}$

$$+ h_k^2 \cdot c_{i,j} \cdot v_{i,j} = h_k^2 f_{i,j}$$

where $1 \leq x_i \leq n-1, \quad 1 \leq y_j \leq n-1$

with boundary conditions $v_{0,0} = v_{0,n} = v_{n,0} = v_{n,n} = 0$

The algebra may be simplified somewhat by considering both systems of equations in matrix form,

4.2.3 $A = D - L - U$

where D_k is the diagonal of the matrix A_k and $-L_k$ and $-U_k$ are the lower and upper triangular parts of A_k respectively. The splitting of the matrix A in this manner allows the definition of the Jacobi and Gauss-Seidel iteration schemes in matrix form. Equations (4.2.1) and (4.2.2) may now be written

4.2.4 $(D - L - U) \cdot v = f$

The subscript, k which serves to signify the grid level has been dropped for the time being. Using this algebra, the Jacobi iteration matrix, P_J may be defined as

4.2.5 $P_J = D^{-1} \cdot (L + U)$

and the overall iteration scheme has the form

4.2.6 $v^{(j)} = P_J \cdot v^{(j-1)} + \omega \cdot D^{-1} \cdot f$

This is in fact the weighted Jacobi method. The weighting constant, ω may be shown to have an optimum value of 0.5 [1]. This was the value used in subsequent calculations. The weighted Jacobi scheme is in such a form as to make use of the vectorising facility of the University IBM 3090 mainframe computer. Despite this however, the algorithm is computationally inefficient in that all of the

components of the new approximation have to be calculated before being used. In the Gauss-Seidel method, components of the approximation are over-written as soon as they are updated. The over-writing process whilst still retaining vectorisation capability, reduces the required computer storage and tends to speed up the iteration routine. The Gauss-Seidel iteration, P_G may be expressed as

4.2.7 $P_G = (D - L)^{-1}.U$

and the iteration scheme has the form

4.2.8 $v^{(j)} = P_G.v^{(j-1)} + (D - L)^{-1}.f$

The red-black Gauss-Seidel method [1,2] was used in this work for equations in the form given by (4.2.1) and (4.2.2). This method makes use of the fact that odd and even elements of the defined grid are never accessed simultaneously. Thus, the odd and even components are updated in separate relaxation sweeps. Algorithms of this sort would have a distinct advantage over normal methods when implemented on parallel processors.

Higher order discretisation schemes may be used to improve on the accuracy of the finite difference approximations. However, these schemes increase the number of calculations to be performed by reducing the sparsity of the matrix A and complicating the necessary relaxation routines. In Chapter 2, it was shown that the introduction of the Numerov correction improved the overall accuracy to $O(h^4)$, without increasing the extent of the calculation. The one-dimensional Numerov correction can be seen to be directly applicable to equation (4.2.1). For the two-dimensional case, a different discretisation scheme is required. The scheme in question, which still approximates the second order differentials to $O(h^2)$ is the following nine-point scheme

4.2.9 $\quad (1/6)\{-(v_{i-1,j-1} + v_{i-1,j+1} + v_{i+1,j-1} + v_{i+1,j+1})$

$$-4(v_{i,j-1} + v_{i,j+1} + v_{i-1,j} + v_{i+1,j}) + 20v_{i,j}\}$$

$$+ h_k^2 . c_{i,j} . v_{i,j} = h_k^2 . f_{i,j}$$

The two-dimensional Numerov correction (as derived in Chapter 2) takes the form

4.2.10 $\quad Y_{i,j} = [1 - (h_k^2/12)c_{i,j}]v_{i,j} - (h_k^2/12)f_{i,j}.$

Following the discussion in Chapter 2, the final equation to be solved is written

4.2.11 $\quad (1/6)\{-(Y_{i-1,j-1} + Y_{i-1,j+1} + Y_{i+1,j-1} + Y_{i+1,j+1})$

$$-4(Y_{i,j-1} + Y_{i,j+1} + Y_{i-1,j} + Y_{i+1,j}) + 20Y_{i,j}\}$$

$$= h_k^2 . c_{i,j} . \frac{Y_{i,j}}{F_{i,j}} + h_k^2 . \frac{f_{i,j}}{F_{i,j}}$$

where $\quad F_{i,j} = 1 - (h_k^2/12)c_{i,j}$

Equation (4.2.11) is now solved for $Y_{i,j}$ and the 'real' solution is obtained by transforming back to the original function $v_{i,j}$ using expression (4.2.10).

The other multigrid elements remaining to be listed are those of the restriction and prolongation operators. In order to transfer between different grids, it is necessary to define explicitly the grids involved in the inter-grid processes. In the expressions that follow, the grid levels are now denoted by the superscripts involving k. The weighted restriction operator (denoted by r in later use), employed in the fine to coarse grid transfers was

4.2.12 $\quad v_i^{k-1} = (1/4)\{v_{2i-1}^k + 2v_{2i}^k + v_{2i+1}^k\}$

in one dimension, and in two dimensions,

4.2.13 $\qquad$ $v_{i,j}^{k-1} = (1/16)\{v_{2i-1,2j-1}^{k} + v_{2i-1,2j+1}^{k} + v_{2i+1,2j-1}^{k} + v_{2i+1,2j+1}^{k}$

$$+ 2(v_{2i,2j-1}^{k} + v_{2i,2j+1}^{k} + v_{2i-1,2j}^{k} + v_{2i+1,2j}^{k}) + 4v_{2i,2j}^{k}\}$$

Linear interpolation (given by the prolongation operator, p) was exclusively used for coarse to fine grid transfers and has the one-dimensional form

4.2.14 $\qquad$ $v_{2i}^{k} = v_{2i}^{k-1}$ for even terms, and

$$v_{2i+1}^{1} = (1/2)\{v_{i}^{k-1} + v_{i+1}^{k-1}\} \quad \text{for odd terms}$$

In two dimensions, the interpolation operator is the nine-point operator given by

4.2.15 $\qquad$ $v_{2i,2j}^{k} = v_{i,j}^{k-1}$

$$v_{2i+1,2j}^{k} = (1/2)\{v_{i,j}^{k-1} + v_{i+1,j}^{k-1}\}$$

$$v_{2i,2j+1}^{k} = (1/2)\{v_{i,j}^{k-1} + v_{i,j+1}^{k-1}\}$$

$$v_{2i+1,2j+1}^{k} = (1/4)\{v_{i,j}^{k-1} + v_{i+1,j}^{k-1} + v_{i,j+1}^{k-1} + v_{i+1,j+1}^{k-1}\}$$

All the necessary elements which make up the building blocks for the multigrid method of calculation have now been presented. The next sections are devoted to their applications to the problems outlined in the introduction.

In all of the calculations that follow, the smoothing algorithms were applied on both the downward and upward slopes of each V-cycle. The number of relaxation iterations on the downward slope (pre-smoothing) is given by ν_1 and the number of iterations on the upward slope (post-smoothing) is denoted by ν_2.

4.3 Inverse Iteration

The method of inverse iteration, as described in section 2.3, was applied to systems involving harmonic oscillators in one and two dimensions using the multigrid approach. The one-dimensional hamiltonian (in the units denoted by u) employed here was that used as an example problem in the same section on inverse iteration

$$4.3.1 \qquad H = -\tfrac{1}{2}\frac{d^2}{dx^2} + \tfrac{1}{2}\omega_x^2 x^2,$$

where $\qquad \omega_x^2 = 1.0u$

with the solution being

$$4.3.2 \qquad E_n = n + 0.5u$$
$$n = 0,1,2,..$$

The two-dimensional problem was once again a pair of coupled oscillators described by the hamiltonian

$$4.3.3 \qquad H = h_x + h_y + \tfrac{1}{2}\alpha x^2 y^2$$

where h_x and h_y are the unperturbed harmonic oscillator hamiltonians and ω_x and ω_y were chosen such that

$$4.3.4 \qquad \omega_x + \omega_y = 2.0u$$

In both cases, the equation to be solved is of the form

$$4.3.5 \qquad (H - E_{corr})\Psi_{new} = \Psi_{old}$$

where E_{corr} is the energy shift from the initial energy guess E_0. Ψ_{old} is initialised with an appropriate guess and the required energy, E is updated after each iteration by calculating

4.3.6　　　　$E_{corr} = \dfrac{\langle \Psi_{new} | \Psi_{old} \rangle}{\langle \Psi_{new} | \Psi_{new} \rangle}$

and

4.3.7　　　　$E = E_0 + E_{corr}$

Each multigrid calculation involved a choice of relaxation routine and multigrid cycle. Relaxation was carried out using either the Jacobi or Gauss-Seidel smoothing routines. The choice of multigrid cycle was between the V- and FMV-cycles. The Numerov correction in one and two dimensions was incorporated throughout. The use of different 'competing' multigrid elements enabled comparisons to be made of the computational timing and efficiency of these various routines.

Results for the One-Dimensional Problem

The first major problem encountered in the set up of any multigrid calculation on systems governed by an operator which is non-positive definite in character is over the tightness of the coarsest grid level. The number of points chosen at this level is closely allied to the range encompassed by the grid used to define the problem. In any quantum mechanical calculation, the ideal range of this grid is that of infinite size. For the purpose of seeking numerical solutions, this is impracticable. The theoretician is thus left with the task of applying artificial bounds to problems whose solutions are not simple, known mathematical forms. In most one-dimensional problems, this does not represent a great problem; it was shown in Chapter 2 that the solution of the radial Schrödinger equation is readily affected for eigenfunctions with many nodes to an acceptable degree of accuracy. In multigrid calculations however, the coarsest grid must contain enough points to include the troublesome low frequency components of the error to the solution. It is these low frequency components that are responsible for the divergence of multigrid schemes [4].

In order to make direct comparisons with the results obtained

using LIDE [3], presented in section 2.3, a zeroth-order vibrational frequency of $\omega_x = 1$ was employed with an initial radial range of 0.0 to 16.0 au. To attempt to find a suitable coarsest grid size, a set of parameters for the various multigrid elements was chosen and the number of points on this grid was varied from 8 up to 64. Some of the results of these calculations are presented in Table I. The chosen multigrid scheme for these calculations consisted of the Gauss-Seidel relaxation routine (the number of smoothing iterations was actually given by $\nu_1 = \nu_2 = 2$) and incorporated the multigrid V-cycle. The maximum number of allowed iterations for the inverse iteration scheme was set at 20 cycles. It can be seen that as the number of points on the coarsest grid is increased, more of the higher frequency converged eigenvalues are obtained. These eigenvalues have converged to the required precision ($\pm 1.0 \times 10^{-06}$). The important point to note from these results is that to obtain converged eigenvalues whose eigenfunctions contain more than two or three nodes requires a coarse grid size in excess of 30 points. Alternatively, the radial range could be shortened to allow a better coverage of the grid with fewer points. To do this however would result in a loss of accuracy for the higher energy eigenvalues - a veritable 'catch-22' situation. Table II gives examples of a scheme whereby the number of points on the coarsest grid is fixed at a reasonably low value and the radial range is reduced. The number of points on this grid was fixed at 16 and the radial range is shortened by degrees from 16.0 to 8.0 au. As predicted, more eigenvalues were obtained on the tighter radial grids than at the outermost limit but the accuracy of these values decreases accordingly.

The other parameters that can have considerable effects on the convergence/divergence of a multigrid scheme are those that control the number of relaxation iterations, ν_1 and ν_2 (both of the smoothing parameters were usually assigned the same value in ensuing calculations). For a problem with fixed radial range and coarsest grid level, calculations were made whereby the number of pre-smoothing steps, ν_1 was varied from 1 to 6. The resulting eigenvalues are listed in Table III. These results indicate that the optimum number of smoothings was 2 or possibly 3 for this system.

Figure I

Comparative timings for the competing multigrid FMV-cycle (upper curves) and V-cycle (lower curves). The upper curve in each couplet refers to timings from the Jacobi routine and the lower curve refers to the Gauss-Seidel iteration. The timings represent an average value for the successful application of the multigrid cycle to the one-dimensional inverse iteration problem to produce one eigenvalue.
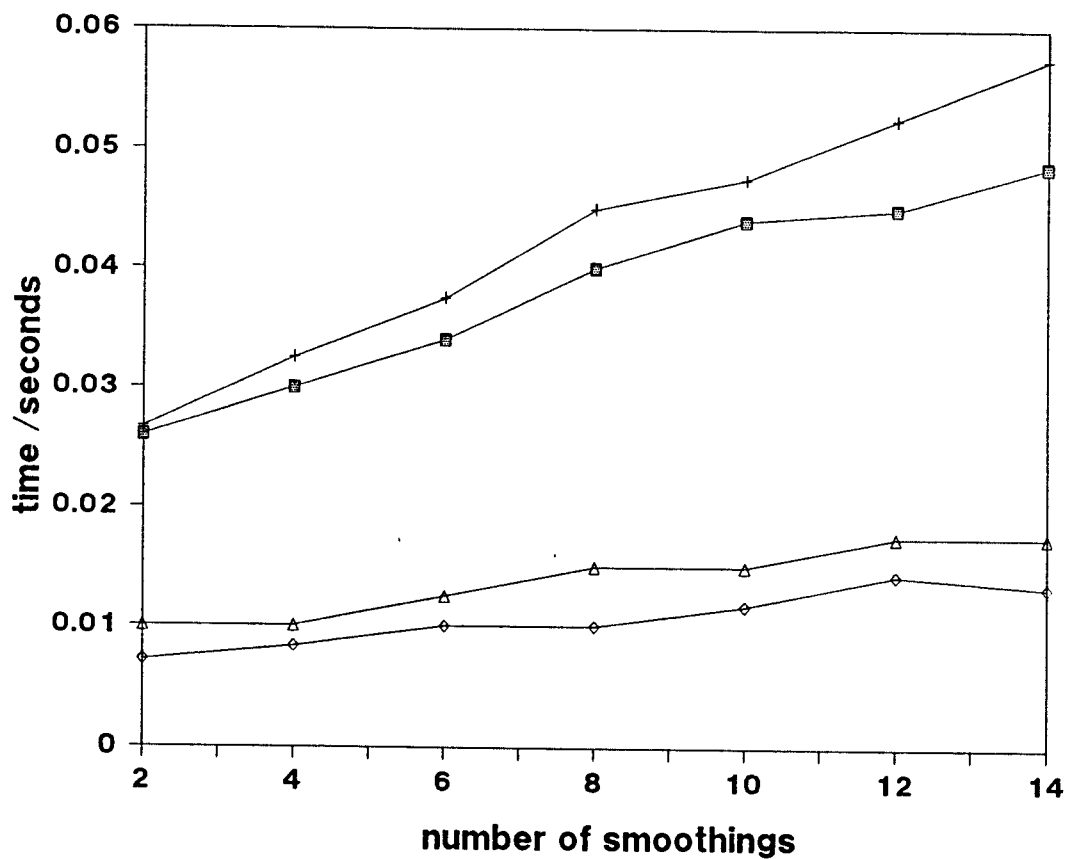
Further relaxation steps served to destabilize the multigrid scheme. It has been shown in past work by Nicolaides that excessive applications of the smoothing algorithm can drive up the low frequency error components to the point where the coarse grid corrections cannot control them [5]. For this reason, in most of the subsequent multigrid calculations, the number of smoothing iterations was set at $\nu_1 = \nu_2 = 2$.

Figure I is designed to give an indication of the relative computational times taken by the alternative multigrid elements. A suitable set of parameters was chosen and the time (in cpu seconds) taken by multigrid schemes involving the V- and FMV-cycle and the Gauss-Seidel and Jacobi smoothing algorithms was recorded. The Gauss-Seidel routine is seen to be computationally faster than the Jacobi method. This is seen to be the case since the Gauss-Seidel algorithm is able to make better use of the vectorisation capabilities of the Southampton University IBM 3090-150 mainframe computer. The multigrid V-cycle has proved to be much more computationally efficient than the FMV-cycle in this particular case. This observation can be attributed to the nature of the inverse iteration process. The wavefunctions calculated on each iteration, Ψ_{new} are only approximations to the required solution and are immediately updated on the next iteration. Thus it is not strictly necessary to utilise the usually much more accurate and reliable FMV-cycle in this problem as the iteration process itself produces converged functions.

Results for the Two-Dimensional Problems

The above one-dimensional problem has served to highlight the many problems associated with the application of multigrid methods to indefinite problems. The two-dimensional scheme is faced with similar problems to be overcome, but there is now a further limitation; the computational size of the problems. To solve directly on a coarse grid of dimension (16 by 16), requires the set up and storage of an array of size (256 by 256). The next highest coarse grid, (32 by 32) will produce an array of size (1024 by 1024).

The repeated use of gaussian elimination techniques on arrays of this magnitude would require the use of supercomputers to be run at all efficiently. Unfortunately, because these matrices are non-positive definite, the standard FORTRAN-NAG routines for solving these systems must incorporate the matrix in its original full form. Whilst the use of supercomputers is by no means an impossibility, the solution of the problems in hand would now be affected by expensive, brute force numerical methods. One of the original aims of multigrid schemes was to provide fast and cheap solutions using elegant and simple algorithms. With this in mind, the approach followed in all of the calculations on two-dimensional systems was to explore the limitations of the multigrid method without resorting to large calculations on not-so-coarse grids.

Once again, the system of a pair of coupled oscillators was used to test the multigrid scheme incorporating inverse iteration. The three systems used were (in the units given by u)

$$4.3.8 \qquad \text{Case A;} \qquad \omega_x^2 = 1.69u, \ \omega_y^2 = 0.49u$$

$$\text{Case B;} \qquad \omega_x^2 = 1.21u, \ \omega_y^2 = 0.81u$$

$$\text{Case C;} \qquad \omega_x^2 = \omega_y^2 = 1.0u.$$

In all calculations on these systems, the direct solution was performed on a coarse grid of (16 by 16) points. The Gauss-Seidel algorithm was employed with $\nu_1 = \nu_2 = 2$ and the multigrid V-cycle was the chosen scheme. The domain of the two-dimensional grid was varied together with the coupling parameter, α.

Table IV contains the first few obtained eigenvalues for the above three cases as a function of α and range of the (x,y) grid. As the (x,y) domain is tightened, the number of observed eigenvalues increases. This is as to be expected from the preceding one-dimensional calculations. The converged eigenvalues have not achieved the precision of accuracy to six significant figures. This is because the highest grid level was fixed at (128 by 128) points

and the step-size over the grid, h is correspondingly large. However, the obtained accuracy is of the order of h^4 and can be attributed to the incorporation of the 2D Numerov correction in the multigrid scheme. The convergence that has been attained by the method is acceptable for step-sizes of the magnitude employed. Even though the scheme was artificially limited by the size of the coarsest grid, the first two or three eigenvalues in each chosen system were obtained. The use of a degenerate system did not seem to pose any more problems than the non-degenerate cases. It was shown in Chapter 3 that the occurrence of accidental degeneracies resulted in the breakdown of the perturbation scheme used to correct for the use of the Born-Oppenheimer approximation as applied to the systems under consideration here. More extensive calculations are required to establish whether such problems would not occur in this method of calculation.

The use of multigrid methods coupled with inverse iteration does allow direct calculations to be made of considerably-sized systems of chemical interest. The two-dimensional form of equation (4.3.5) could in principle be solved directly by gaussian elimination, as was the case in Section 2.5. However, for the fine grid level of (128 by 128) points chosen here, the direct solver would require the set up of a matrix with (16384 by 16384) points. The storage of such an array is not in the realms of computers such as the CRAY XMP-48. Thus, multigrid schemes do have considerable applications in such cases as they have the effect of reducing the magnitude of the problem to more manageable forms.

4.4 Brillouin-Wigner Perturbation Theory

The Brillouin-Wigner perturbation scheme is another example of a quantum mechanical problem that may be solved using the methods of multigrid. Calculations were carried out in one and two dimensions, with systems of perturbed oscillators once more at the source of the problems. The perturbation/iteration scheme used here is that described in Chapter 2 and the equation to be solved for the wavefunction correction is

4.4.1 $\qquad (E - H_0)|\phi> = P.H_1|\psi>$

where E is the energy with corresponding wavefunction ψ, ϕ is the wavefunction correction (orthogonal to ϕ), P is the projection operator (to ensure the orthogonality of ϕ) and H_1 is the perturbation, given by

4.4.2 $\qquad H_1 = \alpha x^4 \qquad$ in the 1-D case

and

$\qquad H_1 = \alpha x^2 y^2 \qquad$ in the 2-D cases

The energy correction is given by

4.4.3 $\qquad E = E_0 + <\psi_0|H_1|\psi>$

The appropriate Numerov corrections were incorporated in both cases. In the one-dimensional case, this enabled comparisons to be made between results obtained from the multigrid scheme and from the routine LIDE [3] for which equation (4.4.1) is in the correct form. For the two-dimensional system, a pair of coupled oscillators was once again used to test the capabilities of the multigrid method for such a scheme. The Numerov-Cooley method [6] was used throughout to obtain the unperturbed 'exact' one-dimensional solutions.

Equation (4.4.1) was solved using the various multigrid elements as described earlier in this chapter. In the example problem of section 2.5, the direct solution of equation (4.4.1) was attempted for a two-dimensional problem. These calculations were limited by the magnitude of the array of inhomogeneous differential equations (a problem comparable to that discussed above in the section on the method of inverse iteration). A more extensive study of the application of multigrid methods with Brillouin-Wigner perturbation theory is possible for the above one-dimensional and two-dimensional problems. As a detailed comparison between the relaxation routines and multigrid cycles was given in Section 4.3, the optimum multigrid scheme for the current problem is simply

presented here. A few preliminary calculations were enough to establish that the best scheme consisted of the Gauss-Seidel algorithm (once again with $\nu_1 = \nu_2 = 2$) and the FMV-cycle. This optimisation applied in both one and two dimensions.

Results for the One-Dimensional Problem

In the one-dimensional case, it was possible to obtain direct solutions to equation (4.4.1) using LIDE [3]. This enabled a detailed comparison to be made between the multigrid approach and the more conventional direct solvers. Table V is designed to give such a comparison of results. The unperturbed hamiltonian was that employed in the radial harmonic oscillator problem involving inverse iteration, where the vibrational frequency is given by $\omega_x^2 = 1$ with zeroth order energies given by

4.4.4 $E_n = (n + 0.5), \quad n = 0,1,2,\ldots$

The value of the perturbation constant, α ranged from 0.05 to 0.35. It was found that a value of 0.3 for α resulted in a 25% increase in the ground state energy from the zeroth order value. Such a large perturbation proved enough to destabilise the perturbation scheme itself and was therefore not suitable for testing the multigrid scheme. Perturbations of this magnitude were also observed to destabilise the direct approach to the problem.

As was found in the inverse iteration case, the number of observed eigenvalues was very much dependent on the nature of the coarsest grid. The number of points allowed on this grid was chosen to relinquish the first few perturbed energy levels. The number of iterations required to converge these eigenvalues is presented in Table V. The converged eigenvalues are seen to be in agreement with those obtained from the direct approach. The perturbation scheme itself appears to be effective for eigenvalues with relatively few nodes, becoming less efficient for higher energies. This problem can in part be attributed to the choice of coarsest grid but not entirely. The direct approach using LIDE also has difficulties in

converging the higher order energy levels. The problem of achieving convergence increases as the magnitude of the perturbation is increased. Overall, these calculations have indicated that multigrid methods are indeed a viable alternative to conventional mathematical solvers, when used with the appropriate coarsest grid level.

Results for the Two-Dimensional Problems

The two-dimensional systems under consideration here are usually solved by indirect methods which involve the uncoupling of variables as was the case in Chapter 3. Once again, a multigrid procedure is applied to a problem to reduce the need for large amounts of computational storage as would be required for a direct numerical approach. However, the resident problem of having to solve the necessary equation on the coarsest grid is still to be overcome. Even though this may limit the full extent of the calculation (as was the case above), the multigrid approach does enable the calculation to be performed on these perturbed systems for the first few eigenvalues and eigenvectors. The capabilities of the scheme when applied to the three cases given in expression (4.3.8) are outlined in Table VI.

The results presented in Table VI confirm all that has already been stated about the use of two-dimensional multigrid schemes. For small perturbations, there is good agreement between the first couple of eigenvalues and the results obtained using the method of secular equations. Given the radial step-size employed in these calculations, these values are accurate to $O(h^4)$. The effectiveness of the iteration scheme is seen to diminish as the size of the perturbation is increased. Once again, the major limitation on these calculations was the allowable size of the coarsest grid and so an extensive set of calculations was not possible.

4.5 Direct Multigrid Approach to a Two-Dimensional Eigenvalue Problem

Introduction

In the previous section on Brillouin-Wigner perturbation theory, an indication was made of the usefulness of projection operators in quantum mechanics. In the direct approach to the eigenvalue problem described by Hackbusch [2], the projection operator once more plays an important rôle in attempts to stabilise the multigrid algorithm. As discussed earlier in Chapter 1, the standard multigrid methods are not suitable for indefinite problems such as those defined by Schrödinger's equation. This is illustrated in the work of Grinstein et al. [6] on a model two-dimensional scattering problem. In this paper, they discuss the limitations of the Gauss-Seidel method of relaxation showing that this scheme is indeed divergent for non-positive definite operators. The problem of divergence is avoided by performing a direct solution on the carefully-chosen coarsest grid. Their multigrid algorithm proved efficient for problems with relatively small domains and for eigenvalues of low energy. However, as the domain of the problem was increased and higher energies were sought, finer grids were required for a stable, convergent scheme. This problem has already been encountered in the present work in both the inverse iteration and perturbation theory approaches.

Hackbusch's method [2] is also reliant on finding a solution (not necessarily exact) at the coarsest grid level but, stability is enhanced by a further constraint. The correction term to be found after relaxation is constrained to be orthogonal to the approximate solution already calculated for that level. This solution itself is obtained by the application of standard relaxation techniques to the eigenvalue problem. The multigrid algorithm employed here is based on the nested iteration, FMV-cycle and incorporates the orthogonalisation step where appropriate. The various elements of this method are outlined below.

A Multigrid Scheme for the Eigenvalue Problem

The multigrid scheme used to directly solve the two-dimensional Schrödinger equation may be best described in terms of a quasi-FORTRAN algorithm. Such an algorithm is given in Figure II and follows that of Hackbusch [2]. The problem under consideration may be cast in the form

$$4.5.1 \qquad L_k e_k = \lambda_k e_k,$$

where the subscript k refers to the grid level, L is the hamiltonian and e is the eigenvector solution with corresponding eigenvalue denoted by λ. The scheme as outlined in Figure II is based on the method of nested iteration. The starting point for the calculation is therefore an approximate solution for the coarsest grid level, given by $k = 0$. The subroutine FMGM is responsible for providing the initial guesses and is thus used to set up the problem. This approximate solution may be represented by e_0'. The eigenvalue approximation corresponding to e_0' is calculated by means of the Rayleigh quotient

$$4.5.2 \qquad \lambda_0' = \frac{\langle e_0' | L_0 | e_0' \rangle}{\langle e_0' | e_0' \rangle}$$

In subsequent usage, the Rayleigh quotient will be expressed in the form $\Lambda_k(e_k')$. The next stage of the calculation involves the transfer of the approximation, e_0' to form an approximate solution at the next finest grid level. This interpolation process is carried out by means of the nine-point prolongation operator, p,

$$4.5.3 \qquad e_k' = p \cdot e_{k-1}'.$$

The final step in this set-up phase is to zero the solution vector for the grid below the current level. Next, the routine EMGM is used to provide an improved approximation at the current grid level. The actual number of calls to this routine, n_i depends on the problem in hand; values of $n_i > 2$ may serve to render the algorithm unstable.

Figure II

Quasi-FORTRAN code for the multigrid solution of the Schrödinger equation.

```
Subroutine FMGM ; nested iteration for solving (4.5.1), with 0≤k≤k_max
        do 10 k = 1,k_max
```
$$e'_{k-1} = \frac{e_{k-1}}{<e'_{k-1}|e'_{k-1}>}$$
$$\lambda'_{k-1} = \Lambda_{k-1}(e'_{k-1})$$
$$e'_k = p.e'_{k-1}$$
$$e_k = 0$$
```
        do 20 i = 1,n_i
20      call EMGM(k,e'_i)
10      continue
```

```
subroutine EMGM(k,e'_k) ; takes e^i_k as input and gives e^{i+1}_k as output
```
$$\lambda'_k = \Lambda_k(e'_k)$$
$$e'_k = S^\nu_k(\lambda'_k;e'_k)$$
$$d_{k-1} = Q_{k-1}.r.(L_k-\lambda'_k.I).e'_k$$
```
        do 10 j = 1,n_j
10      call SMGM(k-1,v_{k-1},f_{k-1})
```
$$e'_k = e'_k - p.v_{k-1}$$

```
subroutine SMGM(m,v_{k-1},f_{k-1}) ; returns the correction at level k-1
        do 10 k = m,1,-1
```
$$v_k = S^\nu_k(\lambda'_k;e'_k;f_k)$$
$$d_{k-1} = Q_{k-1}.r.(L_k-\lambda'_k.I-f_k)$$
$$v_{k-1} = 0$$
```
10      continue
(solve at level k = 0)
```
$$v_0 = (L_0-\lambda'_0.I)^{-1}.d_0$$
```
        do 20 l = 1,m
20      v_k = v_k - p.v_{k-1}
```

The first task of EMGM is to calculate an eigenvalue approximation for the given eigenvector, e_k'. Standard Jacobi or Gauss-Seidel relaxation techniques are then applied to this function. This smoothing step is described by

4.5.4 $\qquad e_k' = S_k^\nu(\lambda_k'; e_k'),$

where the number of smoothing iterations, ν is also dependent on the chosen problem. Once again, a value of ν greater than 2 may cause problems. When λ coincides with the exact discrete eigenvalue, λ_k, the smoothing step leaves the solution vector, e_k' unchanged. In normal circumstances, after one or two iterations, it is necessary to seek the coarse-grid correction. This takes the form of the defect, d_k, which may be written

4.5.5 $\qquad d_k' = (L_k - \lambda_k'.I).e_k'$

At this point, the approximation, e_k' is split into the following sum

4.5.6 $\qquad e_k' = \alpha.e_k + v_k,$

where v_k is orthogonal to the required solution. This is analogous to the expression of the new system wavefunction in the Brillouin-Wigner perturbation scheme (equation (2.4.2) in Chapter 2). The projection operator, Q_k is used to project out the component of d_k orthogonal to the current approximation, e_k

4.5.7 $\qquad d_k = Q_k.d_k = (L_k - \lambda_k'.I).v_k'.$

The correction term is then calculated using the restriction operator, r

4.5.8 $\qquad d_{k-1} = Q_{k-1}.r.(L_k - \lambda_k'.I).$

Having obtained an approximate correction on the grid level given by k-1, the algorithm proceeds in true multigrid style down to the coarsest grid, k = 0. To this end, the subroutine SMGM is simply the

95

normal V-cycle, incorporating the multigrid elements already discussed in this chapter. These cycles may also be called a number of times (n_j) for each of the V-cycles that form the overall, FMV-cycle. Once a solution has been attained at level 0 (by standard gaussian elimination techniques), the routine SMGM is able to return the correction at level k-1. This enables the subroutine EMGM to return an improved approximation at the originally called level, k.

It can be seen that there are a number of parameters to be varied in order to optimize the code. The achievement of such an optimisation may not be enough to ensure a stable algorithm. The successful application of multigrid schemes to indefinite problems such as those under consideration here has already been shown to be greatly dependent on the choice of coarsest grid. The following example problem of a pair of coupled oscillators serves to bring to the fore the importance of choosing the correct parameters, of which the size of the coarsest grid is the most important.

Results

Once again, the test problem was chosen to be a pair of coupled oscillators. The three cases studied have already been outlined in Section 4.3 on the multigrid application of the method of inverse iteration. As with the two previous two-dimensional examples, the computational scope of the problem was greatly restricted by the maximum allowed size of the coarsest grid. The size of this grid was fixed with dimensions (16 by 16) for reasons already outlined. Because of the restrictions on computational size, the scheme could only produce the first couple of eigenvalues in each of the test cases to any reasonable accuracy. Initially, the number of pre-smoothing cycles, ν_1 was restricted to a value of 2 to ensure that at least two or three eigenvalues were returned. The results of these calculations are given in Table VII.

The values given in Table VII are not at first sight, very accurate. From previous calculations, good convergence of at least the ground state level has come to be expected. It was found that

the ground state energies could be prompted to converge by simply increasing the number of smoothing iterations, ν_1. Figures III and IV contain convergence plots for the three cases under consideration as a function of increasing ν_1. It can be seen that by $\nu_1 = 14$, the ground state energies have converged to the expected accuracy of $O(h^4)$. Unfortunately, the use of this number of smoothing iterations results in the breakdown of the whole scheme when applied to the other eigenvalues. However, the converged values are in good agreement with those obtained in the two previous sets of calculations. These values were not, however obtained using the 2D Numerov correction as in the preceding calculations. The application of this correction to the direct approach to the eigenvalue problem was hindered by the necessity of updating the energy correction, λ_k' at various stages in the calculation. The finite difference scheme employed on these calculations was a nine-point scheme which approximates the second order derivatives to an accuracy of $O(h^4)$.

As regards to the optimisation of the code, it was found that the most stable schemes were obtained when the parameters n_i, n_j and ν were all assigned a value of 2. For the ground state eigenvalues, the number of smoothing operations, given by ν could be increased to as large a value as 14 without disrupting the stable algorithm. In general, values of greater than 2 for all of these parameters served to render the algorithm unstable.

Figure III

Ground state convergence plots for the direct multigrid approach to the coupled oscillator problem for case A (upper) and case B (lower) with $\alpha = 0.1$ against number of pre-smoothing iterations, ν_1.
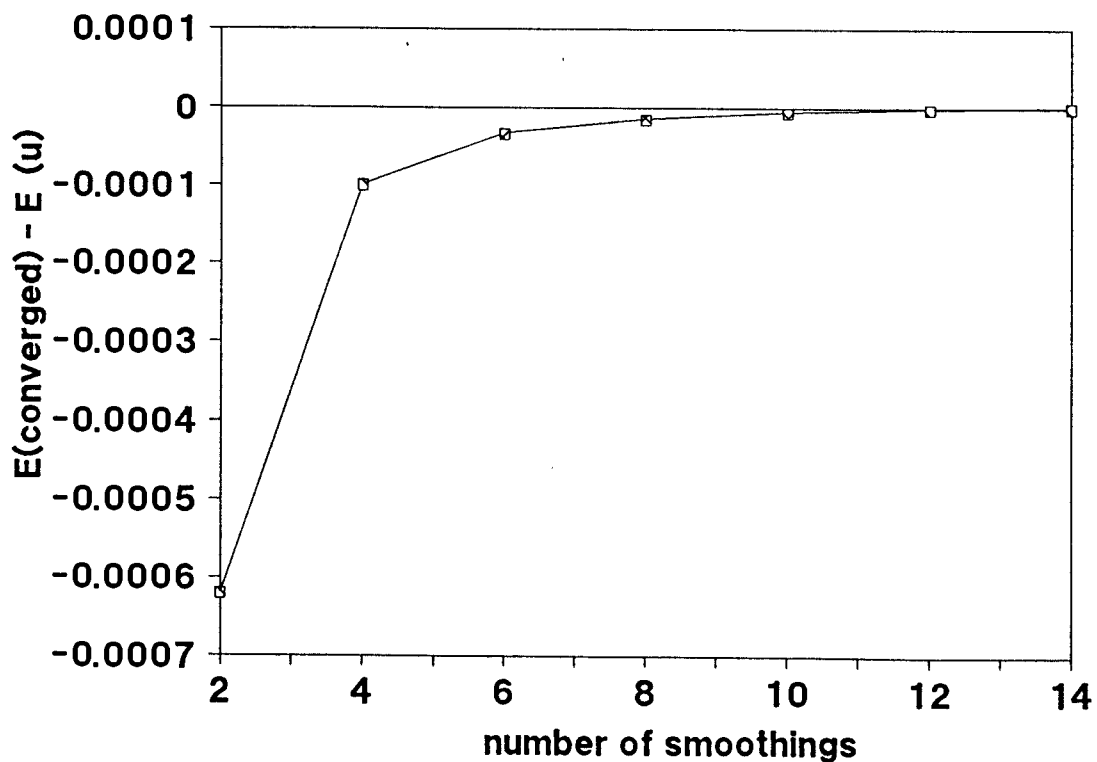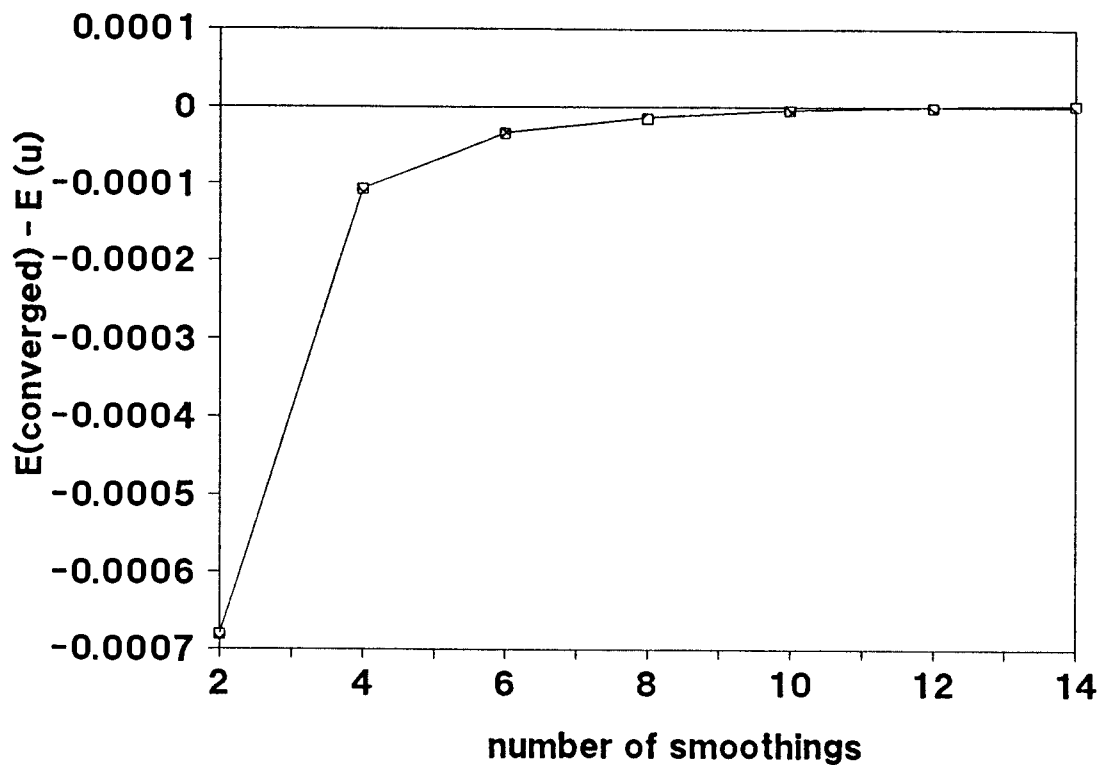
Figure IV

As for Figure III for case C.
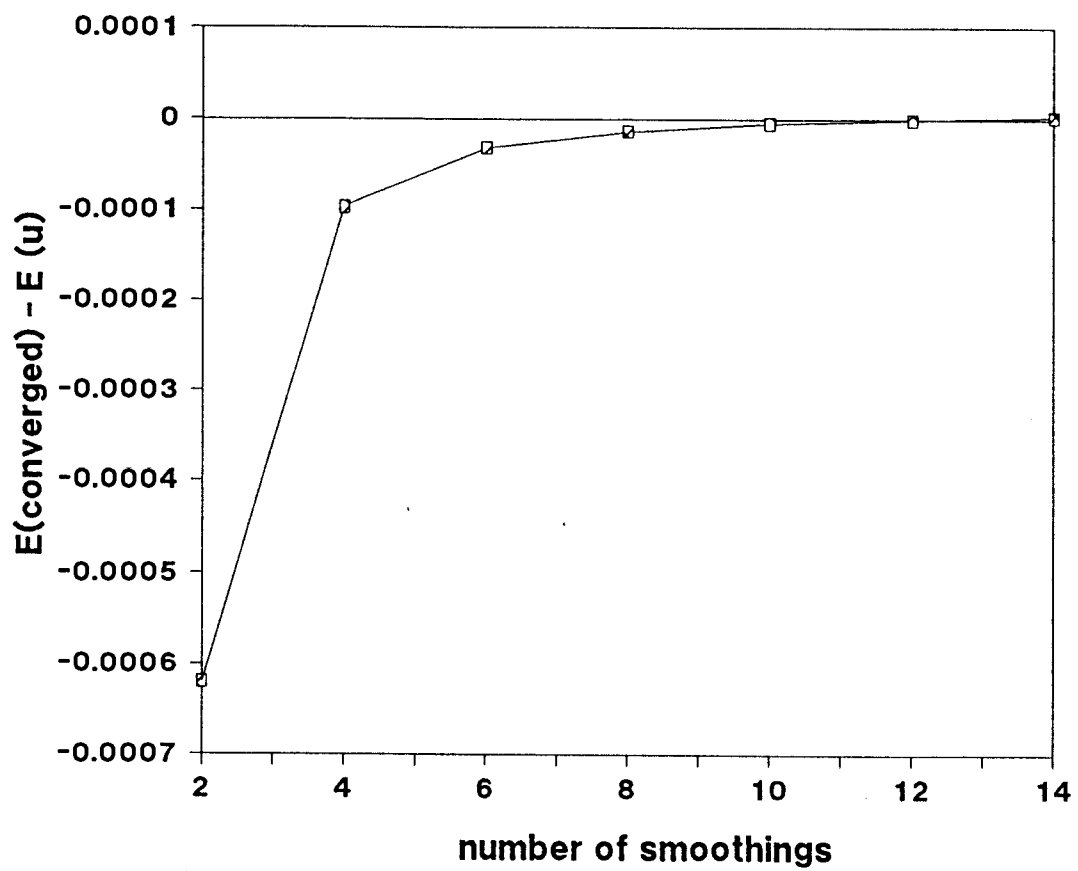
4.6   Conclusions

The results in this chapter have shown that multigrid techniques can be used for a system governed by a non-positive definite operator. The schemes themselves have to be applied with due caution and in the examples given here are only successful when the problem is solved on a suitable coarse grid. The necessity of having to solve exactly at this level stems from the inefficiency of the standard relaxation routines. The Gauss-Seidel and Jacobi smoothing processes are seen to be stable when they are not called upon to do too much work. The Gauss-Seidel scheme is, in general more efficient than the weighted Jacobi method with an optimum value of 2 for the number of smoothing cycles. However, it was also shown in the direct multigrid approach to the Schrödinger equation that provided the algorithm is stable, many iterations of the smoothing algorithm may be possible.

The two-dimensional Numerov correction was successfully employed in the multigrid schemes involving inverse iteration and Brillouin-Wigner perturbation theory. The accuracy of the results obtained using the appropriate correction terms was shown to be of the order of h^4. It has also been shown that multigrid schemes can be applied to the direct calculation of eigenvalues in two-dimensional problems. The performance of this direct approach is limited by computer memory problems and the need for an efficient method of solving the problem at the coarsest level. If the size of the problem at this level could be reduced, the way would be open for wider applications of the scheme. These applications would include problems of increased dimensionality.

Table I

Results obtained from the combined methods of inverse iteration
and multigrid as applied to a one-dimensional harmonic oscillator
(with vibrational frequency, $\omega = 1$). The radial range size is set at
0.0 to 16.0 u and the number of points on the coarse-grid level is
varied from 8 to 64. The number of points at the finest level is
fixed at 512. Gauss-Seidel relaxation was employed ($\nu_1 = \nu_2 = 2$) with a
multigrid V-cycle scheme. E_{guess} is the intial eigenvalue and E_{iter} is
the value obtained from the iterative scheme.

Calculations for a coarse grid of 8 points

Ψ_{old} symmetric

N_{it}	E_{guess}	E_{iter}	ERROR
No observed eigenvalues			

Ψ_{old} antisymmetric

N_{it}	E_{guess}	E_{iter}	ERROR
6	0.800	1.500004	0.000004

Calculations for a coarse grid of 16 points

Ψ_{old} symmetric

N_{it}	E_{guess}	E_{iter}	ERROR
5	0.800	0.499997	0.000003

Ψ_{old} antisymmetric

N_{it}	E_{guess}	E_{iter}	ERROR
6	0.800	1.500000	0.000000

Calculations for a coarse grid of 32 points

Ψ_{old} symmetric

N_{it}	E_{guess}	E_{iter}	ERROR
5	0.800	0.500000	0.000000
13	1.800	2.501204	0.001204
5	2.800	2.499992	0.000008

Ψ_{old} antisymmetric

N_{it}	E_{guess}	E_{iter}	ERROR
6	0.800	1.500000	0.000000
5	1.800	1.500000	0.000000
11	2.800	3.500134	0.000134

Table I continued

Calculations for a coarse grid of 64 points

Ψ_{old} symmetric				Ψ_{old} antisymmetric			
N_{it}	E_{guess}	E_{iter}	ERROR	N_{it}	E_{guess}	E_{iter}	ERROR
5	0.800	0.500000	0.000000	6	0.800	1.500000	0.000000
12	1.800	2.499993	0.000007	5	1.800	1.500000	0.000000
5	2.800	2.500000	0.000000	11	2.800	3.499998	0.000002
12	3.800	4.500158	0.000158	5	3.800	3.500000	0.000000
5	4.800	4.500000	0.000000	11	4.800	5.499997	0.000003
12	5.800	6.500502	0.000502	5	5.800	5.499999	0.000001
5	6.800	6.499999	0.000001	11	6.800	7.499993	0.000007
12	7.800	8.501069	0.001069	5	7.800	7.499998	0.000002
5	8.800	8.499998	0.000002	11	8.800	9.499976	0.000024
12	9.800	10.501962	0.001962	5	9.800	9.499996	0.000004

Table II

As for Table I, with the coarse-grid level fixed at 16 points and the radial size varied from 8.0 to 16.0 u.

Calculations for a radial range of 0.0 to 16.0

Ψ_{old} symmetric				Ψ_{old} antisymmetric			
N_{it}	E_{guess}	E_{iter}	ERROR	N_{it}	E_{guess}	E_{iter}	ERROR
5	0.800	0.499997	0.000003	6	0.800	1.500000	0.000000

Calculations for a radial range of 0.0 to 14.0

Ψ_{old} symmetric				Ψ_{old} antisymmetric			
N_{it}	E_{guess}	E_{iter}	ERROR	N_{it}	E_{guess}	E_{iter}	ERROR
5	0.800	0.500000	0.000000	6	0.800	1.500002	0.000002
19	1.800	2.523240	0.023240	5	1.800	1.500000	0.000000

Table II continued

Calculations for a radial range of 0.0 to 12.0

Ψ_{old} symmetric			
N_{it}	E_{guess}	E_{iter}	ERROR
5	0.800	0.499998	0.000002
14	1.800	2.507510	0.007510

Ψ_{old} antisymmetric			
N_{it}	E_{guess}	E_{iter}	ERROR
6	0.800	1.500001	0.000001
5	1.800	1.500000	0.000000

Calculations for a radial range of 0.0 to 10.0

Ψ_{old} symmetric			
N_{it}	E_{guess}	E_{iter}	ERROR
5	0.800	0.499999	0.000001
11	1.800	2.502304	0.002304
5	2.800	2.499998	0.000002

Ψ_{old} antisymmetric			
N_{it}	E_{guess}	E_{iter}	ERROR
6	0.800	1.500001	0.000001
5	1.800	1.500000	0.000000
11	2.800	3.500132	0.000132

Calculations for a radial range of 0.0 to 8.0

Ψ_{old} symmetric			
N_{it}	E_{guess}	E_{iter}	ERROR
5	0.800	0.500000	0.000000
12	1.800	2.500672	0.000672
5	2.800	2.500202	0.000202
13	3.800	4.515004	0.015004
5	4.800	4.509636	0.009636

Ψ_{old} antisymmetric			
N_{it}	E_{guess}	E_{iter}	ERROR
6	0.800	1.500015	0.000015
5	1.800	1.500015	0.000015
11	2.800	3.501697	0.001697
5	3.800	3.501691	0.001691
13	4.800	5.539505	0.039505

Table III

The results presented here are designed to show the effect of varying the number of pre-smoothing relaxation iterations, ν_1 on the stability of the multigrid scheme for the system studied in Tables I and II. The radial range is 0.0 to 8.0 u, with 15 points on the coarse-grid level (512 on the finest grid). The number of post-smoothing iterations, ν_2 was fixed at a value of 2.

Results for $\nu_1 = 1$

Ψ_{old} symmetric

N_{it}	E_{guess}	E_{iter}	ERROR
5	0.800	0.500000	0.000000
12	1.800	2.499900	0.000100
5	2.800	2.500200	0.000200
13	3.800	4.512415	0.012415
5	4.800	4.509637	0.009637
16	5.800	6.636577	0.136577
5	6.800	6.621123	0.121123
19	7.800	7.649127	0.149127

Ψ_{old} antisymmetric

N_{it}	E_{guess}	E_{iter}	ERROR
6	0.800	1.500015	0.000015
5	1.800	1.500015	0.000015
11	2.800	3.501714	0.001714
5	3.800	3.501692	0.001692
13	4.800	5.539453	0.039453
4	5.800	5.539422	0.039422
3	7.800	7.781348	0.281348

Results for $\nu_1 = 2$

Ψ_{old} symmetric

N_{it}	E_{guess}	E_{iter}	ERROR
5	0.800	0.500000	0.000000
12	1.800	2.500672	0.000672
5	2.800	2.500202	0.000202
13	3.800	4.515004	0.015004
5	4.800	4.509636	0.009636

Ψ_{old} antisymmetric

N_{it}	E_{guess}	E_{iter}	ERROR
6	0.800	1.500015	0.000015
5	1.800	1.500015	0.000015
11	2.800	3.501697	0.001697
5	3.800	3.501691	0.001691
13	4.800	5.539505	0.039505

Table III continued

Results for $\nu_1 = 3$

Ψ_{old} symmetric

N_{it}	E_{guess}	E_{iter}	ERROR
5	0.800	0.500000	0.000000
13	1.800	2.501095	0.001095
5	2.800	2.500201	0.000201
16	3.800	4.516729	0.016729

Ψ_{old} antisymmetric

N_{it}	E_{guess}	E_{iter}	ERROR
6	0.800	1.500015	0.000015
5	1.800	1.500015	0.000015
11	2.800	3.501706	0.001706
5	3.800	3.501692	0.001692

Results for $\nu_1 = 4$

Ψ_{old} symmetric

N_{it}	E_{guess}	E_{iter}	ERROR
5	0.800	0.500000	0.000000
13	1.800	2.501413	0.001413
5	2.800	2.500193	0.000193

Ψ_{old} antisymmetric

N_{it}	E_{guess}	E_{iter}	ERROR
6	0.800	1.500015	0.000015
5	1.800	1.500015	0.000015
11	2.800	3.501719	0.001719

Results for $\nu_1 = 5$

Ψ_{old} symmetric

N_{it}	E_{guess}	E_{iter}	ERROR
5	0.800	0.500000	0.000000
11	1.800	2.501710	0.001710
5	2.800	2.500187	0.000187

Ψ_{old} antisymmetric

N_{it}	E_{guess}	E_{iter}	ERROR
6	0.800	1.500015	0.000015
5	1.800	1.500015	0.000015
11	2.800	3.501745	0.001745

Results for $\nu_1 = 6$

Ψ_{old} symmetric

N_{it}	E_{guess}	E_{iter}	ERROR
5	0.800	0.500000	0.000000
13	1.800	2.502053	0.002053

Ψ_{old} antisymmetric

N_{it}	E_{guess}	E_{iter}	ERROR
6	0.800	1.500015	0.000015
5	1.800	1.500015	0.000015
11	2.800	3.501805	0.001805

Table IV

Results obtained from the combined methods of inverse iteration
and multigrid as applied to a pair of coupled harmonic oscillators
(the three cases of which are given in equation (4.3.8)). The radial
range size is set at 0.0 to 10.0 u and the coarse-grid level is
fixed at (16 by 16) points. The number of points on the finest grid
is (128 by 128). Gauss-Seidel relaxation was employed ($\nu_1=\nu_2=2$) with
a multigrid V-cycle scheme. E_d is the value obtained using the
method of secular equations.

Case A

Results for $\alpha = 0.1$

Ψ_{old} symmetric

n_x,n_y	N_{it}	E_{guess}	E_{iter}	E_d
0,0	3	1.000	1.025451	1.025451
0,1	19	1.700	1.773965	1.773965
0,2	4	2.400	2.517737	2.517722
0,2	5	2.300	2.517737	2.517722
2,0	6	3.600	3.715127	3.715129
0,4	10	4.300	3.998022	3.996671

Ψ_{old} antisymmetric

n_x,n_y	N_{it}	E_{guess}	E_{iter}	E_d
0,0	11	1.000	1.025451	1.025451
0,1	15	1.700	1.773943	1.773965
1,0	13	2.400	2.372086	2.372089
1,1	4	3.000	3.210368	3.210373
1,1	7	3.600	3.210368	3.210373
1,3	11	4.300	4.853456	4.853421

Results for $\alpha = 0.3$

Ψ_{old} symmetric

n_x,n_y	N_{it}	E_{guess}	E_{iter}	E_d
0,0	3	1.000	1.068220	1.068221
0,0	14	1.700	1.068221	1.068221
0,2	6	2.400	2.691336	2.691333
2,2	6	3.700	3.879343	3.879352
2,2	4	3.600	3.879415	3.879352
0,4	4	4.300	4.267813	4.267154

Ψ_{old} antisymmetric

n_x,n_y	N_{it}	E_{guess}	E_{iter}	E_d
0,0	12	1.000	1.068299	1.068221
0,1	10	1.700	3.526632	3.517720
1,2	8	2.400	3.517804	3.517720
1,2	9	2.300	3.520567	3.517720
0,2	6	3.000	3.517712	3.517712
0,4	14	4.300	4.267813	4.267154

Table IV continued

Results for $\alpha = 0.5$

Ψ_{old} symmetric

n_x,n_y	N_{it}	E_{guess}	E_{iter}	E_d
0,0	4	1.000	1.104431	1.104432
0,0	10	1.700	1.104432	1.104432
0,2	8	2.400	2.826234	2.826235
0,4	14	4.300	4.481394	4.473910
0,4	11	5.000	4.474326	4.473910

Ψ_{old} antisymmetric

n_x,n_y	N_{it}	E_{guess}	E_{iter}	E_d
0,0	14	1.000	1.104480	1.104432
1,1	10	1.700	3.766643	3.755110
1,1	8	2.400	3.758744	3.755110
1,1	8	2.300	3.759690	3.755110
1,1	6	3.000	3.755102	3.755110
1,1	7	4.300	3.755097	3.755110

Results for $\alpha = 0.7$

Ψ_{old} symmetric

n_x,n_y	N_{it}	E_{guess}	E_{iter}	E_d
0,0	4	1.000	1.136406	1.136406
0,2	10	2.400	2.939878	2.939882
0,2	4	3.000	2.939878	2.939882
2,0	10	4.300	4.109940	4.109952

Ψ_{old} antisymmetric

n_x,n_y	N_{it}	E_{guess}	E_{iter}	E_d
0,0	15	1.000	1.136439	1.136406
1,1	10	1.700	3.968176	3.954271
1,1	8	2.400	3.959509	3.954271
1,1	9	2.300	3.960596	3.954271
1,1	7	3.000	3.954272	3.954271
1,1	5	3.600	3.954258	3.954271

Results for $\alpha = 0.9$

Ψ_{old} symmetric

n_x,n_y	N_{it}	E_{guess}	E_{iter}	E_d
0,0	4	1.000	1.165328	1.165329
0,2	12	2.400	3.039554	3.039558
2,0	5	4.300	4.202131	4.202149
0,4	6	5.000	4.799791	4.799603

Ψ_{old} antisymmetric

n_x,n_y	N_{it}	E_{guess}	E_{iter}	E_d
0,0	15	1.000	1.165352	1.165329
1,1	10	1.700	4.144460	4.128372
1,1	9	2.400	4.135230	4.128372
1,1	9	2.300	4.136426	4.128372
1,1	5	3.700	4.128356	4.128372

Table IV continued

Case B

<u>Results for $\alpha = 0.2$</u>

Ψ_{old} symmetric

n_x,n_y	N_{it}	E_{guess}	E_{iter}	E_d
0,0	3	1.000	1.044704	1.044704
0,2	7	2.800	2.987879	2.987883
0,1	17	2.100	2.026462	2.026464
0,2	3	3.000	2.987876	2.987883
0,4	4	5.000	4.905802	4.905792

Ψ_{old} antisymmetric

n_x,n_y	N_{it}	E_{guess}	E_{iter}	E_d
0,0	13	1.000	1.044704	1.044704
1,1	9	1.900	3.361763	3.356446
1,1	6	2.800	3.356440	3.356446
1,1	9	2.100	3.359951	3.356446
1,3	10	5.000	5.492700	5.492723

<u>Results for $\alpha = 0.4$</u>

Ψ_{old} symmetric

n_x,n_y	N_{it}	E_{guess}	E_{iter}	E_d
0,0	3	1.000	1.081880	1.081880
0,0	15	1.900	1.082011	1.081880
0,2	8	2.800	3.117589	3.117594
0,1	12	2.100	2.124581	2.124576
0,2	5	3.000	3.117588	3.117594
2,0	8	3.900	3.559914	3.559923
0,2	6	3.200	3.117588	3.117594

Ψ_{old} antisymmetric

n_x,n_y	N_{it}	E_{guess}	E_{iter}	E_d
0,0	13	1.000	1.081927	1.081880
1,1	9	1.900	3.622977	3.615290
1,1	6	2.800	3.615292	3.615290
0,1	11	2.100	2.124581	2.124576
1,1	6	3.000	3.615283	3.615290
1,1	5	3.900	3.615282	3.615290

<u>Results for $\alpha = 0.6$</u>

Ψ_{old} symmetric

n_x,n_y	N_{it}	E_{guess}	E_{iter}	E_d
0,0	4	1.000	1.114468	1.114469
0,0	12	1.900	1.114465	1.114469
0,2	10	2.800	3.222732	3.222738
0,1	18	2.100	2.207547	2.207551
0,2	7	3.000	3.222731	3.222738
2,0	6	3.900	3.687407	3.687418
0,4	6	5.000	5.284755	5.284191

Ψ_{old} antisymmetric

n_x,n_y	N_{it}	E_{guess}	E_{iter}	E_d
0,0	14	1.000	1.114499	1.114469
1,1	9	1.900	3.837459	3.827577
1,1	7	2.800	3.827605	3.827577
1,1	8	2.100	3.835051	3.827577
1,1	6	3.000	3.827571	3.827577
1,1	3	3.900	3.827566	3.827577

Table IV continued

Results for $\alpha = 0.8$

Ψ_{old} symmetric

n_x,n_y	N_{it}	E_{guess}	E_{iter}	E_d
0,0	4	1.000	1.143832	1.143833
0,0	10	1.900	1.143830	1.143833
0,2	11	2.800	3.313455	3.313462
2,0	4	3.900	3.797793	3.797805
0,2	5	3.200	3.313454	3.313462
2,0	7	4.100	3.797793	3.797805
0,4	8	5.000	5.431323	5.431350

Ψ_{old} antisymmetric

n_x,n_y	N_{it}	E_{guess}	E_{iter}	E_d
0,0	15	1.000	1.143853	1.143833
1,1	9	1.900	4.022832	4.010897
1,1	7	2.800	4.010970	4.010897
1,1	9	2.100	4.020245	4.010897
1,1	6	3.000	4.010906	4.010897
1,1	4	4.100	4.010884	4.010897
1,1	12	5.000	4.008454	4.010897

Results for $\alpha = 1.0$

Ψ_{old} symmetric

n_x,n_y	N_{it}	E_{guess}	E_{iter}	E_d
0,0	4	1.000	1.170756	1.170756
0,0	9	1.900	1.170754	1.170756
0,0	17	2.100	1.167286	1.170756
2,0	2	3.900	3.894428	3.896107
0,2	7	3.200	3.394384	3.394393

Ψ_{old} antisymmetric

n_x,n_y	N_{it}	E_{guess}	E_{iter}	E_d
0,0	15	1.000	1.170771	1.170756
1,1	9	1.900	4.187815	4.173942
1,1	8	2.800	4.177035	4.173942
1,1	9	2.100	4.185095	4.173942
1,1	7	3.000	4.173981	4.173942
1,1	4	3.900	4.173926	4.173942

Case C

Results for $\alpha = 0.1$

Ψ_{old} symmetric

n_x,n_y	N_{it}	E_{guess}	E_{iter}	E_d
0,0	3	1.000	1.023397	1.023398
0,1	15	2.000	2.067539	2.067541
2,0	4	3.000	3.147656	3.147662
1,0	15	2.000	2.067539	2.067541
2,0	4	3.000	3.147656	3.147662

Ψ_{old} antisymmetric

n_x,n_y	N_{it}	E_{guess}	E_{iter}	E_d
0,0	11	1.000	1.023397	1.023398
1,1	4	3.000	3.195641	3.195646
1,1	8	2.000	3.195809	3.195646
1,1	4	3.000	3.195641	3.195646
1,1	12	4.000	3.195657	3.195646

Table IV continued

<u>Results for $\alpha = 0.3$</u>

Ψ_{old} symmetric

n_x,n_y	N_{it}	E_{guess}	E_{iter}	E_d
0,0	3	1.000	1.063494	1.063495
2,0	5	3.000	3.357665	3.357673
2,0	9	4.000	3.357664	3.357673
0,4	6	5.000	5.368742	5.368769

Ψ_{old} antisymmetric

n_x,n_y	N_{it}	E_{guess}	E_{iter}	E_d
0,0	12	1.000	1.063553	1.063495
1,1	8	2.000	3.496048	3.490564
1,1	5	3.000	3.490557	3.490564
2,0	5	3.000	3.490557	3.490564

<u>Results for $\alpha = 0.5$</u>

Ψ_{old} symmetric

n_x,n_y	N_{it}	E_{guess}	E_{iter}	E_d
0,0	4	1.000	1.097958	1.097959
0,0	14	2.000	1.098168	1.097959
0,2	7	3.000	3.515627	3.515636

Ψ_{old} antisymmetric

n_x,n_y	N_{it}	E_{guess}	E_{iter}	E_d
0,0	14	1.000	1.097995	1.097959
1,1	8	2.000	3.729899	3.722291
2,0	6	3.000	3.722283	3.722291
0,2	6	3.000	3.722283	3.722291

<u>Results for $\alpha = 0.7$</u>

Ψ_{old} symmetric

n_x,n_y	N_{it}	E_{guess}	E_{iter}	E_d
0,0	4	1.000	1.128673	1.128674
0,0	12	2.000	1.128837	1.128674
0,2	8	3.000	3.645940	3.645951
4,0	18	5.000	5.708980	5.708962

Ψ_{old} antisymmetric

n_x,n_y	N_{it}	E_{guess}	E_{iter}	E_d
0,0	14	1.000	1.128697	1.128674
1,1	9	2.000	3.927906	3.918287
1,1	6	3.000	3.918287	3.918287
1,1	6	3.000	3.918287	3.918287

<u>Results for $\alpha = 0.9$</u>

Ψ_{old} symmetric

n_x,n_y	N_{it}	E_{guess}	E_{iter}	E_d
0,0	4	1.000	1.156634	1.156635
0,0	10	2.000	1.156628	1.156635
0,2	9	3.000	3.758581	3.758595
4,0	20	5.000	5.864273	5.848743

Ψ_{old} antisymmetric

n_x,n_y	N_{it}	E_{guess}	E_{iter}	E_d
0,0	15	1.000	1.156651	1.156635
1,1	9	2.000	4.101976	4.090446
1,1	7	3.000	4.090468	4.090446
3,3	9	5.000	4.090181	4.090446

Table V

Results obtained from the multigrid application of the one-dimensional Brillouin-Wigner perturbation scheme as applied to a harmonic oscillator ($\omega^2=1$). The radial range is 0.0 to 8.0 u with 32 points on the coarsest grid and 256 on the finest. Gauss-Seidel relaxation was employed ($\nu_1=\nu_2=2$) with a multigrid V-cycle. The first few converged eigenvalues (E_{B-W}) as a function of the magnitude of the applied perturbation, α in comparison with results obtained directly using the Numerov-Cooley method [6] (E_{N-C}) are presented.

$\alpha = 0.05$

N_{it}	E_{B-W}	E_{N-C}
23	0.532643	0.532643
27	1.653442	1.653436
29	2.874054	2.873980
33	4.176877	4.176342

$\alpha = 0.10$

N_{it}	E_{B-W}	E_{N-C}
25	0.559146	0.559146
28	1.769510	1.769503
28	3.138713	3.138624

$\alpha = 0.15$

N_{it}	E_{B-W}	E_{N-C}
26	0.582024	0.582024
29	1.866250	1.866242

$\alpha = 0.20$

N_{it}	E_{B-W}	E_{N-C}
26	0.602405	0.602405
44	1.950552	1.950543

$\alpha = 0.25$

N_{it}	E_{B-W}	E_{N-C}
27	0.620927	0.620927

$\alpha = 0.30$

N_{it}	E_{B-W}	E_{N-C}
36	0.637992	0.637992

$\alpha = 0.35$

N_{it}	E_{B-W}	E_{N-C}
101	0.653869*	0.653874

* this value is not converged to the specified accuracy ($\pm 1.0 \times 10^{-06}$) since the allowed number of the iterations for the scheme has been exceeded.

Table VI

As for Table V, in two dimensions. The radial range is 0.0 to 10.0 u with (16 by 16) points on the coarsest grid and (128 by 128) on the finest. Gauss-Seidel relaxation was employed ($\nu_1=\nu_2=2$) with a multigrid V-cycle. The first few converged eigenvalues (E_{B-W}) as a function of the magnitude of the applied perturbation, α in comparison with results obtained directly using the method of secular equations (E_d) are presented.

Case A

Results for $\alpha = 0.1$

n_x,n_y	N_{it}	E_{iter}	E_d
0,0	14	1.025448	1.025451
0,1	18	1.773962	1.773965
0,2	19	2.517725	2.517722
1,0	18	2.372084	2.372089
1,1	19	3.210365	3.210373
1,2	19	4.036066	4.036081

Results for $\alpha = 0.3$

n_x,n_y	N_{it}	E_{iter}	E_d
0,0	18	1.068217	1.068221
0,1	19	1.891393	1.891400
0,2	19	2.691323	2.691333
1,0	19	2.481932	2.481939

Case B

Results for $\alpha = 0.2$

n_x,n_y	N_{it}	E_{iter}	E_d
0,0	17	1.044253	1.044704
0,1	19	2.025237	2.026464
1,0	19	2.223399	2.224936
1,1	19	3.353787	3.356446
2,0	19	3.402165	3.405678

Results for $\alpha = 0.4$

n_x,n_y	N_{it}	E_{iter}	E_d
0,0	19	1.081382	1.081880
0,1	19	2.123210	2.124576
1,0	19	2.318936	2.320610

Table VI continued

Case C

Results for $\alpha = 0.1$

Results for $\alpha = 0.3$

n_x,n_y	N_{it}	E_{iter}	E_d
0,0	14	1.022979	1.023398
0,1	18	2.066266	2.067541
0,2	20	3.144052	3.068870
1,0	18	2.066266	2.067541
1,1	19	3.193294	3.195646
1,2	19	4.332200	4.336284
2,0	20	3.144052	3.147662
2,1	19	4.332200	4.336284
2,2	19	5.521857	5.547657

n_x,n_y	N_{it}	E_{iter}	E_d
0,0	16	1.063023	1.063495
0,1	19	2.173919	2.175364
1,0	19	2.173919	2.175364
1,1	19	3.487723	3.490564

Results for $\alpha = 0.5$

n_x,n_y	N_{it}	E_{iter}	E_d
0,0	18	1.097445	1.097959

Table VII

Results obtained from the direct multigrid approach to the system of a pair of coupled harmonic oscillators. The three sets of harmonic frequencies are those given in the text and the range of the perturbation constant, α is 0.1 to 0.5. The radial range is 0.0 to 16.0 u with (16 by 16) points on the coarsest grid and (128 by 128) on the finest. Gauss-Seidel relaxation was employed ($\nu_1=\nu_2=2$) with a multigrid FMV-cycle. The first few eigenvalues (E_{mg}) as a function of the magnitude of the applied perturbation, α are compared with results obtained using the method of secular equations (E_d).

Case A

n_x,n_y	$\alpha = 0.1$		$\alpha = 0.3$		$\alpha = 0.5$	
	E_{mg}	E_d	E_{mg}	E_d	E_{mg}	E_d
0,0	1.026131	1.025451	1.069473	1.068221	1.105484	1.104432
0,1	1.774108	1.773965	1.886785	1.891400	1.963720	1.986872
0,2	2.422919	2.517722	1.817841	2.691333	2.201475	2.826235
1,0	2.283965	2.372089	2.571979	2.481939	2.536320	2.569129
1,1	3.011230	3.210373	2.760212	3.517720	1.544976	3.755110
1,2	2.367895	4.036081	2.486618	4.493109	1.742253	4.822112
2,0	2.232320	3.715129	2.528196	3.879352	2.689749	4.004795
2,1	1.353415	4.634669	2.228473	5.133199	1.973785	5.483410
2,2	1.972169	5.544587	1.649515	6.216079	2.635917	7.927464

Table VII continued

Case B

$\alpha = 0.1$			$\alpha = 0.3$			$\alpha = 0.5$	

n_x, n_y	E_{mg}	E_d	E_{mg}	E_d	E_{mg}	E_d
0,0	1.024229	1.023610	1.065012	1.063990	1.099552	1.098643
0,1	1.964420	1.968369	2.059541	2.077918	2.252356	2.167543
0,2	3.037732	2.905966	2.397807	3.056890	2.598658	3.172399
1,0	2.166630	2.167856	2.270930	2.275201	1.969211	2.362319
1,1	3.076197	3.197190	1.823947	3.493469	1.702767	3.725835
1,2	1.692264	4.201162	2.438545	4.797306	1.854280	5.120836
2,0	1.723864	3.312286	2.310480	3.487082	3.018761	3.626252
2,1	1.790939	4.423253	2.371397	4.885813	1.678395	5.233111
2,2	2.471274	5.461104	1.736859	6.290590	2.163371	6.793580

Case C

$\alpha = 0.1$			$\alpha = 0.3$			$\alpha = 0.5$	

n_x, n_y	E_{mg}	E_d	E_{mg}	E_d	E_{mg}	E_d
0,0	1.024017	1.023398	1.064263	1.063495	1.098859	1.097959
0,1	2.061741	2.067541	2.151172	2.175364	2.214612	2.263372
0,2	3.015819	3.068870	2.092616	3.183002	3.383498	3.515636
1,0	2.061905	2.067541	2.164830	2.175364	2.239591	2.263372
1,1	2.873599	3.195646	1.825450	3.490564	1.789286	3.722291
1,2	1.757899	4.336284	2.398052	4.804833	1.652264	5.155909
2,0	3.021021	3.147662	2.095087	3.357673	3.255946	3.278902
2,1	2.747321	4.336284	2.427802	4.804833	1.608232	5.155909
2,2	2.464778	5.547657	1.658886	6.270241	2.096362	6.790278

4.7 References

1. W. L. Briggs, "A Multigrid Tutorial", Society for Industrial and Applied Mathematics (SIAM), (1987).

2. W. Hackbusch, "Multi-Grid Methods and Applications", Springer-Verlag, (1985).

3. J. M. Hutson and B. J. Howard, Mol. Phys., **41**, 1113, (1980).

4. F. F. Grinstein, H. Rabitz and A. Askar, J. Comp. Phys., **51**, 423, (1983).

5. R. A. Nicolaides, Math. Comp., **32**, 1082, (1978).

6. J. K. Cashion, J. Chem. Phys. **39**, 1872, (1963).

5. Vibration-Rotational energy levels for "plane" motion of X_3 molecules and the He atom using hyperspherical coordinates.

5.1   Introduction

Quantum mechanical calculations using hyperspherical
coordinates have been successfully performed on a range of scattering
and bound state problems associated with three body systems in
nuclear [1], atomic [2] and chemical physics [3]. The methods of
calculation employed range from full secular equation methods with a
basis set describing the wavefunction dependence on all the
coordinates to coupled channel calculations in which one coordinate,
usually the hyper-radius, is treated separately giving rise to the
set of coupled differential equations. The basis set used in some of
these calculations consists of the eigenfunctions of the kinetic
energy operator in hyperspherical coordinates, the hyperspherical
harmonics. For even relatively small, but non-zero, values of the
total angular momentum, J, the hyperspherical harmonic functions are
difficult to express in a simple closed analytical form [4]. The
calculations performed using this type of basis set in three
dimensions have thus been mainly restricted to cases with $J = 0$, for
which it is much easier to deal with the hyperspherical functions
[5]. The applications to the structure of nuclei do not suffer so
much from this difficulty because the number of basis functions
required is smaller than that needed for a typical chemical physics
application, mainly owing to the range and strength of the forces
involved.

In his discussion of the various 3-body hyperspherical
coordinate systems, Johnson [6] describes an example of a situation
in which angular momentum is readily included. This is achieved by
reducing the dimensionality of the problem; the three particles are
restricted to motion within a fixed plane (designated as the xy
plane) [7]. The resulting "planar hyperspherical harmonics" are now
readily defined for all values of J_z, where J_z defines motion about
the coincident space and molecule fixed z axes. For the planar
system used in this work, the total angular momentum is denoted by m.
Calculations on the model X_3 system studied in this work were
performed for values of angular momentum up to and including $m = 50$.
The range of angular momentum studied opens up the possibility of

investigating the effect of angular momentum on the structure and dynamics of weakly bound and floppy molecular systems and comparing the quantum predictions with classical results [8].

5.2   The hyperspherical coordinate system

There are two distinct types of hyperspherical coordinates that can be defined for a three particle system, differing in the degree of symmetry displayed by the coordinates to particle permutation. The "democratic" coordinate set [7] which treats all the particles in an even handed manner, (that is no one particle is selected as a special central particle), and the asymmetric set most suitable for the treatment of an atom-diatomic system.   For each type of coordinate system there exists a family of coordinates as a variation on a theme, differing in the scaling and range of the individual coordinates.   The coordinate systems considered in this work are related to the "democratic" set as this is ideal for the consideration of X_3 systems, especially ones for which particle exchange is a "feasible" process.

The definition of the hyperspherical coordinate system used in this work is essentially that given by Johnson [6], and thus only a brief summary is presented here.   Three Euler angles (α,β,γ) are required to describe the orientation of the plane containing the three particles with respect to the space-fixed axes.   However, in the planar motion problem, since the particles can only move on a stationary plane surface only one Euler angle, γ, is required to specify the "external" motion.   The three remaining internal coordinates consisting of a hyper-radius, ρ and the two angles θ and ϕ are the same in both the planar and "full spatial" cases, except for the range of θ.   Johnson [6] modified the original Smith [7] angles θ_S and ϕ_S^k (the superscript indicating the labelling sequence used) to ease the mapping of the internal coordinates into a three dimensional cartesian configuration space representation

5.2.1 $\qquad \theta_J = \pi/2 - 2\theta_S$

5.2.2 $\qquad \phi_J^k = \pi/2 - 2\phi_S^k$

Johnson's definition of θ is employed, but for symmetry reasons, ϕ^k is defined by equation (5.2.4)

5.2.3 $\qquad \theta = \pi/2 - 2\theta_S$

5.2.4 $\qquad \phi^k = 2\phi_S^k$

The ranges of these coordinates can be chosen as

5.2.5 $\qquad 0 \leq \rho \leq \infty$

5.2.6 $\qquad 0 \leq \gamma \leq 2\pi$

5.2.7 $\qquad 0 \leq \theta \leq \pi$

5.2.8 $\qquad 0 \leq \phi^k \leq 4\pi$

In order to cover the whole of configuration space without any avoidable discontinuities appearing in the definition of the moments of inertia in the molecular frame, the range of θ has had to be extended from $\pi/2$ (in three dimensions [7]) to π. This has significant effects on the symmetry of the planar wavefunction, see section 5.3. The relationship between some of the different sets of democratic coordinates that have been used for "planar problems" are given in Table I.

In terms of these definitions, equations (5.2.3) and (5.2.4) the inter-particle distances r_{ij} are

5.2.9 $\qquad r_{ij} = \rho(d^k/2^{\frac{1}{2}})[1+\sin\theta\cos\phi^k]^{\frac{1}{2}}$

where d^k are scale parameters as defined by Johnson [6], see Table II which also lists possible values for ϕ^k. The internal coordinates

Table I

The relationship between the different democratic hyperspherical coordinates

Johnson [6]	Child [8]	This work
$\rho_J = \rho_S$	$\rho_C = \rho_S$	$\rho = \rho_S$
$\theta_J = \pi/2 - 2\theta_S$	$\theta_C = 2\theta_S$	$\theta = \pi/2 - 2\theta_S$
$\phi_J = \pi/2 - 2\phi_S$	$\phi_C = 2\phi_C$	$\phi = 2\phi_S$
$0 < \rho_J < \infty$	$0 < \rho_C < \infty$	$0 < \rho < \infty$
$0 < \theta_J < \pi/2$ or π	$-\pi/2 < \theta_C < \pi/2$	$0 < \theta < \pi/2$ or π
$0 < \phi_J < 4\pi$	$0 < \phi_C < 2\pi$	$0 < \phi < 4\pi$

Table II

The d^k scale parameters and ϕ^k as defined by Johnson [6]

	XY_2 $m_1 = m_2$, $m_3 = \infty$	X_3 $m_1 = m_2 = m_3$
d^1	$2^{\frac{1}{2}}$	$2^{\frac{1}{2}}/3^{\frac{1}{2}}$
$d^2 = d^3$	1	$2^{\frac{1}{2}}/3^{\frac{1}{2}}$
ϕ^1	ϕ	ϕ
ϕ^2	$\phi+\pi/2$	$\phi+2\pi/3$
ϕ_3	$\phi-\pi/2$	$\phi-2\pi/3$

Table III

Cartesian Coordinate Maps

Johnson [6]	Kupperman	This work
$x = \rho\sin\theta_J\cos\phi_J$	$x = \rho\cos\theta_S\cos\phi_S$	$x = -\rho\sin\theta\sin\phi$
$y = \rho\sin\theta_J\sin\phi_J$	$y = \rho\cos\theta_S\sin\phi_S$	$y = \rho\sin\theta\cos\phi$
$z = \rho\cos\theta_J$	$z = \rho\sin\theta_S$	$z = \rho\cos\theta$

span a 3D subspace which can be covered by a cartesian map in a number of ways to make the visualisation of the internal configuration of the atoms more apparent, some of the mappings employed are illustrated in Table III.

The hamiltonian, H, for this restricted plane motion can be expressed as

5.2.10 $H = (1/2\mu)\{P_\rho^2 + \Lambda_4^2/\rho^2\} + 3\hbar^2/8\mu\rho^2 + V$

     $P_\rho = i\hbar\partial/\partial\rho$

The $3\hbar^2/8\mu\rho^2$ term arises when the wavefunctions are scaled so as to transform the hyper-radial volume element to $d\rho$. The four-dimensional grand angular momentum operator, Λ_4^2, can be decomposed in to the sum of the three dimensional angular laplacian, L^2, and angular momentum operators corresponding to the angles γ and ϕ

5.2.11 $\Lambda_4^2 = 4L^2(\theta,\phi) + \{P_\gamma(P_\gamma - 4P_\phi\cos\theta)\}/\sin^2\theta$

     $P_\gamma = i\hbar\partial/\partial\gamma$ and $P_\phi = i\hbar\partial/\partial\phi$

The planar hyperspherical harmonic functions, the eigenfunctions of Λ_4^2 are solutions of

5.2.12 $[\Lambda_4^2 - \lambda(\lambda+2)]X_{\lambda,\sigma,m}(\phi,\theta,\gamma) = 0$

where λ is the hyperangular momentum quantum number with components σ and m. The functions are simultaneously eigenfunctions of P_γ and P_ϕ with the angular momentum about the z axis given by $m\hbar$. The integers λ,σ and m are all of the same parity (either all even or all odd) and take the values

5.2.13 $\lambda = 0,1,2,3,4....$
     $\sigma = \lambda,\lambda-2.....-\lambda$
     $m = \lambda,\lambda-2.....-\lambda$

The hyperspherical harmonic functions, $X_{\lambda,\sigma,m}(\phi,\theta,\gamma)$ have the explicit form

5.2.14 $\qquad X_{\lambda,\sigma,m}(\phi,\theta,\gamma) \;=\; e^{-i\sigma\phi/2}d^{\lambda/2}_{\sigma/2,m/2}(\theta)e^{-im\gamma}$

$$= D^{\lambda/2}_{\sigma/2,m/2}(\phi,\theta,2\gamma)$$

The sign convention used in the definition of these 'D' functions follows that given by Brink and Satchler [9].

5.3 Coordinate symmetry properties

The elegant symmetry properties of the democratic hyperspherical coordinates are a powerful reason for their wider use in quantum mechanical calculations on systems of identical particles. The symmetry properties of hyperspherical coordinates have been examined by past workers for the full three dimensional case [6],[10],[11] and similar, but not identical, behaviour is obtained for the restricted motions being considered here. The transformation properties for the X_3 and XY_2 systems will be considered. As for the full 3D case the coordinate ρ remains unchanged under all particle permutations, that is under all operations in the group S_3, but in contrast to the full 3D case the θ coordinate is altered under the action of particle exchange. The action of the particle interchange, (ij), and cyclic permutation, (ijk) operators, on the angle ϕ produce rotations, see Table IV. In order to simplify the consideration of the symmetry operations, only the parameterisation labelled by (123) will be considered, and in the subsequent description the label k, (k = 3, ij = 12) will be dropped from the angle ϕ. The details of the derivation of the effect of the symmetry operations are given in a separate work [12].

The spacial inversion operator, E^*, has two possible representations, in one all the internal coordinates remain unaltered but the Euler angle γ is shifted by π. The alternative is a shift in ϕ by π with all the other coordinates remaining the same.

5.3.1 $E^* \gamma = \gamma + \pi$

OR

5.3.2 $E^* \phi = \phi + \pi$

The parity of the wavefunctions under E^* as represented by either equation (5.3.1) or (5.3.2) must be the same so that the functions given in equation (5.2.14) must always satisfy the condition that

5.3.3 $\Psi(\rho,\theta,\phi,\gamma) = \Psi(\rho,\theta,\phi+\pi,\gamma+\pi)$

The effect on the coordinates of reflection in the "equatorial plane" [12],[13] defined by $z = 0$ (ie. $\theta = \pi/2$), σ_{eq}, must be considered for the planar case. The extended coordinate range for θ is such that the wavefunction must be symmetric or anti-symmetric with respect to the z coordinate. In the more detailed study of the effect of the symmetry operations on the various 2D and 3D hyperspherical coordinate systems [12], it is shown that the exchange operation (12) is different in the planar and three-dimensional cases. In the planar problem, this difference can be alleviated by defining the operation (12)' from the combination

5.3.4 $(12)' = \sigma_{eq}.(12)$

The operator (12)' is seen to be crucial to the assignment of symmetry species to the observed energy levels of states with zero angular momentum. The consequences of these symmetry operations for the angles θ, ϕ and γ are given in Table V.

124

Table IV

Symmetry Properties of ϕ^k

E	(12)	(23)	(13)	(123)	(132)
ϕ^3	$-\phi^3$	$-\phi^3+4\pi/3$	$-\phi^3-4\pi/3$	$\phi^3+4\pi/3$	$\phi^3-4\pi/3$
ϕ^1	$-\phi^1-4\pi/3$	$-\phi^1$	$-\phi^1+4\pi/3$	$\phi^1+4\pi/3$	$\phi^1-4\pi/3$
ϕ^2	$-\phi^2+4\pi/3$	$-\phi^2-4\pi/3$	$-\phi^2$	$\phi^2+4\pi/3$	$\phi^2-4\pi/3$

Table V

(Only the results for k=3 are given here)

Symmetry Properties

	$\theta_S\ \phi_S\ \gamma$	$\theta_J\ \phi_J\ \gamma$	$\theta_C\ \phi_C\ \gamma$	$\theta\ \phi\ \gamma$
E^*	$\theta_S \dashrightarrow \theta_S$	$\theta_J \dashrightarrow \theta_J$	$\theta_C \dashrightarrow \theta_C$	$\theta \dashrightarrow \theta$
	$\phi_S \dashrightarrow \phi_S$	$\phi_J \dashrightarrow \phi_J$	$\phi_C \dashrightarrow \phi_C$	$\phi \dashrightarrow \phi$
	$\gamma \dashrightarrow \gamma+\pi$	$\gamma \dashrightarrow \gamma+\pi$	$\gamma \dashrightarrow \gamma+\pi$	$\gamma \dashrightarrow \gamma+\pi$
$(12)'$	$\theta_S \dashrightarrow \theta_S$	$\theta_J \dashrightarrow \theta_J$	$\theta_C \dashrightarrow \theta_C$	$\theta \dashrightarrow \theta$
	$\phi_S \dashrightarrow -\phi_S$	$\phi_J \dashrightarrow -\phi_J$	$\phi_C \dashrightarrow -\phi_C$	$\phi \dashrightarrow -\phi$
	$\gamma \dashrightarrow \pi-\gamma$	$\gamma \dashrightarrow \pi-\gamma$	$\gamma \dashrightarrow \pi-\gamma$	$\gamma \dashrightarrow \pi-\gamma$
σ_{eq}	$\theta_S \dashrightarrow -\theta_S$	$\theta_J \dashrightarrow \pi-\theta_J$	$\theta_C \dashrightarrow -\theta_C$	$\theta \dashrightarrow \pi-\theta$
	$\phi_S \dashrightarrow \phi_S$	$\phi_J \dashrightarrow \phi_J$	$\phi_C \dashrightarrow \phi_C$	$\phi \dashrightarrow \phi$
	$\gamma \dashrightarrow 2\pi-\gamma$	$\gamma \dashrightarrow 2\pi-\gamma$	$\gamma \dashrightarrow 2\pi-\gamma$	$\gamma \dashrightarrow 2\pi-\gamma$
(12)	$\theta_S \dashrightarrow -\theta_S$	$\theta_J \dashrightarrow \pi-\theta_J$	$\theta_C \dashrightarrow -\theta_C$	$\theta \dashrightarrow \pi-\theta$
	$\phi_S \dashrightarrow -\phi_S$	$\phi_J \dashrightarrow -\phi_J$	$\phi_C \dashrightarrow -\phi_C$	$\phi \dashrightarrow -\phi$
	$\gamma \dashrightarrow \pi+\gamma$	$\gamma \dashrightarrow \pi+\gamma$	$\gamma \dashrightarrow \pi+\gamma$	$\gamma \dashrightarrow \pi+\gamma$

5.4 Zero angular momentum functions

In the construction of the symmetrised function appropriate for considering the X_3 and XY_2 molecules, the simplest case is provided by the S-state, m=0, functions. These functions are necessary for the expansion of the potential

$$5.4.1 \qquad \tilde{S}(\lambda\sigma) = X(\lambda\sigma 0).$$

The $\tilde{S}(\lambda\sigma)$ will all be even under $\mathbf{E}^*$ since they are not dependent on γ and since $m = 0$, λ and σ must both be even so that $\tilde{S}$ will also be unchanged by a shift in ϕ by π. The transformation properties under (12), σ_{eq} and (12)' are given by (5.4.2). The symmetry properties of the zero angular momentum functions are classified with respect to the operations (12)' and σ_{eq}.

5.4.2

E	(12)'	σ_{eq}	(12)
$\tilde{S}(\lambda\sigma)$	$(-1)^{\sigma/2}\tilde{S}(\lambda\text{-}\sigma)$	$(-1)^{(\lambda+\sigma)/2}\tilde{S}(\lambda\sigma)$	$(-1)^{\lambda/2+\sigma}\tilde{S}(\lambda\text{-}\sigma)$

so the linear combinations

$$5.4.3 \qquad S(\lambda\sigma s) = N_{\lambda\sigma}\{\tilde{S}(\lambda\sigma) + (-1)^s(-1)^{\sigma/2}\tilde{S}(\lambda\text{-}\sigma)\} \text{ with } \sigma \geq 0$$

$$= \frac{2\left[(\lambda\text{-}\sigma)!\right]^{\frac{1}{2}}}{\left[(\lambda+\sigma)!\right]} P_\lambda^\sigma(\cos\theta) \begin{cases} \cos(\sigma\phi/2) & s = 0 \\ \sin(\sigma\phi/2) & s = 1 \end{cases}$$

($P_\lambda^\sigma(\cos\theta)$ are the associated legendre polynomials)

are symmetric (s=0) or antisymmetric (s=1) to (12)'. The functions are symmetric or antisymmetric under σ_{eq} according to the parity of $(\lambda+\sigma)/2$. The expansion of the potential which must be symmetric to σ_{eq} only requires the functions $S(\lambda\sigma s)$ with $(\lambda+\sigma)$ a multiple of 4.

In order to construct the fully symmetrised hyperspherical harmonic basis, consider the two general cases

5.4.4

$$|\alpha\rangle \quad = \qquad\qquad\qquad X(\lambda\sigma 0)$$

$$|\beta\rangle \quad = \qquad (-1)^{\sigma/2} \qquad X(\lambda\text{-}\sigma 0)$$

where σ is restricted to values of greater than or equal to 0. The linear combinations

5.4.5 $\qquad |\psi\rangle = N_{\lambda\sigma}\{|\alpha\rangle + (-1)^s|\beta\rangle\}$

5.4.6 $\qquad N^2_{\lambda\sigma} = (2\text{-}\delta_{\sigma 0})(\lambda+1)/16\pi^2$

give the fully symmetrised hyperspherical harmonic functions. The functions $|\psi\rangle$ are symmetric (s=0) or antisymmetric (s=1) to (12)' and symmetric (p=0; if $(\lambda+\sigma)/2$ is even) or antisymmetric (p=1; if $(\lambda+\sigma)/2$ is odd) to σ_{eq}. These functions may be classified under the symmetry species as follows

5.4.7

E	(12)'	σ_{eq}	(12)
$|\alpha\rangle$	$(-1)^s|\beta\rangle$	$(-1)^p|\alpha\rangle$	$(-1)^S|\beta\rangle$

where $\qquad$ S = s + p

The matrix elements of the potential in the symmetrised basis have the form

5.4.8 $\qquad \langle\psi_1|V|\psi_2\rangle$

where ψ_1 and ψ_2 are given in (5.4.5). The calculation may be simplified somewhat by considering only the terms in the integration (5.4.8) involving $|\alpha_1\rangle$; all of the possible symmetries are then linear combinations of the two resulting integrals;

5.4.9

$$A_1 = <\alpha_1|V|\alpha_2>$$

$$A_2 = <\alpha_1|V|\beta_2>$$

The final expression for the matrix elements of the potential has the form

5.4.10 $\quad <\psi_1|V|\psi_2> = N_{\lambda\sigma}^2\{A_1 + (-1)^sA_2\}$

5.4.11 $\quad N_{\lambda\sigma}^2 = (2-\delta_{\sigma 0})(\lambda+1)/8\pi^2$

In X_3 molecules, the symmetry operation (123) must be considered and it is more appropriate to classify the basis functions under a group isomorphic to $D_{3h}(M)$, generated by the elements $\{E, (12), \sigma_{eq}$ and (123)$\}$. From Table IV, the effect of (123) on the angle ϕ produces a rotation of $4\pi/3$ and so the functions $S(\lambda\sigma s)$ transform as one dimensional irreducible representations of $D_{3h}(M)$ if σ is a multiple of 3, but as a two dimensional representation if $\sigma = 3n+1$ or $3n+2$; these results are summarised in Table VI. In XY_2 molecules, the different symmetry classes can be classified under a group isomorphic to $C_{2v}(M)$ generated by the symmetry operations (E, (12) and σ_{eq}). These are shown in Table VII.

5.5 Non-zero angular momentum functions

For the more general problem including angular momentum, the construction of a symmetrised basis is simplified by the redundancy of the two symmetry operations σ_{eq} and (12)'. The effect of these operations on the angle γ is such to transform functions of positive angular momentum, +m to functions of negative angular momentum, -m, see Table V. Since the potential is independent of m, there can be no coupling between functions of positive and negative m. The symmetry species for non-zero angular momentum are therefore simply classified

Table VI

Symmetry classification of zero angular momentum planar harmonic functions for X_3.

$D_{3h}(M)$	(12)'	σ_{eq}	σ
A_1'	$s = 0$	$(\lambda+\sigma)/2$ even	$\sigma = 3n$
A_2'	$s = 1$	$(\lambda+\sigma)/2$ even	$\sigma = 3n$
E'		$(\lambda+\sigma)/2$ even	$\sigma \neq 3n$
A_1''	$s = 0$	$(\lambda+\sigma)/2$ odd	$\sigma = 3n$
A_2''	$s = 1$	$(\lambda+\sigma)/2$ odd	$\sigma = 3n$
E''		$(\lambda+\sigma)/2$ odd	$\sigma \neq 3n$

Table VII

Symmetry classification for the zero angular momentum planar harmonic functions for XY_2

$C_{2v}(M)$	(12)'	σ_{eq}
A_1	$s = 0$	$(\lambda+\sigma)/2$ even
A_2	$s = 0$	$(\lambda+\sigma)/2$ odd
B_1	$s = 1$	$(\lambda+\sigma)/2$ odd
B_2	$s = 1$	$(\lambda+\sigma)/2$ even

as symmetric or antisymmetric under (12) and J_z. The parity of the functions under E^* is given by $(-1)^m$. The action of (12) on the hyperspherical harmonic function, $X(\lambda\sigma m)$ produces

5.5.1 $\qquad (12)X(\lambda\sigma m) \;=\; (-1)^S(-1)^{(\lambda+2\sigma+3m)/2}X(\lambda\text{-}\sigma m)$

Defining

5.5.2 $\qquad |\alpha\rangle \;=\; \qquad\qquad X(\lambda\sigma m)$

$\qquad\qquad |\beta\rangle \;=\; (-1)^{(\lambda+2\sigma+3m)/2}X(\lambda\text{-}\sigma m)$

the linear combinations

5.5.3 $\qquad |\psi\rangle = N_{\lambda\sigma}\{|\alpha\rangle + (-1)^S|\beta\rangle\}$

5.5.4 $\qquad N^2_{\lambda\sigma} \;=\; (2-\delta_{\sigma 0})(\lambda+1)/16\pi^2$

are symmetric (S=0) or antisymmetric (S=1) with respect to particle exchange, (12). The symmetry classification for X_3 and XY_2 molecules with non-zero angular momentum with respect to a simple molecular point group is not possible with the symmetry operations so far discussed in this work. The redundancy of the two symmetry operations σ_{eq} and (12)', combined with the fact that the observed energy levels are degenerate with respect to positive and negative values of m suggest a much higher symmetry group than those already discussed for the case of non-zero angular momentum.

5.6 Calculation of the matrix elements

To facilitate the calculation of the hamiltonian matrix, the potential, V is expanded in a series of the hyperspherical harmonics. The expansion of the potential is thus of the form

5.6.1 $\qquad V \;=\; \sum\limits_{\lambda'',\sigma''} c_{\lambda''\sigma''}S(\lambda''\sigma''0)$

where $S(\lambda''\sigma''0)$ are the S-state harmonics as defined by equation (5.4.3) and $c_{\lambda''\sigma''}$ represent the coefficients of the potential

expansion. Details of these coefficients are presented in the
appendix to this chapter. The required matrix elements of the
potential can then be evaluated using angular momentum algebra and
reduce to a sum over products of 3-j symbols.

To show these integrals more explicitly, consider the integral
A_1 from expression (5.4.9) which may be written in the form

$$5.6.2 \qquad A_1 = \langle D^\lambda_{\sigma,m}(\theta,\phi,2\gamma) | V | D^{\lambda'}_{\sigma',m'}(\theta,\phi,2\gamma) \rangle$$

where $D^\lambda_{\sigma,m}(\theta,\phi,2\gamma)$ are the hyperspherical harmonic functions given in
equation (5.2.14). It may be noted that in this case, $m = m'$. Each
term in the expansion of the potential, equation (5.6.1) has the form

$$5.6.3 \qquad V = \sum_{\lambda'',\sigma''} c_{\lambda''\sigma''} (D^{\lambda''}_{\sigma'',0}(\theta,\phi,2\gamma) + (-1)^{\sigma''} D^{\lambda''}_{-\sigma'',0}(\theta,\phi,2\gamma))$$

Substituting for V from equation (5.6.3) into equation (5.6.2) and
dropping the dependence of the D-functions on $(\theta,\phi,2\gamma)$ gives

$$5.6.4 \qquad A_1 = \sum_{\lambda'',\sigma''} c_{\lambda''\sigma''} \langle D^\lambda_{\sigma,m} | (D^{\lambda''}_{\sigma'',0} + (-1)^{\sigma''} D^{\lambda''}_{-\sigma'',0}) | D^{\lambda'}_{\sigma',m} \rangle$$

In terms of angular momentum algebra, this integral (5.6.4) may be
written

$$5.6.5 \qquad A_1 = (-1)^{\sigma-m} \left[\begin{pmatrix} \lambda & \lambda'' & \lambda' \\ -\sigma & \sigma'' & \sigma' \end{pmatrix} \begin{pmatrix} \lambda & \lambda'' & \lambda' \\ -m & 0 & m \end{pmatrix} \right.$$
$$\left. + (-1)^{\sigma''} \begin{pmatrix} \lambda & \lambda'' & \lambda' \\ -\sigma & -\sigma'' & \sigma' \end{pmatrix} \begin{pmatrix} \lambda & \lambda'' & \lambda' \\ -m & 0 & m \end{pmatrix} \right]$$

A similar derivation of the integral in terms of 3-j symbols applies
to the other term that constitutes the matrix elements, namely A_2.
The calculation is carried out for each element in the hyperspherical
basis defined by λ, σ, λ' and σ' by choosing the appropriate value
for σ'' and calculating the set of non-zero symbols for all possible
λ''. The value of σ'' may be easily determined from angular momentum
algebra. For a 3-j symbol of the form

5.6.6
$$\begin{pmatrix} \lambda & \lambda'' & \lambda' \\ -\sigma & \sigma'' & \sigma' \end{pmatrix}$$

the value of σ'' required to give a non-zero value is given by [14]

5.6.7
$$\sigma'' = \sigma - \sigma'$$

The calculation can be performed efficiently because a whole series of 3-j symbols can be evaluated using the recurrence relations and algorithm outlined by Schulten and Gorden [15].

5.7 Solution of the Schrödinger equation

The approximate bound state energies are obtained by a Born-Oppenheimer separation between ρ and the angular coordinates $\Omega \equiv (\theta,\phi)$ [11]. The implied diagonalisation of the "clamped-rho", H_ρ, is performed in the symmetrised basis formed by $|\lambda\sigma m\rangle$ at each value of ρ. H_ρ which is obtained by neglecting the terms involving radial derivatives, has the form, in units scaled so that $\hbar^2/2\mu = 1$

5.7.1
$$H_\rho = (A_4^2 + 3/4)/\rho^2 + V(\rho,\Omega)$$

and

5.7.2
$$H_\rho Q_i(\Omega;\rho) = U_i(\rho)Q_i(\Omega;\rho)$$

where

5.7.3
$$\psi(\rho,\Omega) = \sum_i f_i(\rho)Q_i(\Omega;\rho)$$

Equation (5.7.3) shows the total wavefunction expressed as products of the radial function, $f_i(\rho)$ and a channel function, $Q_i(\Omega;\rho)$. $Q_i(\Omega;\rho)$ is chosen to depend only parametrically, that is slowly, on ρ. A sequence of channel potentials, $U_i(\rho)$ is specified at selected values of ρ (up to 50 points) by solving equation (5.7.2). Cubic spline interpolation is used to give the channel potentials on a fine grid (for this work a step size of 0.001 atomic units was used). In

the Born-Oppenheimer approximation only a single product term is
retained in equation (5.7.3) so that the solution is completed by
solving a one-dimensional Schrödinger equation in ρ with $U_i(\rho)$ as the
potential function, equation (5.7.4). This is achieved by using the
Numerov-Cooley finite difference algorithm [16].

5.7.4 $[-(\hbar^2/2\mu)\partial^2/\partial\rho^2 + U_i]f_{ni}(\rho) = E_{ni}f_{ni}(\rho)$

The physical picture as described by these calculations is a series
of stretching energy levels in each of the bending channels [11].
Thus, with the ability to include angular momentum in the planar
three body problem, a good understanding of the overall motion of
such small systems can be obtained.

5.8   The potential expansions

Coupled morse oscillators

The potential for the model X_3 system is that developed by
Child et al [8] and consists of a sum of morse pair potentials

5.8.1 $V_m = \sum_{k=1,3} D\{1 - \exp[-\alpha(r_k-r_e)]^2\}$

with parameter values in atomic units, $D = 0.08896269$ E_h, $\alpha = 0.85$ Å^{-1}
and $r_e = 1.66$ Å.

For a pairwise additive X_3 potential, the matrix elements of
the potential in the symmetrised basis can be obtained directly from
those of $V(r_{12}) = V(\rho d^3(1+\sin\theta\cos\phi)^{\frac{1}{2}})$. The potential expansion is
outlined in the appendix but has the form

5.8.2 $V(r_{12}) = \frac{1}{2}\sum_{n=0}^{\infty}\sum_{k=0}^{n}(2-\delta_{k0})(2n+1)\frac{(n-k)!}{(n+k)!}P_n^k(0)P_n^k(\cos\theta)\cos(k\phi)I_n$

Details of the one-dimensional integral I_n are given in the appendix.

The Helium Atom

The potential energy for the helium atom of nuclear charge $Z = 2$ and with infinite nuclear mass is, in atomic units,

5.8.3 $V_c = -2(1/r_{13} + 1/r_{23}) + 1/r_{12}$

while, in terms of the hyperspherical coordinates

5.8.4 $V_c(\rho,\theta,\phi) = (1/\rho)\{ - 2\sqrt{2}[1+\sin\theta\cos(\phi+\pi/2)]^{-\frac{1}{2}}$
$- 2\sqrt{2}[1+\sin\theta\cos(\phi-\pi/2)]^{-\frac{1}{2}}$
$+ [1+\sin\theta\cos\phi]^{-\frac{1}{2}}\}$

The derivation of the expansion of the pairwise additive coulomb potential is akin to that described in the appendix. The only difference in the expansion between the two systems under consideration here is shown in the integral I_n. For helium, this integral is in a standard form [17]

5.8.5 $I_n(\text{coulomb}) = \int_{-1}^{1} \frac{P_n(t)}{(1+t)^{\frac{1}{2}}} dt$

$= (-1)^n \frac{2^{3/2}}{2n+1}$

Substituting for I_n from (5.8.5) into (5.8.2) produces the following expression for the expansion of $V(r_{12})$ of the coulomb potential

5.8.6 $V(r_{12}) = \sum_{n=0}^{\infty} \sum_{k=0}^{n} (2-\delta_{k0})(-1)^n 2^{1/2} \frac{(n-k)!}{(n+k)!} P_n^k(0)P_n^k(\cos\theta)\cos(k\phi)$

The overall expansion is given by

5.8.7 $V_c = \{1 - 4\sqrt{2}\cos(k\pi/2)\}V(r_{12})$

134

5.9   Results

Model X$_3$ System

Calculations using the potential as defined in equation (5.8.1) were performed for values of m up to and including m = 50.

For m = 0, there are six symmetry species required to describe the vibrational symmetry of the system, A_1', A_2', E', A_1'', A_2'' and E'' states. Results were obtained for the first three channels for each symmetry species. Table VIII contains the first few rovibrational energy levels in the three obtained channels for all possible symmetries. The maximum value of λ required for the convergence of these level was λ_{max}=50. It may be noted that there are only minor differences between states that are symmetric or antisymmetric under σ_{eq}. The rovribational ground state is symmetric as expected and the morse oscillators have equilateral equilibrium symmetry.

As explained in section 5.5, the inclusion of angular momentum into the system has a dramatic effect on the number of allowed vibrational symmetries. The allowed vibrational symmetries are simply those of the symmetric, anti-symmetric and non-symmetric vibrations. Table IX shows the ground state energies for each symmetry species as a function of increasing m. It can be seen that only when m is a multiple of three is the lowest rovibrational level totally symmetric. This is to be expected since it is only then that the basis functions with σ as a multiple of three are accessed (the requirement for symmetric/antisymmetric functions - see section 5.4). Thus when m is not a multiple of three the basis functions which contribute to the non-symmetric states predominate. Table X contains further levels for the different symmetry species in each of the first three channels for m ranging from 1 to 50.

Figure I

Plot of the ground state energy levels against increasing m for the model X_3 system.
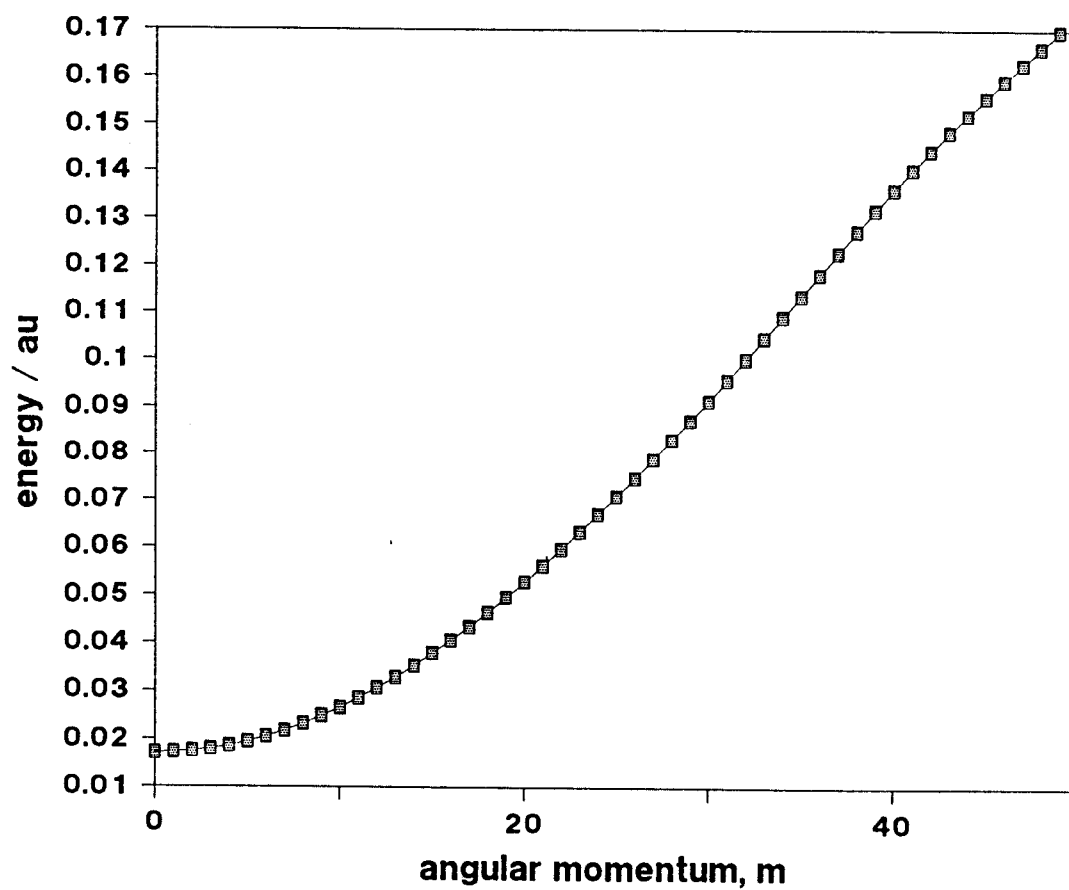
Figure II

Zeroth order potential wells for m = 38 to 42. The radial range has been limited to concentrate on the central well regions. The curve for m = 38 is the outermost potential (ie the lower energy curve).
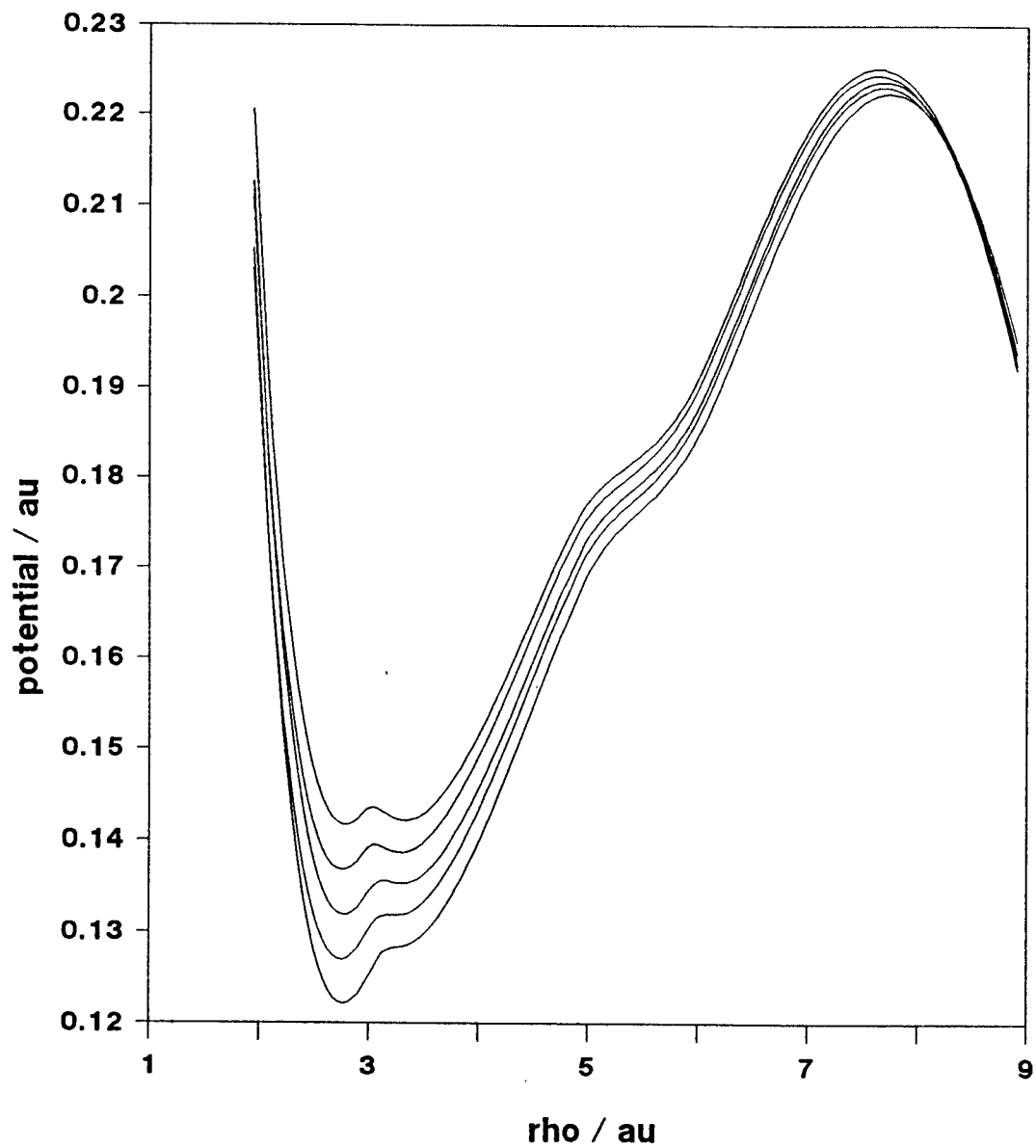
The zeroth order energy rises smoothly as the value of m increases. As the value of m exceeds 40, the rate of this energy rise is seen to decrease. This is shown in Figure I where the ground state energy is plotted against m. Physically, this point on the curve corresponds to a change in the equilibrium geometry of the system. For values of m less than 40 the equilibrium geometry of the three particles is equilateral, but for greater values of m a collinear geometry is favoured. This feature of the system is described in the work by Child et al [10]. Figure II contains a set of the zeroth order potential wells $(U_0(\rho))$ plotted as energy versus ρ with m ranging from 38 to 42. The double minima in these plots with high values of m are those of the collinear and equilibrium geometries. The collinear arrangement is favoured when the equilibrium bond distance exceeds 3.295 Å - this occurs when m > 39 [8].

The examination of the shape of the wavefunction at selected values of ρ on these potential curves requires knowledge of the channel functions $Q_0(\rho)$. These functions are simply the eigenvectors resulting from the diagonalisation of H_ρ in the symmetrised basis formed by $|\lambda\sigma m\rangle$. The angular wavefunction may now be plotted over the ranges of θ and ϕ for fixed ρ. The geometry of the system can be determined by the angular components θ and ϕ. When $\theta = 0$ and π, the three particles occupy the vertices of an equilateral triangle whereas $\theta = \pi/2$ corresponds to a collinear formation. When $\phi = \pi/3$, π and $5\pi/3$, the system is in a symmetric collinear geometry. Hence the behaviour of the angular wavefunction at these points will indicate the preferred formation of the particles. The wavefunctions of the ground state potential curves for m = 38 - 42 were examined. The point of reference on each curve is that which corresponds to the zeroth order energy level on the curve at the higher ρ side of the potential minimum. The calculations were performed at a value of λ_{max} sufficient to converge this level to an acceptable accuracy - these details are to be found in Table XI.

Table XI

Details of the contour plots for m = 38 to 42. This table contains the value of λ_{max} (and the resulting basis size) used in the wavefunction expansion, the value E_0 and the corresponding value, ρ_0 on the potential curve for each m.

m	λ_{max}	E_0	ρ_0	Basis	Symmetry
38	48	0.127185	3.08415	88	E
39	49	0.131672	3.13285	45	A_1
40	50	0.136068	3.51835	92	E
41	51	0.140328	3.63512	94	E
42	52	0.144413	3.7225	48	A_1

Table XII

Details of the contour plots for m = 9, energy levels 0,5,10 and 15. This table contains the value E_n and the corresponding value, ρ_n on the potential curve for each energy, n. The symmetry is given by the symmetric, A_1 species. The chosen value for λ_{max} is 50 which corresponds to a basis set size of 105 functions.

n	E_n	ρ_n
0	0.024799	2.55905
5	0.083582	3.6675
10	0.125990	4.578725
15	0.159987	5.62225

Figure III

Contour plots for m = 38 to 42. The x coordinate refers to the angle θ and the y coordinate represents the angle ϕ.

J = 38
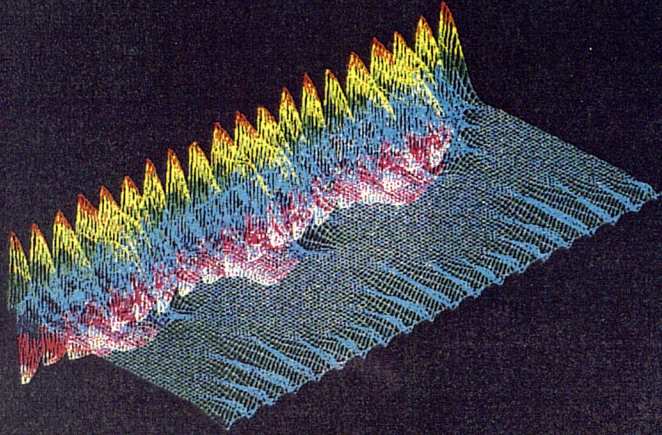
J = 39
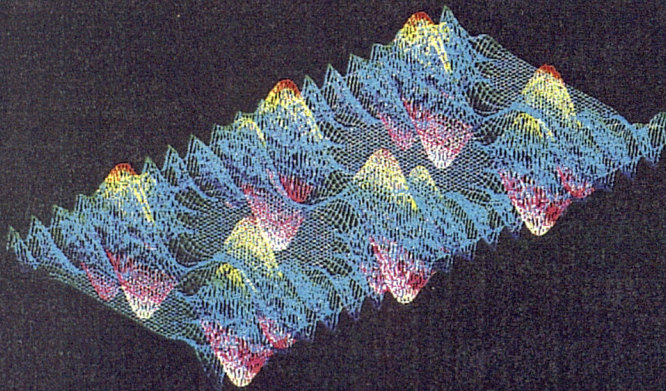
J = 40
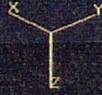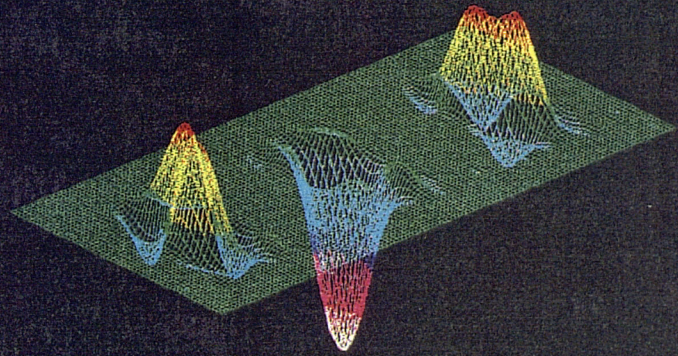
J = 41
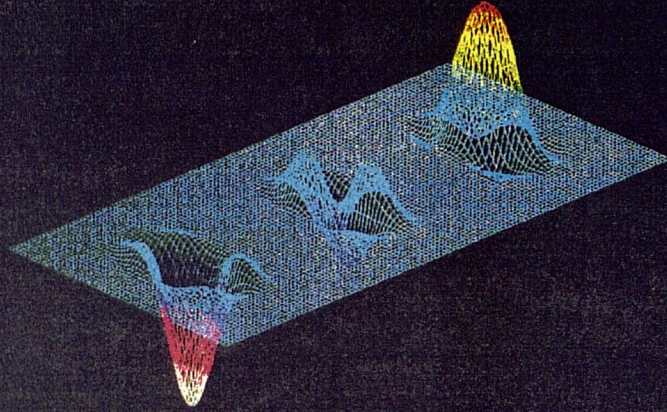
J = 42
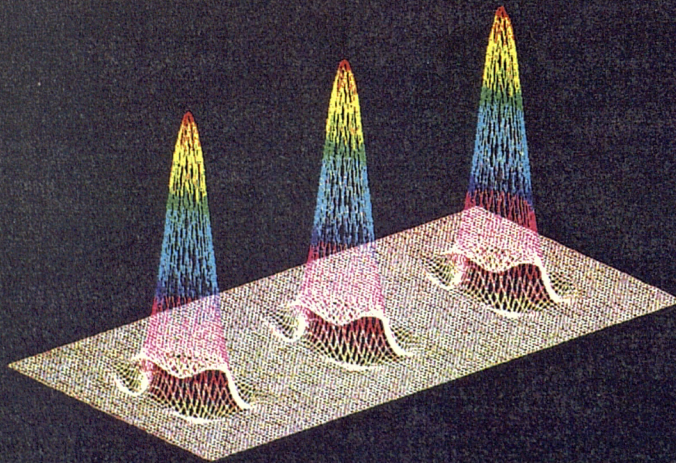
The plots in Figure III show the appropriate angular wavefunction (whose value is given by the z coordinate) plotted as a function of θ (the x coordinate) and ϕ (the y coordinate) at fixed rho (the values of which are given in Table XI). The full range of θ ($0 < \theta < \pi$) and one full rotation of ϕ ($0 < \phi < 2\pi$) have been employed in the plots. The plot for J = 38 indicates that the wavefunction is largely to be found at $\theta = 0$ and π thus favouring the equilateral geometry. The differences in the behaviour of the wavefunction at $\theta = 0$ and π can be attributed to the E state symmetry of this curve. The corresponding plot for m = 39 is symmetric through the plane defined by $\theta = \pi/2$ (the curve has A state symmetry). It can be seen in this plot that the system is beginning to move away from the equilateral geometry. The wavefunction is mostly to be found around $\theta = 0$ and π but there are approaches to the collinear formation at $\phi = \pi/3$, π and $5\pi/3$. At m = 40, the change over to the collinear geometry is now apparent. The major wavefunction amplitude is found at the intersections between $\theta = \pi/2$ and $\phi = \pi/3$, π and $5\pi/3$. This is also the case for m = 41 and m = 42. The symmetric A state of m = 42 accounts for the difference in the behaviour of this function as opposed to that of m = 40 and m = 41 which are both E states.

The changeover in the preferred geometry of the system is seen to occur as the X_3 system approaches dissociation. This may be shown by examining the ground state potential well for a value of m that is well away from the changes at high angular momentum. The potential chosen was that for m = 9. The system has an A state symmetry and the equilibrium geometry is equilateral. The wavefunction was examined at various points on the curve corresponding to the zeroth, fifth, tenth and fifteenth energy levels. Figure IV consists of views of the wavefunction at each value of ρ up the potential curve (the values of which are given in Table XII). The coordinate system is that described for Figure III. It can be seen from these plots that there is indeed a switch from equilateral to collinear geometry as dissociation is approached. The function corresponding to the zeroth order level is mainly to be found around $\theta = 0$ and π.

Figure IV

Contour plots for m = 9, E_0, E_5, E_{10} and E_{15}. The x coordinate refers to the angle θ and the y coordinate represents the angle ϕ.

J = 9, E0
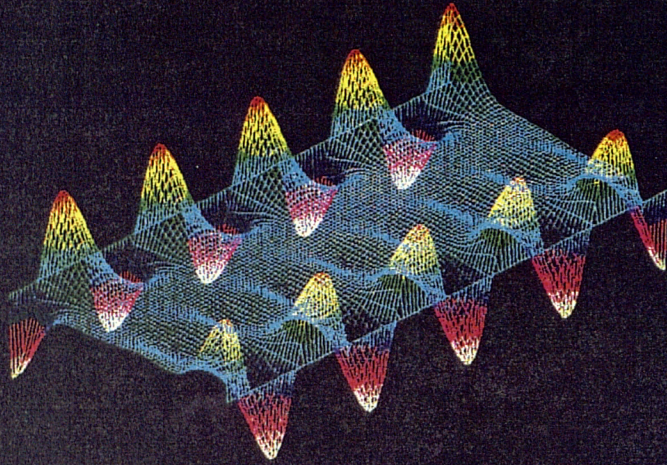
J = 9, E5
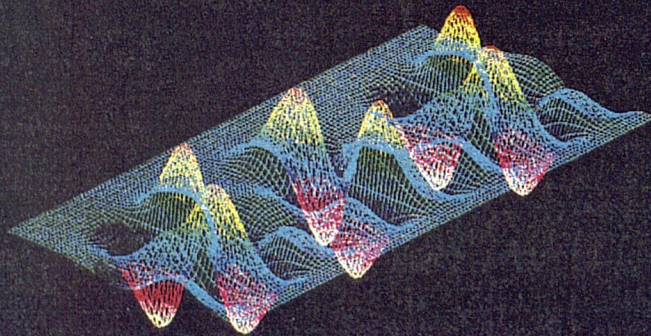
J = 9, E10
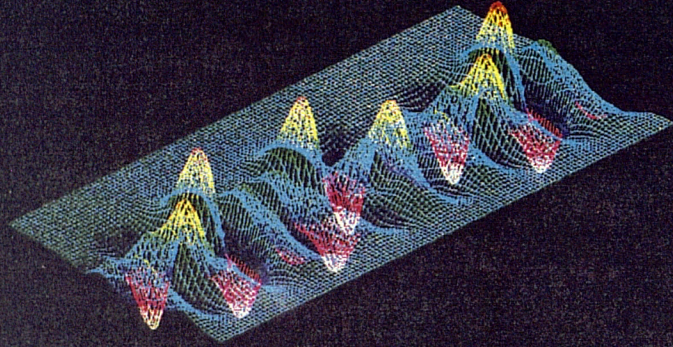
J = 9, E15
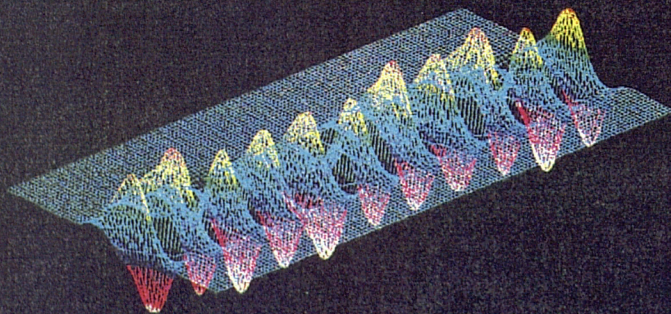
As energy increases towards dissociation the system moves away from the equilateral geometry. The higher order wavefunctions contain a high degree of structure but the general trend is for oscillations about $\theta = \pi/2$. The collinear geometry enables the system to dissociate smoothly from X_3 to $X + X_2$.

The He atom in two dimensions

The system consisting of a He atom confined to motion in a plane proved to be a stringent test of the hyperspherical harmonic scheme. The coulombic potential as described in section 5.8 above is much more strongly binding in two dimensions than the corresponding full spatial case. The hyperspherical harmonic basis set is ideally suited to describe "kinetic energy dominated motion" [11] and for such systems (for instance, the X_3 system already discussed) a relatively small set of functions is required in the wavefunction expansion. However, for the problem in hand, it was found that a very large basis was required (calculations up to $\lambda_{max} = 148$ for the m = 0 levels) to obtain a convergence of approximately $\pm 5.0 \times 10^{-04}$. The huge computing resources required for such large bases ($\lambda_{max} = 148$ corresponds to the diagonalisation of a matrix of size (1444 by 1444) for the ground state) limited the extent of the calculations.

For m = 0, there are four symmetry species required to describe the vibrational symmetry of the system, A_1', A_2', A_1'' and A_2''. The convergence of the ground state energy level (with A_1 symmetry) as a function of λ_{max} is shown in Figure V. It can be noted from this plot that the rate of convergence is approaching a plateau but has not yet attained a satisfactory level (that is in terms of the level of convergence attained for the model X_3 system). Similar convergence rates were observed for the other symmetry species.

The final value obtained for the ground state energy (with λ_{max} = 148) is $E_{BO} = -12.033786$au. In their work on dimensional expansions for two-electron atoms, Loeser and Herschbach [18] put forward a number of empirical approaches to the calculation of ground state energies for such systems over a range of dimensionalities.

Figure V

Convergence plot for the ground state energy of the planar helium atom plotted as a function of λ_{max}.
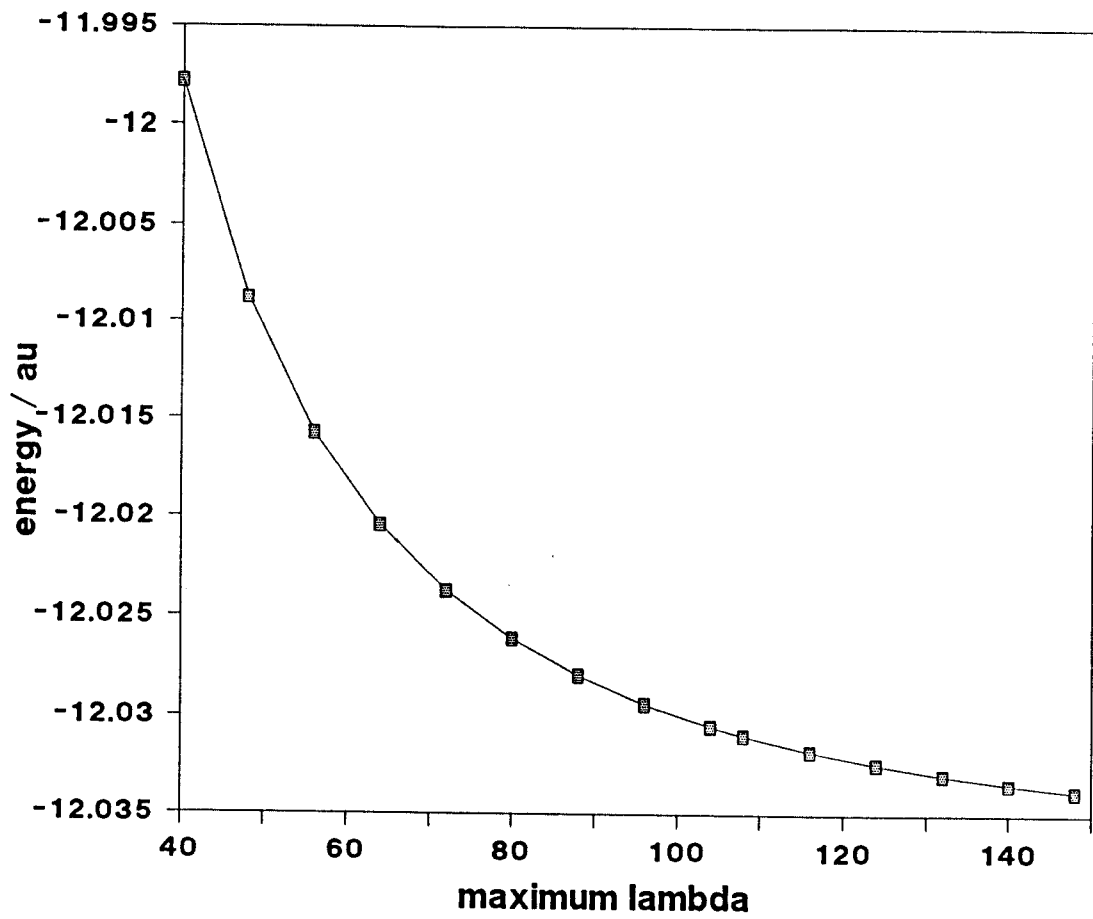
For helium, with Z = 2 and D = 2, the best value for this energy was obtained using a Taylor series expansion with a shift in origin [18]. The calculated value is E_{Emp} = -11.8998au (converged to $\pm 1.0 \times 10^{-04}$). This means that the 'unconverged' Born-Oppenheimer energy is within about 1% of this empirical value. Further calculations incorporating the adiabatic and non-adiabatic corrections should improve further on this result. The Born-Oppenheimer value, E_{BO} is seen to be lower than E_{Emp}, a point-of-fact which often results from using the Born-Oppenheimer approximation. Table XIII contains the first few energy levels in the bottom two channels for each of the four symmetry species with λ_{max} = 148.

As was found in the X_3 system, the inclusion of angular momentum in the calculation served to half the number of observed symmetry species. The symmetries that remain are simply those of the symmetric A_1 and anti-symmetric A_2. The range of angular momentum employed was that of m = 0 to 4, corresponding in atomic terms to the s, p, d, f and g shells of atomic structure. As already stated, these calculations were severely limited by available computing resources and thus only a selection of results at a fixed value of λ_{max} are presented. Table XIV contains the first few energy levels in each of the first two channels for m = 1 to 4, with λ_{max} = 70.

Table VIII

The first ten stretching energy levels (n_s) in the zeroth order bending channel potential for each of the six observed symmetry species of the model X_3 system with zero total angular momentum.

n_s	A_1'	A_1''		n_s	A_2'	A_2''
0	0.017170	0.017170		0	0.046190	0.046190
1	0.030759	0.030759		1	0.058137	0.058138
2	0.043886	0.043889		2	0.069511	0.069523
3	0.056399	0.056440		3	0.080132	0.080224
4	0.067781	0.068051		4	0.089720	0.090109
5	0.077571	0.078365		5	0.098450	0.099255
6	0.086836	0.087961		6	0.106847	0.107922
7	0.095791	0.097188		7	0.114915	0.116220
8	0.104455	0.106042		8	0.122702	0.124184
9	0.112869	0.114623		9	0.130156	0.131791
10	0.121036	0.122911		10	0.137267	0.139015

n_s	E'	E''
0	0.026661	0.026661
1	0.039631	0.039633
2	0.051998	0.052017
3	0.063434	0.063585
4	0.073540	0.074111
5	0.082845	0.083851
6	0.091895	0.093170
7	0.100609	0.102121
8	0.109107	0.110785
9	0.117353	0.119175
10	0.125312	0.127253

Table IX

Ground state energies for the three observed symmetry species for the model X_3 system with m = 1 to 50.

m	A_1	A_2	E
1	0.026921	0.026921	0.017265
2	0.026691	0.026691	0.017552
3	0.018029	0.018029	0.026981
4	0.028789	0.028789	0.018695
5	0.028111	0.028111	0.019549
6	0.020589	0.020589	0.028947
7	0.032243	0.032243	0.021813
8	0.031157	0.031157	0.023217
9	0.024799	0.024799	0.032524
10	0.037189	0.037189	0.026556
11	0.035772	0.035772	0.028484
12	0.030579	0.030579	0.037645
13	0.043483	0.043483	0.032836
14	0.041872	0.041872	0.035253
15	0.037823	0.037823	0.044217
16	0.050931	0.050932	0.040542
17	0.049349	0.049349	0.043406
18	0.046409	0.046409	0.052127
19	0.059335	0.059334	0.049546
20	0.058081	0.058080	0.052812
21	0.056202	0.056202	0.061247
22	0.068590	0.068592	0.059710
23	0.067933	0.067932	0.063331
24	0.067060	0.067061	0.071440
25	0.078689	0.078684	0.070892
26	0.078761	0.078764	0.074820
27	0.078841	0.078839	0.082562
28	0.C39563	0.089576	0.082944
29	0.090427	0.090419	0.087130
30	0.091389	0.091394	0.094462

Table IX continued

m	A_1	A_2	E
31	0.101143	0.101111	0.095716
32	0.102742	0.102764	0.100104
33	0.104561	0.104546	0.106964
34	0.113147	0.113233	0.109033
35	0.115589	0.115523	0.113556
36	0.118100	0.118152	0.119834
37	0.125617	0.125382	0.122648
38	0.128423	0.128635	0.127184
39	0.131869	0.131671	0.132650
40	0.137348	0.137955	0.136064
41	0.141456	0.140813	0.140327
42	0.144411	0.145128	0.144708
43	0.149824	0.148626	0.148312
44	0.152158	0.153482	0.152067
45	0.157186	0.155711	0.155760
46	0.159336	0.161046	0.159283
47	0.164641	0.162821	0.162808
48	0.166301	0.168220	0.166308
49	0.171792	0.169780	0.169772
50	0.173228	0.175297	0.173226

N.B. The double degeneracy, implicit with E state symmetries was indeed observed but has not been included in this table.

Table X

The first three stretching vibrations (of each symmetry type) in each of the first three bending channels for the planar X_3 system with m = 35 to 45.

	A_1	A_2	E
m = 35	0.115589	0.115523	0.113556
	0.124308	0.123549	0.122463
	0.131558	0.130340	0.129050
	0.120961	0.120701	0.117341
	0.129888	0.128891	0.125480
	0.137825	0.136587	0.132821
	0.125508	0.124881	0.119213
	0.134787	0.134090	0.127730
	0.142183	0.141970	0.135369
m = 36	0.118100	0.118152	0.119834
	0.126271	0.127027	0.127214
	0.132790	0.134008	0.133989
	0.123233	0.123444	0.121474
	0.131408	0.132404	0.129174
	0.138892	0.140122	0.136393
	0.127490	0.127883	0.124556
	0.136481	0.137162	0.132457
	0.144157	0.144352	0.139987

Table X continued

	A_1	A_2	E
m = 37	0.125617	0.125382	0.122648
	0.132872	0.131737	0.130022
	0.139987	0.138690	0.136571
	0.129887	0.129350	0.124287
	0.137974	0.136817	0.131917
	0.145310	0.144022	0.138922
	0.132658	0.131905	0.127274
	0.140483	0.139750	0.135087
	0.147613	0.147364	0.142440
m = 38	0.128423	0.128635	0.127184
	0.134528	0.135698	0.133743
	0.141340	0.142630	0.140370
	0.132314	0.132779	0.129756
	0.139676	0.140896	0.136579
	0.146941	0.148256	0.143595
	0.135862	0.136571	0.131334
	0.144663	0.145372	0.138773
	0.152110	0.152028	0.146007
m = 39	0.131869	0.131671	0.132650
	0.138681	0.137464	0.138225
	0.145439	0.144153	0.145007
	0.135816	0.135391	0.133873
	0.143719	0.142468	0.140303
	0.150888	0.149577	0.147208
	0.139447	0.138922	0.136222
	0.148108	0.147393	0.143304
	0.154565	0.154666	0.150427

Table X continued

	A₁	A₂	E
m = 40	0.137348	0.137955	0.136064
	0.142758	0.144049	0.141228
	0.149398	0.150820	0.147899
	0.140681	0.141517	0.137249
	0.147680	0.148991	0.143280
	0.154597	0.155998	0.150041
	0.143578	0.144522	0.139440
	0.151261	0.151901	0.146174
	0.157915	0.157833	0.153146
m = 41	0.141456	0.140813	0.140327
	0.147110	0.145816	0.145078
	0.153722	0.152290	0.151613
	0.144793	0.143997	0.141981
	0.151933	0.150604	0.147824
	0.158822	0.157402	0.154427
	0.148001	0.147180	0.143472
	0.155774	0.155173	0.149897
	0.161994	0.162222	0.156709
m = 42	0.144411	0.145128	0.144708
	0.149036	0.150311	0.149722
	0.155300	0.156749	0.155921
	0.147462	0.148266	0.145939
	0.153637	0.154975	0.151627
	0.160259	0.161696	0.158031
	0.150589	0.151296	0.147867
	0.158129	0.158702	0.154276
	0.164993	0.164775	0.160891

Table X continued

	A_1	A_2	E
m = 43			
	0.149824	0.148626	0.148312
	0.155449	0.154193	0.153082
	0.161634	0.160146	0.158988
	0.153166	0.151959	0.149585
	0.159858	0.158476	0.154891
	0.166399	0.164942	0.161050
m = 44	0.152158	0.153482	0.152067
	0.157605	0.158817	0.157154
	0.163242	0.164712	0.162704
	0.155495	0.156732	0.153632
	0.161632	0.162991	0.159275
	0.167858	0.169321	0.165240
	0.158676	0.159655	0.155292
	0.165683	0.166062	0.161161
	0.172231	0.172053	0.167336
m = 45			
	0.157186	0.155711	0.155760
	0.162349	0.161174	0.161488
	0.167903	0.166470	0.166955
	0.160430	0.159116	0.157370
	0.166259	0.164924	0.163079
	0.172329	0.170869	0.168852
	0.163243	0.162306	0.159255
	0.169147	0.168838	0.165308
	0.174976	0.175123	0.171337

Table XIII

This table presents the first few energy levels (if applicable) in the first three channels for each of the four observed symmetry species of the planar He atom with zero total angular momentum. λ_{max} has a value of 148.

A_1', basis set size = 1444

	0		1		2
0	-12.033786	0	-1.456205	0	-1.035701
1	-8.209274	1	-1.034225	1	-0.924070

A_1'', basis set size = 1406

	0		1		2
0	-1.283080	0	-0.515066	0	-0.412335
1	-0.991666				

A_2', basis set size = 1406

	0		1		2
0	-8.276688	0	-1.041668	0	-0.963265
1	-7.817407				
2	-7.504063				

A_2'', basis set size = 1369

	0		1
0	-1.011193	0	-0.404680

Table XIV

This table contains the first few energy levels (if applicable) in the first three channels for the two observed symmetry species of the planar He atom with angular momentum of m = 1 to 4. The chosen value for λ_{max} was 76.

<u>m = 1</u>

A_1, basis set size = 741

	0		1		2
0	-8.114942	0	-1.175523	0	-1.010899
1	-7.469874				
2	-6.976385				

A_2, basis set size = 741

	0		1		2
0	-8.059884	0	-1.412998	0	-0.995551
1	-7.432993				
2	-6.945550				

<u>m = 2</u>

A_1, basis set size = 760

	0		1		2
0	-7.620810	0	-1.258591	0	-0.945802
1	-7.128746			1	-0.901447
2	-6.701479				

Table XIV continued

A_2, basis set size = 760

	0		1		2
0	-7.621746	0	-1.021841		
1	-7.130059				
2	-6.702971				

<u>m = 3</u>

A_1, basis set size = 740

	0		1		2
0	-7.293130	0	-0.975786	0	-0.897461
1	-6.848326	1	-0.916628		
2	-6.452060				

A_2, basis set size = 740

	0		1		2
0	-7.293101	0	-0.992647	0	-0.897623
1	-6.848268	1	-0.924615		
2	-6.451978				

<u>m = 4</u>

A_1, basis set size = 759

	0		1
0	-7.032727	0	-0.925374
1	-6.625289		
2	-6.257857		

A_1, basis set size = 758

	0		1
0	-7.032727	0	-0.925462
1	-6.625292		
2	-6.257861		

5.10 Appendix - The morse potential expansion

The matrix elements of the potential in the symmetrised basis have the form

5.10.1 $\qquad \langle \lambda_1 \sigma_1 m | V_m | \lambda_2 \sigma_2 m \rangle = 3 \langle \lambda_1 \sigma_1 m | V(r_{12}) | \lambda_2 \sigma_2 m \rangle$

where

$$V(r_{12}) = V(\rho d^1 (1+\sin\theta\cos\phi)^{\frac{1}{2}})$$

5.10.2 $\qquad \langle \lambda_1 \sigma_1 m | V(r_{12}) | \lambda_2 \sigma_2 m \rangle$

$$= \quad \langle \lambda_1 \sigma_1 m | V(\rho d^3 (1+\sin\theta\cos\phi)^{\frac{1}{2}}) | \lambda_2 \sigma_2 m \rangle$$

$$= \quad \langle \lambda_1 \sigma_1 m | V(f(t)) | \lambda_2 \sigma_2 m \rangle$$

where

5.10.3 $\qquad t = \sin\theta\cos\phi = \cos\alpha$

The result presented in equation (5.10.3) shows that the length r_{12} may be written in terms of the scalar product of the two spherical unit vectors ξ and η.

The potential is expanded as a series of the S-state hyperspherical harmonics which form a set of orthonormal functions akin which are essentially the spherical harmonic functions, $S_{n,k}(\theta,\phi)$

5.10.4 $\qquad S_{n,k}(\theta,\phi) = \left[\dfrac{(2n+1)(n-k)!}{2\pi \quad (n+k)!} \right]^{\frac{1}{2}} P_n^k(\cos\theta)\cos(k\phi)$

for $k=1,2,\ldots n$

$$= \left[\dfrac{(2n+1)}{4\pi} \right]^{\frac{1}{2}} P_n(\cos\theta)$$

for $k=0$

5.10.5 $\qquad V(r_{12}) = \sum_{n,k} c_{nk} S_{n,k}(\theta,\phi)$

Since $S_{n,k}(\theta,\phi)$ form a complete orthonormal basis, the coefficients c_{nk} are given by

5.10.6
$$c_{nk} = \int V(r_{12}) S_{n,k}(\theta,\phi) \; d\tau$$

$$= \int V(V(\rho d^3(1+t)^{\frac{1}{2}})) S_{n,k}(\theta,\phi) \; d\tau$$

The matrix elements depend only on the scalar product, t, between the vectors ξ and η. The application of the Hecke-Funk theorem [19] to equation (5.10.6) then reduces the two-dimensional integral (over θ and ϕ) to a single integration over t. The full form of this theorem for spherical harmonics in p-dimensional space is

5.10.7
$$\int_{|\eta|=1} f((\xi \cdot \eta)) S_n(\eta) \; dw_p$$

$$= w_{p-1} S_n(\xi) \int_{-1}^{1} f(t) P_n(t) (1-t^2)^{(p-3)/2} \; dt$$

Applying the Hecke-Funk theorem to equation (5.10.6) with $w_2 = 2\pi$ and using the definition of $S_{n,k}(\theta,\phi)$ given in equation (5.10.4) the coefficients c_{nk} may be written

5.10.8
$$c_{nk} = 2\pi S_{n,k}(1,0) I_n$$

5.10.9
$$I_n = \int_{-1}^{1} V(d^k \rho (1+t)^{\frac{1}{2}}) P_n(t) \; dt$$

The expansion of the $V(r_{12})$ part of a pairwise additive potential is now in the form

5.10.10
$$V(r_{12}) = \tfrac{1}{2} \sum_{n=0}^{\infty} \sum_{k=0}^{n} (2-\delta_{k0})(2n+1) \frac{(n-k)!}{(n+k)!} P_n^k(0) P_n^k(\cos\theta) \cos(k\phi) I_n$$

The I_n are single dimensional integrals over the variable t, given by

5.10.11
$$I_n = \int_{-1}^{1} V(d^k \rho (1+t)^{\frac{1}{2}}) P_n(t) \; dt$$

157

and $t = \sin\theta\cos\phi$

For the Morse potential, I_n is given by

$$5.10.12 \qquad I_n = \int_{-1}^{1} D\{1 - \exp(-\alpha(r_{12}-r_e))^2\}P_n(t) \; dt$$

$$= D \int_{-1}^{1} P_n(t)dt - 2D\exp(\alpha r_e)J_n(\alpha) + 2D\exp(2\alpha r_e)J_n(2\alpha)$$

where the $J_n(\alpha)$ are given by

$$5.10.13 \qquad J_n(\alpha) = \int_{-1}^{1} P_n(t)\exp(-\alpha\rho(1+t)^{\frac{1}{2}}) \; dt$$

$$= \sum_{m=0}^{\infty} \frac{(-\alpha\rho)^m}{m!} \int_{-1}^{1} (1+t)^{m/2} \; P_n(t) \; dt$$

$$= \sum_{m=0}^{\infty} \frac{(-\alpha\rho)^m}{m!} \; \frac{2^{m/2+1}[\Gamma(m/2+1)]^2}{\Gamma(m/2+n+2)\Gamma(1+m/2-n)}$$

The stability of the summation shown in (5.10.13) is largely dependent on the value of ρ as well as the order, n, of the legendre polynomial.

5.11 References

1. J. L. Ballot and M. Fabre de la Ripelle, Ann. Phys. (NY),
    127, 62, (1980) and references contained therein.

2. H. Klar and M. Klar, J. Phys. B, 13, 1057, (1980);
    C. D. Lin, Phys. Rev. A, 10, 1986, (1974);
    U. Fano, Rep. Prog. Phys., 46, 97, (1983).

3. J. A. Kaye and A. Kupperman, Chem. Phys. Lett., 78, 546,
    (1981);
    J. Röhmelt, Chem. Phys. Lett., 74, 263, (1980);
    R. Wallace, Chem. Phys., 37, 93, (1979).

4. M. I. Mukhtarova and V. D. Efros, J. Phys. A, 19, 1589,
    (1986);
    E. Chacón, O. Castaños and A. Frank, J. Math. Phys., 25,
    1442, (1984);
    F. del Aguila, J. Math. Phys., 21, 2327, (1980);
    H. Mayer, J. Phys. A, 8, 1562, (1975);
    V. D. Efros, Sov. J. Nucl. Phys., 13, 758, (1971).

5. V. Aquilanti, S. Cavalli And G. Grossi, J. Chem. Phys.,
    85, 1362, (1986).

6. B. R. Johnson, J. Chem. Phys., 79, 1916, (1983).

7. F. T. Smith, J. Math. Phys., 3, 735, (1962).

8. A. V. Chambers, M. S. Child and R. Pfeiffer, J. Chem.
    Soc. Faraday Trans. 2, 84, (1988).

9. D. M. Brink and G. R. Satchler, "Angular Momentum",
    Second Edition, Oxford University Press, (1968).

10. H. Mayer, J. Phys. A, 8, 1562, (1975).

11.   J. G. Frey and B. J. Howard, Chem. Phys., **99**, 415, (1985).

12.   J. G. Frey, (1989) to be published.

13.   M. S. Child, private communication.

14.   L. D. Landau and E. M. Lifshitz, "Quantum Mechanics; Non-relativistic theory", Third Edition, Revised and Enlarged, Pergamon Press, (1977).

15.   K. Shulten and R. G. Gorden, J. Math. Phys., **16**, 1961, (1975).

16.   J. K. Cashion, J. Chem. Phys. **39**, 1872, (1963).

17.   M. Abramowitz and I. A. Stegun, "Handbook of Mathematical Functions", Dover, New York, (1965).

18.   J. G. Loeser and D. R. Herschbach, J. Chem. Phys., **86**, 2114, (1987).

19.   H. Hochstadt, "Functions of Mathematical Physics", Dover, (1986).